

Application of Image Analysis Techniques to Determine Strain Distribution in Leather

**A Thesis submitted for the degree of
Doctor of Philosophy
The University of Northampton**

**FOR
REFERENCE
ONLY**

SAQIB KABEER

B.E (*Mechanical Engineering*), M.Sc (*Design Engineering*)

April 2006



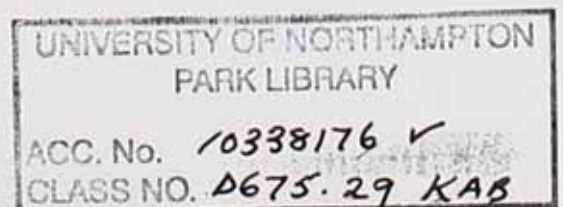
Disclaimer

The content of this dissertation describes the original work by the candidate, except where specific reference is made to the work of others. No part of this dissertation has been submitted for a higher degree to any other university.

SAQIB KABEER

British School of Leather technology

The University of Northampton



Acknowledgments

I am grateful to *Prof. G.E. Atteburrow, Prof. Phil Picton* and *Dr Malcolm Wilson* for their academic support, productive advice and systematic guidance throughout my PhD studies. I am also grateful to all of the British School of Leather Technology, the Graduate School and IT staff members.

Finally I would like to give my gratitude to my parents who gave me great strength, encouragement and to the EPSRC (*Engineer and Physical Sciences Research Council*) for providing financial support to carry out this research work.

I dedicate my theses to my niece *Miss Moomal Bhatti* and to Cancer Research UK.

ABSTRACT

The optimum cutting of various parts of a shoe, prior to shoe manufacture requires knowledge of the topographical variation of what are termed "lines of tightness". Currently the cutting operation for shoe parts is guided by a general assumption about the pattern of the lines of tightness. There is a need to have available a system which can determine, in a non-destructive way, the lines of tightness in an individual piece of leather.

Initially an image analysis system was developed to investigate the uni-axial deformation behaviour of leather. This technique provided more information about the stress-strain behaviour of a leather sample along the gauge length than a conventional mechanical test and it was possible to accurately measure the strain distribution along the gauge length. A system was developed which could determine the relative displacement of marked spots along the gauge length of the sample using images captured during a uni-axial, bi-axial or multi-axial tensile test. The separation of the marked spots along the direction of applied stroke allowed the determination of longitudinal strain while contraction across the width was also measured in some cases, which was useful in calculating the Poisson's ratio of leather for which a great variation was observed between different locations (Butt, Belly, Neck etc).

Various approaches were investigated to determine the lines of tightness. Firstly, the local Poisson's ratio was observed since a higher value of this parameter was associated with these lines of tightness. Secondly, biaxial stretching of leather by a series of actuators for each axis indicated the lines of tightness along the actuator with lower strain values. Thirdly, the strain was measured when the leather was stretched along number of known axes. This latter technique appeared to be best approach and mathematical modeling was investigated to provide further refinement. A mechatronics-based device for industrial application of the third approach was also

proposed. The software was written using a graphical programming system (LabVIEW).

NOMENCLATURE

Symbol	Definition
δ	Stress
E	Modulus of Elasticity
ϵ	Strain
ϵ_l	Lateral Strain
L_0	Original Length
L_f	Final Length
L_r	Retract Length
ν	Poisson's Ratio
N_x	Pixels in the columns
N_y	Pixels in the rows
Abbreviation	Definition
CCD	Charged Couple Device
FOV	Field of View
VI	Virtual Instrumentation
BCG	Brightness, Contrast, Gamma
PNG	Portable Network Graphics Format
TIFF	Tag Image File Format

TABLE OF CONTENTS

CONTENTS	PAGE NUMBER
Title	i
Disclaimer	ii
Acknowledgement	iii
Abstract	iv
Nomenclature	vi
Contents	vii
CHAPTER ONE: INTRODUCTION	2
1.1 Structure of Skin/Hide	6
1.1.1 Fibrous Structure of Collagen	9
1.1.2 Mechanical Function of Skins/Leather	10
a) Engineering Stress	13
b) Engineering Strain	13
1.1.3 Stress-Strain behaviour of Leather	14
1.1.4. Effects of Mechanical Processes on the Fibre Network	17
1.1.5 Set in Leather	19
1.2 The Leather Making Process	21
1.2.1 Curing	21
1.2.2 Soaking	22
1.2.3 Liming	22
1.2.4 Fleshing	23
1.2.5 Deliming	23
1.2.6 Bating	23
1.2.7 Pickling	23
1.2.8 Degreasing	24

1.2.9 Tanning	24
a) Mineral Tannage	24
b) Aldehyde Tannage	24
c) Vegetable Tannage	24
1.2.10 Splitting	24
1.2.11 Shaving	25
1.2.12 Neutralization	25
1.2.13 Dyeing	25
1.2.14 Fatliquoring	25
1.2.15 Sammying	26
1.2.16 Setting Out	26
1.2.17 Drying	26
1.2.18 Staking	28
1.2.19 Buffing and Brushing	29
1.2.20 Finishing	30
1.2.21 Final Grading	30
1.2.22 Measurement	30
1.3 Leather as a Material for Shoes	32
1.3.1 Availability	32
1.3.2 Elasticity and Plasticity	32
1.3.3 Strength and Stretch	33
1.3.4 Flexibility	33
1.3.5 Permeability to Air and Water Vapour	33
1.3.6 Thermal Conductivity	34
1.3.7 Abrasion Resistance	34
1.3.8 Ease of Working	34
1.3.9 Maintenance	34

1.4 Shoe Making	36
1.4.1 Clicking Department (or Cutting Department)	37
1.4.1.1 Lines of Tightness	41
1.4.1.2 Effects of Mechanical Processes on Lines of Tightness	43
1.4.2 Closing Department (or Machining Department)	44
1.4.3 Lasting & Making Department	45
1.4.4 Finishing/Shoe Room	46
CHAPTER TWO: FUNDEMENTALS OF IMAGING SYSTEM	48
2.1 Electronic Video Cameras	48
2.2 Digitisation	49
2.2.1 Sampling	49
2.2.2 Quantisation	50
2.3 Analogue and Digital Cameras	51
2.4 Image Storing	52
2.5 Camera Calibration	53
2.5.1 Lenses	53
2.5.2 Field of View	53
2.5.3 Basic Lens Calculations	53
2.5.4 Resolution	54
2.5.5 Contrast	56
2.6 Processing the Acquired Data	57
2.6.1 System Setup	57
2.6.2 Software Selection and Development	58
2.6.2.1 Graphical Programming	58
2.6.2.2 Image Acquisition	58

2.6.2.3 Software Development	59
2.6.2.3.1 IMAQ-BCG Look-up	59
2.6.2.3.2 IMAQ- Edge Detection	60
2.6.2.3.3 IMAQ – Clamp	61
2.6.2.3.4 IMAQ – Thresholding	62
2.6.2.3.5 Improvement of the Binary Image (Extraction of Dots)	63
2.6.2.3.6 Calliper (Measuring Distance)	63
2.7 Tensile Testing	64
2.8 Selection of the Camera	64
CHAPTER THREE: ACCURACY OF MEASUREMENT	67
3.1 Accuracy of Image Processing Software	
3.1.1 System Setup	67
3.1.2 Acquiring images	68
3.1.3 Calibration Using a Grid	69
3.1.3.1 Placing Calibration Marks on the Sample	69
3.1.3.2 Programming the Acquisition Software	71
3.1.4 Measurement by Image Analysis Software	73
3.2 Measurement of Strain Distribution in Rubber	75
3.2.1 Experimental Set-up	76
3.2.2 Image Processing	79

CHAPTER FOUR: APPLICATION OF IMAGE ANALYSIS TO EVALUATE LINEAR STRETCHING OF LEATHER	84
4.1 Determination of Stress-Strain Behaviour of Leather by Image Analysis	84
4.1.1 Material	84
4.1.2 Experimental Procedure	84
4.1.3 Sample Preparation	84
4.1.4 Methodology	85
4.1.5 Results and Discussion	88
4.2 Measurement of Strain Distribution in Leather	88
4.3 Determination of Poisson's Ratio of Leather	92
4.3.1 Methodology	93
4.3.2 Results and Discussion	97
4.4 Poisson's Ratio and the Lines of Tightness	101
4.4.1 Experimental Setup and Methodology	103
4.4.2 Results and Discussion	104
4.5 Analytical Model for Poisson's Ratio at Low Strain Values	109
4.6 Auxetic Behaviour of Leather	113
4.7 Conclusion	114
 CHAPTER FIVE: BI-AXIAL STRETCHING OF LEATHER	 116
5.1 Determination of Lines of Tightness of Leather for Large Pieces	117
5.2 Method 1: Lateral Contraction Method	117
5.2.1 Material	117

5.2.2 Sample Preparation	117
5.2.3 Methodology	118
5.2.4 Results and Discussion	120
5.3 Method 2: Uni-Axial Constraint Method	122
5.3.1 Results and Discussion	125
5.4 Method 3	131
5.4.1 Results and Discussion	133
5.4.2 Mathematical Modelling	135
CHAPTER SIX: PROPOSED SYSTEM	144
6.1 Lateral Contraction Method	144
6.2 Uni-Axial Constrained Method	146
6.3 Angular Stretching Method	147
6.4 Proposed Design of a Commercial System	148
6.5 System Description	150
6.5.1 Upper Grip Mechanism	152
6.5.2 Lower Grip Mechanism	153
6.5.3 Software Development to measure strain	155
6.5.4 Digital Spot- Displacement measurement	155
CHAPTER SEVEN: CONCLUSION AND FUTURE WORK	162
7.1 Conclusion	162
7.2 Future Work	165
References	166

Appendix A	174
Appendix B	176
Appendix C	177
Appendix D	179
Appendix E	183
Appendix F	184
Publication	185

CHAPTER I

CHAPTER 1

1 Introduction

The technology of leather making is, in the broad sense, a series of operations, which aim to remove unwanted material (hair, epidermis, and ground substance) from hide/skin and to isolate a network of collagen fibres. These fibres have a sub-structure of fibrils and fibril bundles. The fibres themselves are also aggregated to form bundles which divide, branch and interweave to form a three-dimensional network. The morphology of this network depends on the degree of tissue development and on the topographical location on the hide/skin [1]. The density and form of the three-dimensional (non-woven) network of these natural fibres play an key role in determining the varying physical properties of leather from hide to hide, skin to skin and from point to point across the whole hide/skin [2]. However the pattern of variation of a property e.g. tensile strength is similar for each separate skin regardless of whether its overall strength is high or low. This pattern of variation in physical properties of leather is highly dependent on, not only thickness but also the frequency with which the collagen fibres interweave and cross over each other. The directional run of fibres with different interweave frequency along the surface of the hide/skin plays a key role in determining the local stress-strain properties of a piece of leather and due to this directional run of fibres this property varies from point to point over the whole surface of hide/skin. This variation in stress-strain relationship plays a key role in determining the final quality of a region of leather for shoemaking and the particular stress-strain relation in a region needs to be known before a correct decision can be made as to which parts of the shoe should be cut from that region. This is because different part of shoe are required to stretch by different degrees during lasting. The ease with which leather can be stretched is governed by the direction of fibre run which determines the so-called lines of tightness. Knowledge about the magnitude and direction of these lines of tightness over a piece of leather is vital in order to guide the optimum cutting of various parts of the shoe. Currently there is no way of non-destructively determining the pattern

of lines of tightness and shoe parts cutting is a imprecise "operation" relying on general assumptions about the lines of tightness (about which there is no agreement). Clearly a method to determine the pattern of lines of tightness and their magnitude on an individual piece of leather would be of great benefit to the shoe making industry. Together with this around 70% of leather produced in the world is used in shoe manufacturing industry and this further obliges us to carry out research in this area to maximise its utilisation and to produce high quality shoes.

Non-destructive testing (NDT) may be defined as the application of an inspection method to a component or structure in which the test piece is not adversely affected by the testing method. Great achievements have been obtained in this field by the introduction of Holography, Speckle Photography, and Laser Speckle Photography. In general, the purpose of NDT is to determine material properties e.g. detecting discontinuities, defects, location of defects and especially the strain distribution over the surface of a material. The most commonly used NDT techniques with their lack of application on leather are discussed below.

a) Ultrasonic Testing

Ultrasonic inspection provides a sensitive method of non-destructive testing in most materials, metallic, non-metallic, magnetic or nonmagnetic. It operates on the principle of measuring the intensity of a 'transmitted' and 'reflected' ultra sound wave. Although the technique could be use to determine the density of fibres along the surface of leather but it could not reveal their preferred orientation. Also this methodology would be a slow process as the sensor to collect the sound waves would need to roll all over the surface of hide/skin.

b) Speckle Photography

Speckle photography is a remote, non-contact, whole field technique and has found particular use in metrology. The methodology involves the use of coherent

laser light to illuminate the surface of interest. A lens collects the reflected light, which is then recorded by a suitable medium, e.g. photographic film or a CCD array. Because the surface is rough, the reflected light will necessarily contain speckle. An applied strain, or in-plane displacement of the surface, causes a shift in the speckle pattern, which is proportional to the direction of the local deformation [3]. The requirement of a rough surface to obtain a speckle pattern would make this technique inconvenient to apply on finished leather also the technique is best suited to measure strain over relatively smaller areas and therefore its application on large pieces of leather would be time consuming.

c) Radiographic Testing

In this method X-rays are used to produce images of objects using film or other detector that is sensitive to radiation. The test object is placed between the radiation source and detector. The thickness and the density of the material that X-rays must penetrate affects the amount of radiation reaching the detector. This variation in radiation produces an image on the detector that often shows internal features of the test object. Although the method might be used to find the orientation of fibres. The following points must be born in mind

- Extensive operator training and skill are requited
- Access to both sides of material is needed
- Orientation of the radiation beam to non-volumetric defects is critical.
- Relatively expensive equipment investment is required.
- There is a possible radiation hazard for personnel.

The above mentioned NDT methods have been successfully applied for quantitative measurement of temperature [4], strain field [5] and surface displacement [6]. Several of the methods mentioned above have some drawbacks such as sensitivity to the environment, a requirement for surface preparation, difficult to automate: also they may be time consuming and so unsuitable for routine production solution. Therefore their use is limited to specific materials and

situation. The physical testing of leather is currently a destructive process, whereby samples are cut out for mechanical testing. Such destructive tests are not only time consuming, but also wasteful of leather. Therefore there is great incentive to develop a non-destructive test that will allow much improved characterisation of leather quality control. Although some significant achievements have been made in the non-destructive testing of leather [7-12] they have major drawbacks of being time consuming, non automated and hard to apply on an industrial basis.

Most of the non-destructive testing measured work carried out on leather has been carried out at the footwear industry since this industry is the major one utilising leather. For centuries, the cutting of shoe parts (Section 1.4) out of leather hides has been done manually by highly skilled operators using a swing beam press and sets of knives. This practice continues but in the future it may be replaced by computerised automation following the introduction of nesting system analysis software (Section 1.4.1). The development of vision systems for leather fault inspection [12] and measurement of grain structure [13], suggests that this technique could be used to perform some other forms of NDT on leather.

To the author's knowledge no research work has been carried out to determine the stress-strain behaviour of leather in a non-destructive way. It is hypothesised that this can be best achieved by using computerised image analysis of stretched leather to measure local variations in strain. The use of digital images to measure strain fields is an emerging area of research in polymer science [14] and biomedical science [15] and an early study of the response of leather to mechanical stretching in a setting machine [16] also suggested that the approach was feasible for leather. If successful it should be possible to non-destructively determine the lines of tightness in leather, thus eliminating the ambiguity about the form of lines of tightness following suggestions by different authors (Section 1.4.1). Therefore the research described in this theses was carried out with following aims and objectives.

- To investigate a route to non destructively measure lines of tight ness in leather

- To develop image analysis software and a practical system which can be used to measure strain distribution in leather
- To determine the accuracy with which strain can be measured using such a system
- To apply the system to measure variation in uni-axially strained leather and compare it with homogeneous material (rubber)
- To evaluate the system for measuring strain in two orthogonal directions simultaneously and evaluate this approach for measuring Poisson's ratio
- To investigate the route where by the measurements made using the system may be used to indicate the magnitude and direction of lines of tightness in leather
- To develop a basic design for a mechatronics system which could be used to measure lines of tightness in whole piece of leather

In the following section structure of hide/skin, leather, shoe-making processes and lines of tightness are discussed in detail.

1.1 Structure of Skin/Hide

Skin and hide can be considered as a protective sheath for animals. Skin and hide are composed of randomly interwoven fibres made of collagen. Some animals are protected primarily by a heavy coating of hair, scales or feathers, while others by the denseness of the network of fibres of the skin itself. In Figure 1.1, a cross sectional view of cattle hide with its major components is shown [17].

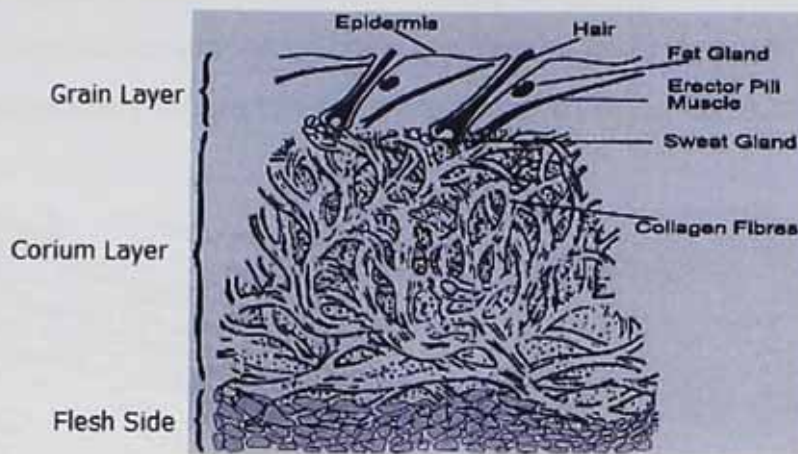


Fig 1.1 A cross section of cattle hide^[17]

The hair follicle contains the hair root. Hair itself is a sulphur bearing protein called keratin. The lining of the hair follicle is also made up of keratin which is spread along the surface of the skin down into the hair follicle and up out again. Next to hair follicle are the sebaceous glands, sweat glands and blood vessels. Sebaceous glands release oil into the hair follicle and on the surface of skin, while sweat glands release water and body wastes through the pores of skin.

The extreme outer layer of skin is called the epidermis and is hard, quite inert chemically and constantly in the state of flaking. The fibre structure has a pattern related to the slope of the hair follicles. The fibre structure through this area is generally quite fine in nature. Below the layer at the bottom of hair root, known as corium layer, the fibres are coarser and stronger, and the predominant angle at which they are woven can indicate the properties of resultant leather [17]. If the fibres are more upright and tightly-woven, one expects a firm, hard leather with little stretch, whereas if they are more horizontal and loosely-woven, one expects soft stretchable leather [18].

In the corium layer the fibre bundles are large and strong. They lie at varying angles to the grain layer above. This angle varies in different animals, but to some extent, the angle can be altered during the leather manufacturing process. This angle is known as the 'angle of weave' and it affects the physical properties

of the leather. A lower angle of weave produces softer, weaker and less elastic leather. The cross sectional view of grain and corium layer is shown in Figure 1.2 (a) and (b) respectively where the compactness of collagen fibres in corium layer is quite clear.

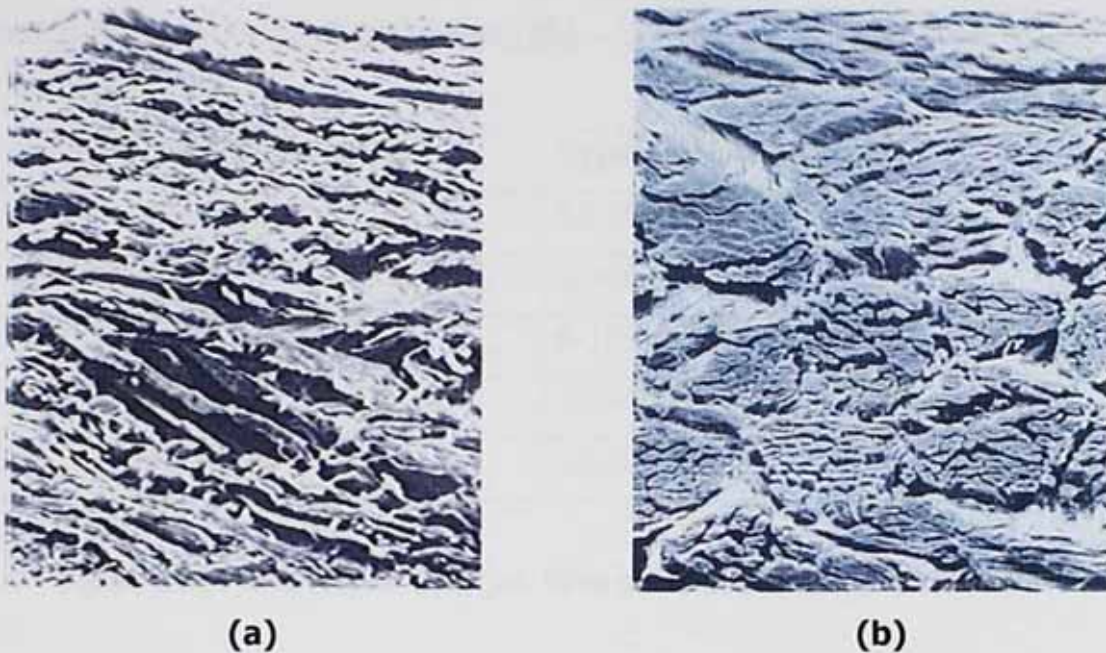


Fig 1.2 A cross section of grain (a) and corium layer (b) ^[18]

In the corium layer of skin the orientation of the fibres more approaches the horizontal and the longer fibres run parallel to the surface of the skin. This layer of hide is composed almost entirely of collagen and is the source of the strength of leather. The lower stratum of the hide is known as the flesh layer; it contains small amounts of flesh and fatty or adipose tissue. In addition to collagen, hides contain about one percent of elastin. Most of this is in the grain layer and its presence in this part of the hide is believed to be responsible for some adverse properties in the finished leather [19].

The residue of hide/skin after applying different chemical processes which will be described later (*Section 1.2*) forms the stabilised collagen fibre network structure, which is called leather. Understanding the mechanical properties of the hide fibre network leads to a better understanding of the leather fibre network.

1.1.1 Fibrous Structure of Collagen

Five hierarchical fibrous units are reported for the corium fibres of bovine leather. The individual units of this hierarchical structure were shown to have varying diameters as shown in table 1.1 below [20].

Structural unit	Typical diameter
Fibre bundle	60-200 μm
Fibres	30-60 μm
Fibril bundle	5-10 μm
Fibril	100-400 nm
Micro fibril	10 nm

Table 1.1 Hierarchy of collagen fibre structure within the skin [20]

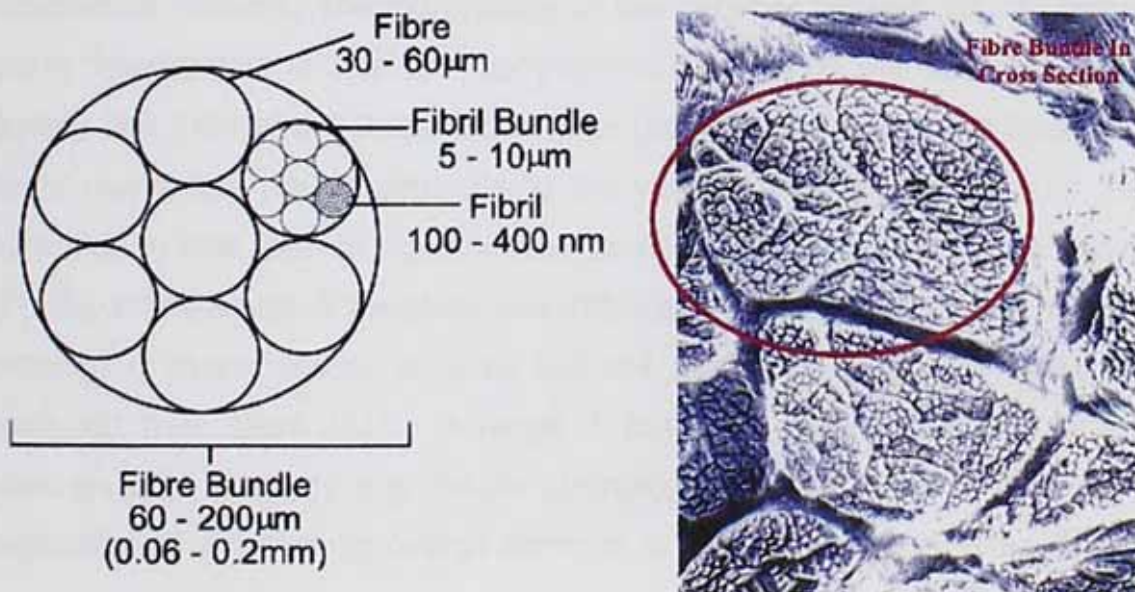


Fig 1.3 The Hierarchy of the Fibre structure [20]

The most fundamental units of collagen fibres have been shown to be the micro-fibrils with diameters of about 0.01 μm . The micro-fibrils aggregate to form fibrils

whose diameters range from 0.1 to 0.2 μm . The fibrils in turns aggregate to form fibril bundles with diameters ranging from 3 to 6 μm . The fibril bundles are also aggregated to form the fibre with typical diameters in the range of 30-60 μm . The fibres finally aggregate to form fibre bundles of diameters within the range 60-200 μm [20]. It is from these collagen fibres and fibre bundles that a fibre network is constructed. The outstanding property of leather is due to this unique collagen fibre network structure.

1.1.2 Mechanical Function of Skins/Leather

The technology of leather making is, in the broad sense, a series of operations which aim to remove unwanted material (hair, epidermis, and ground substance) from hide/skin and to isolate a network of collagen fibres. These fibres have a sub-structure of fibrils and fibril bundles. The fibres themselves are also aggregated to form bundles which divide, branch and interweave to form a three-dimensional network. The morphology of this network depends on the degree of tissue development and on the topographical location on the hide/skin [17]. The density and form of the three-dimensional (non-woven) network of these natural fibres play a key role in determining the varying physical properties of leather from hide to hide, skin to skin and from point to point across the whole hide/skin [2]. An animal's age at slaughter also influences the biochemical, biophysical and histological characteristics of skins and the properties of leather subsequently produced from them [21]. However it has been stated that the pattern of variation of a property e.g. tensile strength, is similar for each separate skin regardless of whether its overall strength is high or low [22]. This pattern of variation in physical properties of leather is highly dependent on not only thickness but the frequency with which the collagen fibres interweave and cross over each other. These fibres are more closely interwoven or compact in the butt area and this compactness of fibre weaves decreases from butt to belly, shoulder, and shank and neck side. In Figure 1.4 (b), (c) and (d) the fibre's compactness

for corium, belly and shank region respectively is shown while in Figure 1.4 (a); the topographical division of skin/hide along its surface is shown.

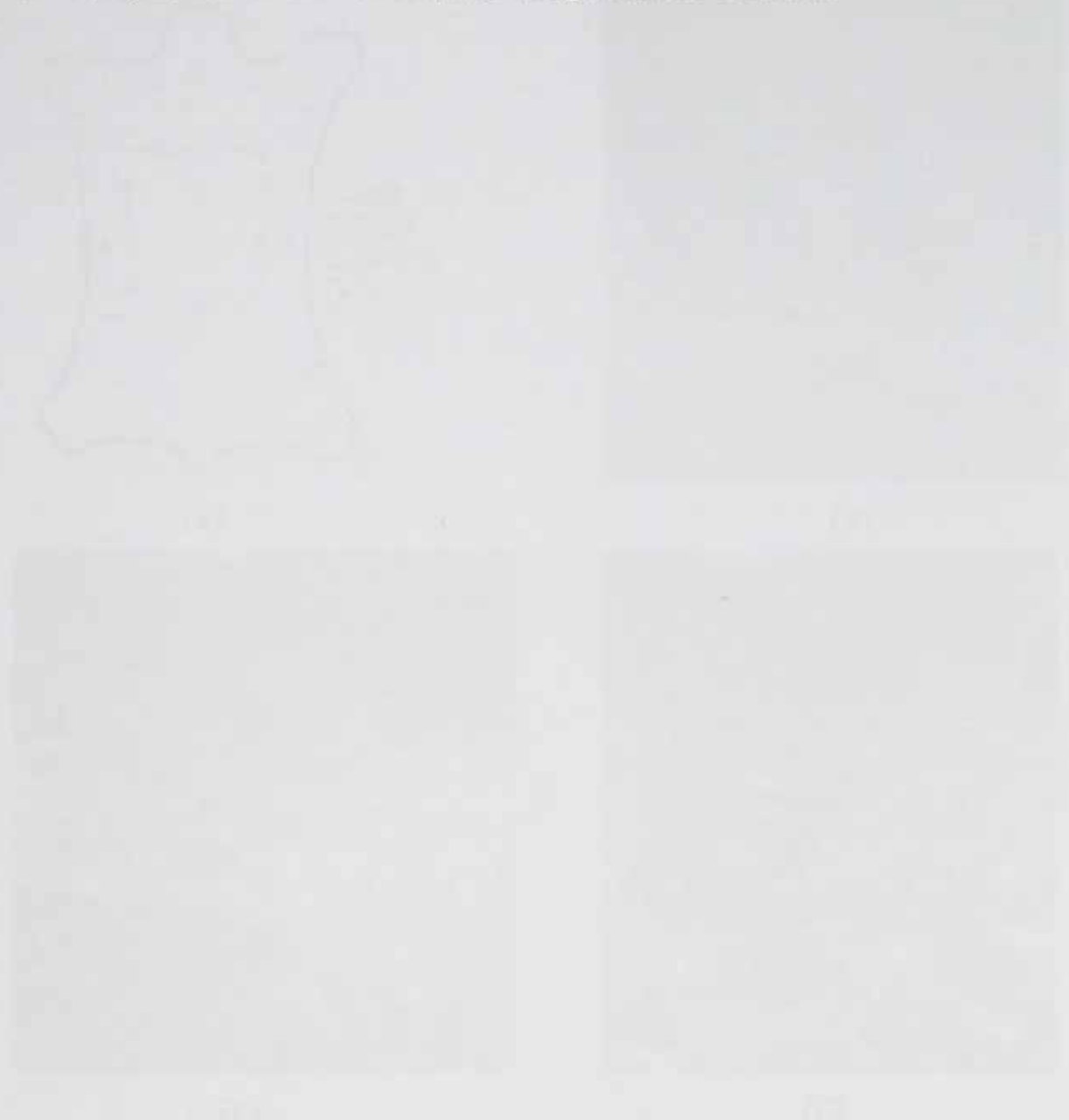
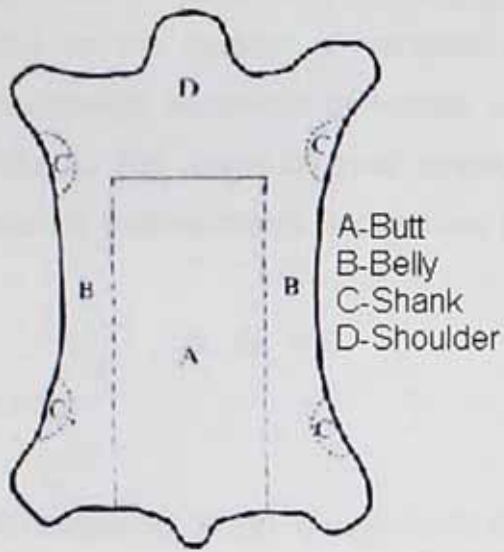


Fig. 1.4 (a) Topographical division of skin/hide along its surface.

The topographical division of skin/hide along its surface is shown in Figure 1.4 (a). The diagrams illustrate the division of the skin/hide into different regions: corium, belly, and shank. The topographical division is shown along the surface of the skin/hide.



(a)



(b)



(c)



(d)

Fig 1.4 (a)-(d) Hide sections with its fibres compactness for different regions^[18]

The angle of weave is the average angle between leather surface and the interweaving fibres with in leather structure. It plays an important role in determining the breaking strength and elongation at break of leather. For high tensile strength the fibres need to interweave at a low angle so that the load can be transferred along the fibre axes. The tensile strength of leather is a function of

the number of fibres in the woven fibre network that become oriented in the direction of applied load at the point of failure [20].

Due to the pattern of variation in the collagen fibre network structure the mechanical behaviour of leather is very difficult to define in detail for a given hide. In the range of small stress, unless the network of collagen fibres is not altered, leather obeys Hooke's law [1].

$$d\delta/d\varepsilon = E$$

Where

δ represents stress, ε represents strain and E is constant

The most commonly used method to characterise the mechanical properties of a material is to determine the stress-strain behaviour in a tensile test. By plotting the stress-strain graph many characteristics such as modulus, breaking strength, strain at break can be obtained. For many engineering applications, the use of 'engineering stress and strain' values for material stress-strain curves will be sufficient for obtaining correct answers in a plasticity analysis. The engineering stress and strain in a material can be defined as

Engineering Stress

$$\delta \text{ (Stress)} = F/A$$

where

F = Force acting on the material

A = Area

Its unit is Pascal or N/mm^2

Engineering Strain

Strain is normally expressed in percentage. It is change in length per unit length, when the material is subjected to any deformation.

$$\% \varepsilon = \left[\frac{L - L_0}{L} \right] \times 100$$

Where

ε = Strain in percentage

L_0 = Original Length of material before application of load

L = Length of material after application of load

In the tensile test a dumb-bell sample of material is clamped between the jaws of the testing machine. The sample is then stretched by the application of a load on the sample and the deformation is measured by the load cell. Then by using the above formulae stress and strain are calculated. The form of the stress-strain behaviour for many materials (e.g. metals and plastics) is shown in Figure 1.5 [23].

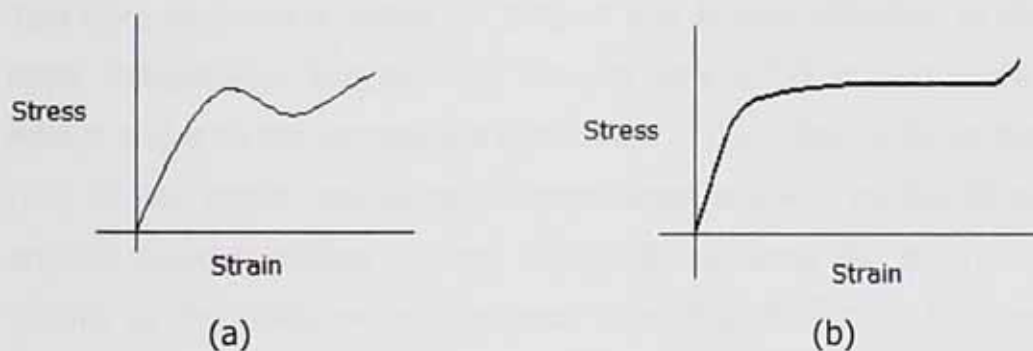


Fig 1.5 (a, b) The form of the stress-strain curve found for most metals and plastics^[23]

1.1.3 Stress-Strain Behaviour of Leather

As stated earlier, leather consists of a network of bundles, comprised of fibrils. There are also spaces between the fibrils. Due to this unusual structure, leather

shows a non-linear stress strain curve tending to bend away from the strain axis at high strain as indicated in Figure 1.6.

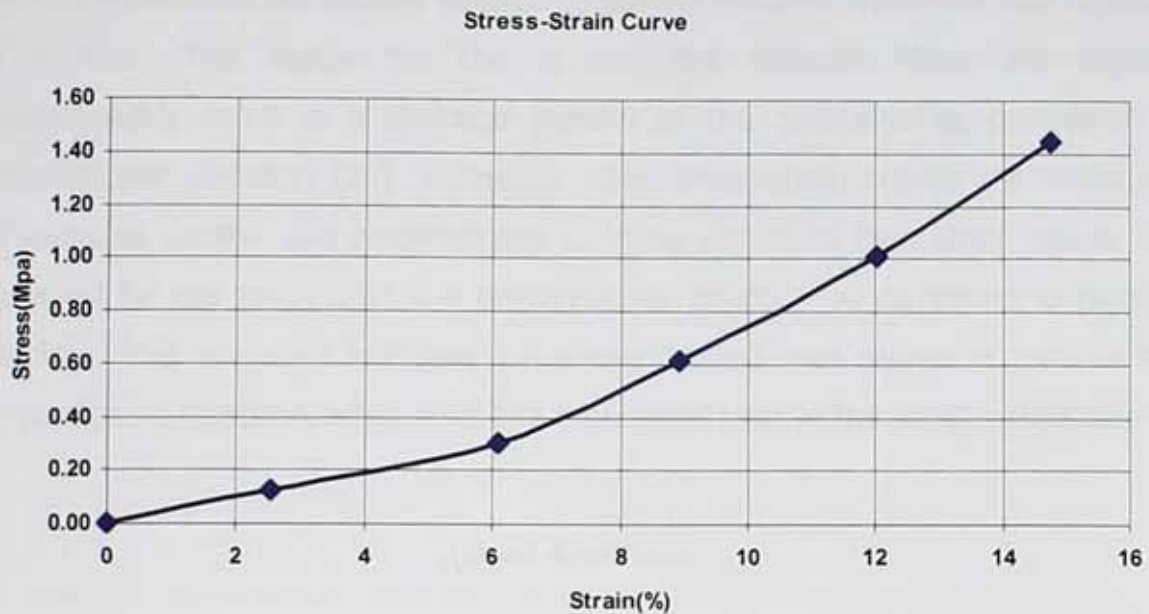


Fig 1.6 Stress-Strain behaviour of leather

This form of curve is called "J" shaped and is also observed in skin and some other collagenous tissues. One view of why a "J" shaped curve is found in leather is due to the progressive orientation of the collagen fibres during straining [24]. At low strains resistance to deformation is low since the fibres themselves are not being stretched but are being aligned along the strain axis. At higher strains, as the fibres become aligned along the strain axis, further deformation can only occur by straining the fibres themselves and this requires increasingly greater stresses. The same behaviour is also observed in partially processed leather, depending upon the moisture content. At high moisture contents the curve has the similar characteristic "J" shape with an initially low slope, which increased dramatically above a given strain. At lower values of moisture content the stress-strain curve acquires as "S" shape with an initially high slope region. This phenomenon is due to the formation of adhesions between various levels of the fibrous structure of the leather, which occur on drying [21]. When tensile strength data were compared with the average and plotted together, all the

samples cut parallel to the backbone showed the same general pattern of variation over the hide, and the samples cut perpendicular to the backbone showed a different but equally definite pattern of variation from one hide location to another. The reason for this is that the collagen fibres are aligned predominately more in a direction parallel to the backbone as compared to perpendicular direction [25]. Therefore when stress-strain curves are measured for samples parallel and perpendicular to these directions high strain values are observed for the same load in a perpendicular direction as compared to parallel direction. This is shown in Figure 1.7 where dashed lines represent tests in the perpendicular direction, while solid line represents tests in the parallel direction.

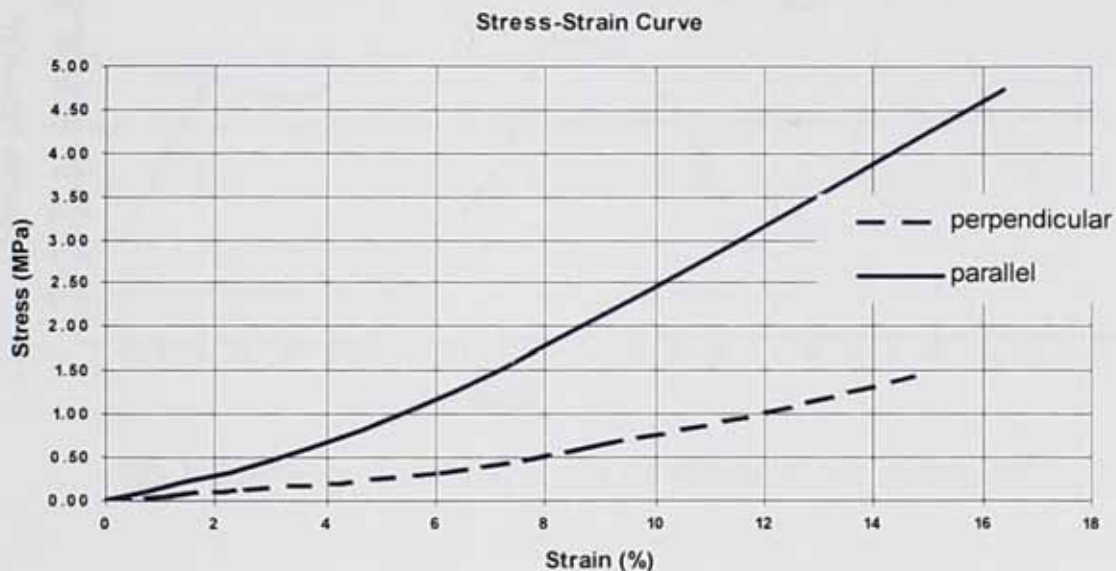


Fig 1.7 Stress-Strain curve for samples cut parallel and perpendicular to the backbone

When stress-strain behaviour for different hide locations was examined then the pattern of variation from one position to another in a given side is, in general, much larger than the variation from one side to another [26]. These variations along different hide locations when averaged using the method introduced by Maeser [22] can be plotted as tensile strength versus elongation. The highest value of tensile strength is observed in the middle of the flank and the adjacent

position of the middle flank, while lowest strength is found in tail area. The elongation in the direction perpendicular to the backbone is higher than in the parallel direction but a great variation is found between the two directions for different positions [27]. Some results of tensile strength parallel to the backbone for different locations are shown in Figure 1.8.

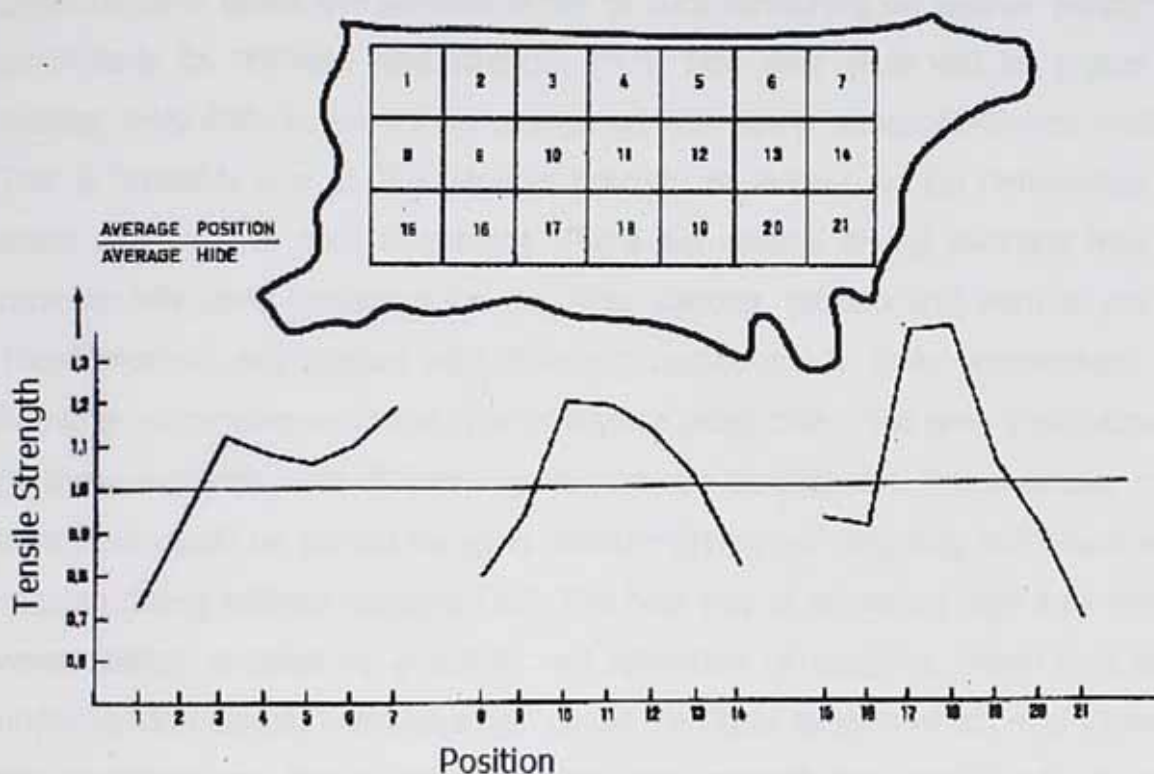


Fig 1.8 Average Tensile strength for different hide locations [27]

This variation can also be observed along the thickness of side or hide, when the stress strain behaviour of split hide was determined for different location i.e. Belly, Butt and Flank. The pattern of stress distribution through the thickness shows substantial differences depending on location on the skin [28]. This difference is due to partial freeing of fibres.

1.1.4. Effects of Mechanical Processes on the Fibre Network

The production of leather comprises chemical process (Liming, Deliming, Bating etc), and some mechanical processes. The most important of these mechanical

processes is drying. At this stage of manufacturing the tanners can achieve considerable interest by increasing the area yield which they achieve by maintaining the leather under stretched condition during drying [29]. The amount of area yield obtained at the time of drying depends upon the moisture content in leather [21], which helps in stretching the leather. However there is great concern about the adverse effect of such stretching on leather properties, particularly its stiffness and strength [30]. This area yield will be higher for heavier weight/thickness leather compared with lower weight/thickness leather. This is probably due to the variable porosity of leather, which determines the space available for fibre alignment. There are several drying methods that are commercially used nowadays i.e. toggling, pasting, tacking and vacuum drying. These methods are applied with different conditions e.g. time, temperature and humidity, depending upon the type of leather being dried. The area yield obtained by these methods with different conditions can be different. For example, more area yield would be gained by using vacuum drying with toggling as compared to vacuum drying without toggling [31]. The best way of achieving high area yield is when leather is dried by a pulling out operation or toggling. When it is dried under tension certain linkages which cause the fibres to stick which might impede the stretching, are broken down by the water present and various new linkages are formed. This results in a more stable form of leather, and permits only a partial recovery when the load is removed, so that a further contraction occurs if these linkages are again weakened by absorption of water [32]. The inherent softness imparted to leather during the earlier chemical processes of opening up and lubrication can be influenced by the adhesion of fibre structure when the leather is dried under stress. For the drying process it is concluded that:

- i) Gentle drying (lower temperature, higher relative humidity, and therefore slower rate) produces soft leather [33].
- ii) The method of moisture removal influences the character and physical properties of leather, particularly if there is a constraint on dimensional change during drying [34]. This has been observed when leather dried under strain (e.g. by using clamps each carrying a load of 7 kp per clamp)

there is a rapid increase of tension on clamps after two hours of drying with higher temperature. But on drying for a long period of time no further increase on load is observed [2].

- iii) Leather dried at higher temperatures becomes firm [2].

1.1.5 Set in Leather

Typically the leather drying process is carried out with a constant applied load to the leather, and under controlled conditions of temperature and humidity. The application of load to the leather results in a deformation of the fibre network which becomes aligned in the direction of applied load. During the drying process, as soon as water is removed from the surface, shrinkage of leather commences and this continues until it reaches an equilibrium state when the drying process is completed [2]. This shrinkage of the surface is not completely recoverable [35]. Similar behaviour is also observed while drying the individual collagen fibres [32]. The amount of shrinkage depends upon the humidity maintained in the drying chamber. At the same dry bulb temperature shrinkage will be higher if humidity is low. Too much drying would result in shrinking of the fibre network to a level that excessive adhesion between the fibres can occur. The purpose of fatliquoring is to minimize this re-sticking. During the toggle drying process leather is dried under an applied extension and so the shrinking tendency of fibres that would lead to a surface area reduction is inhibited. On the completion of this stretching/drying process leather would not return to its original shape but would retain a certain amount of the extension referred to as set [30]. In fact, whenever leather is stretched and allowed to recover it displays some set to a greater or lesser degree. This has been illustrated in the following Figure 1.1.1.

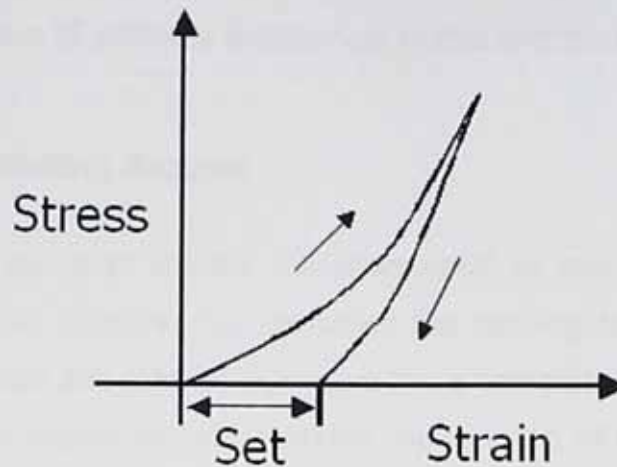


FIG 1.1.1 Illustrating the behaviour of leather in a stress-strain cycle. When leather is extended to a certain strain and then allowed to recover the stress falls to zero when the strain still has a positive value. This retained strain is called set.

The fact that leather displays set effects is due to its viscoelastic properties [24]. In the case of linear set, a sample has an original length L_o , is stretched to a final length L_f and is held for a period of time at this length. Upon release the sample will retract to a length L_r , and set may then be defined as the recovered strain divided by the applied strain and is expressed in percentage as indicated below.

$$\text{Linear Set} = \left[\frac{L_r - L_o}{L_f - L_o} \right] \times 100$$

A direct relation is observed between the amount of set induced and the applied strain which consequently increases the stiffness or tensile modulus of the material. This has been modelled by Attenburrow in relation to the fibre orientation with respect to the applied strain, in which it has been shown that a decrease in fibre's angle with respect to the applied strain would increase the stiffness [30]. This increase in stiffness depends upon the direction in which the sample is cut with respect to the applied strain before drying, and the amount of

strain applied. As the fibres try to realign themselves in the direction of applied strain, a greater value of stiffness is observed in this direction [36].

1.2 The Leather Making Process

Leather is one of the most ancient materials used by mankind to manufacture clothes and everyday objects. For centuries the tanning technology constantly evolved, making hides and leather more and more versatile, opening new original and creative usage scenarios, and making the tanning of more and more skin kinds possible, including even fish skins. Nowadays leather is used to create an incredible variety of objects, such as garments and accessories, footwear, bags, cases, diaries, photo albums, sport gear, car interiors, furniture parts and an almost infinite variety of items to which leather gives prestige and style. The major animal hides (outer covering for big animals) and skins (outer covering for small animals) used for leather making process are bovine, buffaloes, goats, sheep and a variety of other wild living animals. The hide or skin of each species of animal has its own characteristic length, width, thickness, and fibre structure and grain surface. However in general there is much more in common to all animals' hides and skin e.g. proteins, hair, epidermis, proteoglycans, melanin and fats [17]. Therefore almost the same process is applied while converting hides/skins to leather. The manufacturing process is a combination of many mechanical and chemical operations. An overview of the steps involved in leather making is presented below.

1.2.1 Curing

Curing is the method of preserving the hides and skins from bacterial attack before they are tanned. The hide is made up of:

- 1) Fibrous proteins, Keratin, Collagen, Elastin
- 2) The soluble or soft proteins, Albumins, Globulins, Mucoproteins and soft Keratin
- 3) Fat components of the body both physiological and Fat storing.

The most resistant to chemical or bacterial attack are fibrous protein, hair and elastin. The next most resistant is collagen.

The following methods are most commonly used for curing.

- 1) Drying
- 2) Salt Curing
- 3) Brine Curing
- 4) Chilling
- 5) Freezing

1.2.2 Soaking

The first process on arrival of the hides at the tannery (whatever the source or cure) is that of soaking. This is a necessary first step whatever the type of leather is to be produced. Its objectives are:

- 1) To soften the hide and to restore it to its former state of hydration (specially in the case of dry salted and dry hides)
- 2) To remove blood, dung and dirt if present.
- 3) To remove certain (but not necessarily all) soluble proteins which may have been coagulated during drying or curing.
- 4) To remove salt used in the curing process.

1.2.3 Liming

The function of the liming process is to make possible the removal of the epidermis and to weaken or digest the hair roots, or alternatively it may be claimed to weaken the layers attaching the hairs to the hair root thereby making it possible to remove the hair at the end of liming process [17]. In the case of sheepskins for which hair saving is necessary, the process is applied in a different way to save the hairs. This process consequently results in opening up the fibres thereby facilitating the penetration of the tannins into the hide during the subsequent tanning process.

The following methods of liming are normally used:

- 1) Flat liming in pits.
- 2) Suspension liming in pits.
- 3) Paddle liming.
- 4) Drum liming using normal concentrations of lime and sulphide.
- 5) Drum digestion of hair with or without subsequent liming in pits.
- 6) Sweating or Painting process to save hair for liming of sheep skin.

Drum liming is the most frequently used as its fast and cheap.

1.2.4 Fleshing

After liming, the pelt is passed through a machine to remove fleshy tissue from the flesh side. Hides may be split into layers at this stage or after tanning.

1.2.5 Deliming

The principal action of deliming is to gradually neutralize the alkali in the pelt, avoiding rapid changes in pH, which could lead to the distortion or disruption of the tissues [17].

1.2.6 Bating

A long delime can significantly improve the removal of any remaining lime, scud (miscellaneous debris) and residual components broken down during liming. Bating - based on the use of enzymes - completes this process so that the pelt is flat, relaxed, clean and ready for pickling and tanning.

1.2.7 Pickling

Weak acid and salt solutions are used to bring the pelt to the weakly acid state required for most tanning processes. Stronger pickling solutions are used to

preserve pelts so that they can be stored or transported in a stable form over periods of several months.

1.2.8 Degreasing

Solvents or water-based systems can be used to remove excess grease before tanning.

1.2.9 Tanning

Tanning converts the protein of the raw hide or skin into a stable material which will not putrefy and is suitable for a wide variety of purposes. Tanning materials form cross links in the collagen structure and stabilize it against the effects of acids, alkalis, heat, water and the action of micro-organisms [2]. The main types of tanning materials are:

Mineral tannage

Most leather is tanned using salts of chromium.

Aldehyde and oil tannage

Tanning with aldehydes and oils produces very soft leathers and this system can be used to produce dry cleanable and washable fashion leathers and also chamois leather.

Vegetable tannage

Various plant extracts are used to produce brown colour leathers, which tend to be thick and firm. This type of tannage is used to produce stout sole leather [37], belting leather and leathers for shoe linings, bags and cases.

1.2.10 Splitting

A splitting machine slices thicker leather into two layers. The layer without a grain

surface can be turned into suede or have an artificial grain surface applied.

1.2.11 Shaving

A uniform thickness is achieved by shaving the leather on the non-grain side using a machine with helical blades mounted on a rotating cylinder.

1.2.12 Neutralization

Neutralizing removes residual chemicals and prepares the leather for further processing and finishing. Additional tanning material may be applied to give particular properties which are required in the finished leather.

1.2.13 Dyeing

The dyeing of leather into a wide variety of colours plays an important part in meeting fashion requirements. Some leathers are only surface dyed, while others need a fully penetrated dye, as is the case with suede leathers.

1.2.14 Fatliquoring

The preliminary processes of unhairing and bating remove most of the natural oil from skin. A sufficient amount of lubrication is therefore required to prevent leather to dry into a hard mass. The proper lubrication or fatliquoring greatly affects the physical properties of break, stretch, stitch tear, tensile strength and comfort of leather. Over lubrication will result in excessive softness and raggy leather in the bellies and flanks. Under lubrication or improper penetration, results in hard bony leather that may crack in use.

A fatliquoring system that is good for one type of leather might be inadequate for another. Adjustment must be made to compensate for the tannage, retannage dyes, and anticipated finishing systems.

1.2.15 Sammying

This process is carried out by using two cylinders which compress the semi-processed leather to remove water and bringing about a uniform distribution of water in the leather of about 40 to 50% (by weight) depending upon the pressure applied on the cylinders

1.2.16 Setting Out

The leather is stretched out and the grain side is smoothed.

1.2.17 Drying

Drying is one of the key mechanical operations in the leather making process. Leather can acquire its final texture, consistency and flexibility in the drying operations. It is more than the simple removal of the moisture to bring the leather to a final usable form. The tanners purchase hides/skin by weight and sell leather by area. There is a considerable interest in maximizing the area yield of product for a given weight of raw material. Therefore several methods have been introduced to achieve the maximum area yield with flexible and workable effects. The methods currently being used are toggling, pasting, tacking, vacuum drying, electrical radiation drying and microwave drying [38].

Most of these methods for leather drying involve conductive and convective processes such as air-drying and vacuum drying. The air-drying method includes hang drying, toggle drying and past drying. The simplest air-drying method is hang drying, in which leather is hung freely in the open air or in the heated chamber or tunnel. Past drying on the other hand is the most complex drying method, yielding relatively smooth grain and a higher area yield of leather than hang drying [17]. Radiation drying, including radio frequency drying and microwave drying, has not gained popularity due to its high capital cost. The physical properties of leather e.g. stiffness, strength, apparent density, retention

area, compliance and tear strength are significantly affected by the drying method used. It has been discovered for the vacuum drying method that the area retention, stiffness and apparent density of dried leather increase with increasing residual water content. Also the drying rate is one of the key factors controlling the tear strength of leather besides the thickness of leather [31]. The attraction of leather fibre's for one another which exists in almost any type of leather will result in some stiffness upon drying. In causing the physical dimensions to be decreased the fibres attraction will also result in some physical shrinkage of the leather. Drying methods that involve mechanically holding of leather in an extended position will result in a large area yield and may prevent leather curling from the uneven attractive forces with in the fibres [17]. Therefore toggle drying which involves mechanically holding of leather in an extended position produces high area yield as compare to other methods while hang drying produces minimum area yield, so toggle drying is most widely used. Both methods are shown in Figure 1.2.1 [38].

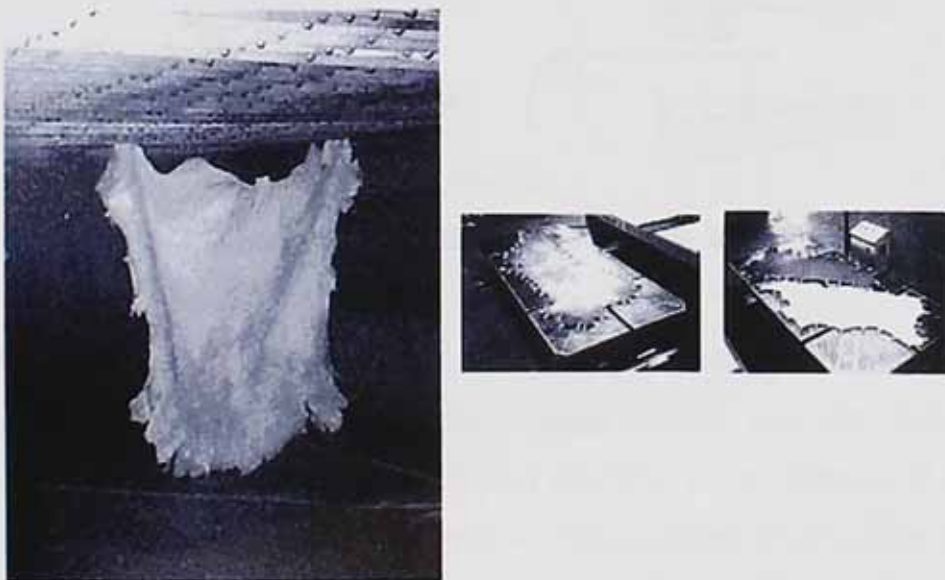


Fig 1.2.1 Hang and Toggle drying methods for leather^[38]

The drying process is always carried out under controlled condition i.e. temperature and humidity. Too much drying would result in shrinking of fibre

network to a level that the bonding between the fibre chains can be feasible. The purpose of fatliquoring is to minimize this re-sticking. Leather is normally dried to a water content level of 10-20%. The properties of leather achieved after this process also depends on the type of tanning agent used. For example synthetic and aldehyde tannage will give soft leather while vegetable tannage will give firm leather upon drying [17].

1.2.18 Staking

On removal from the drying machine, in which the temperature and humidity are controlled, the skins are flat and generally quite firm. After an inspection and light trim, the skins are taken to the finishing department where they are initially softened. The softening process is carried out in one of three ways, all of which work on the same principle of flexing the leather around a blunt blade. The action of flexing separates the fibres from each other. This is shown in Figure 1.2.2.

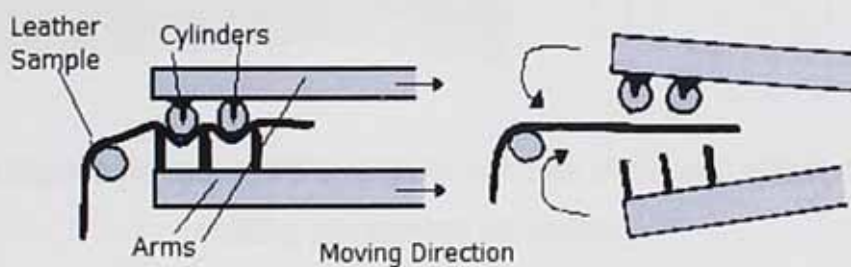


Fig 1.2.2 Staking operation to soften the leather ^[38]

The method used depends on the type of leather and also the end product being produced. The method mentioned above is called cylinder and arm type staking. This is now replaced by the vibration staking machine which instead of using the cylinders uses articulated staking pin system. This consists of an upper fixed twin bridge carries two cast tool plates, each usually with 10 to 12 rows of staking pins spanning the working width of the machine, and a lower cross member housing the vertically oscillating tool plates with 9 to 11 rows of pins meshing with the ones of the upper tool plate. The driven motor provides synchronized oscillating

motion at a fixed number of strokes. The stroke rate is dictated by the type and substance of the leather in conjunction with the degree of staking intensity required. The leather is carried into the machine and the upper and lower staking pins between a pair of stretchy lycra belts, feeding out at the rear of the machine. Alternatively the leather may be carried back to the operator at the feed-in position with a transfer conveyer running over the top of the machine. These pins while holding the leather produces both flexing and significantly stretch and enlarger the surface of a given leather. The schematic diagram of the pin is shown in Figure 1.1.3.

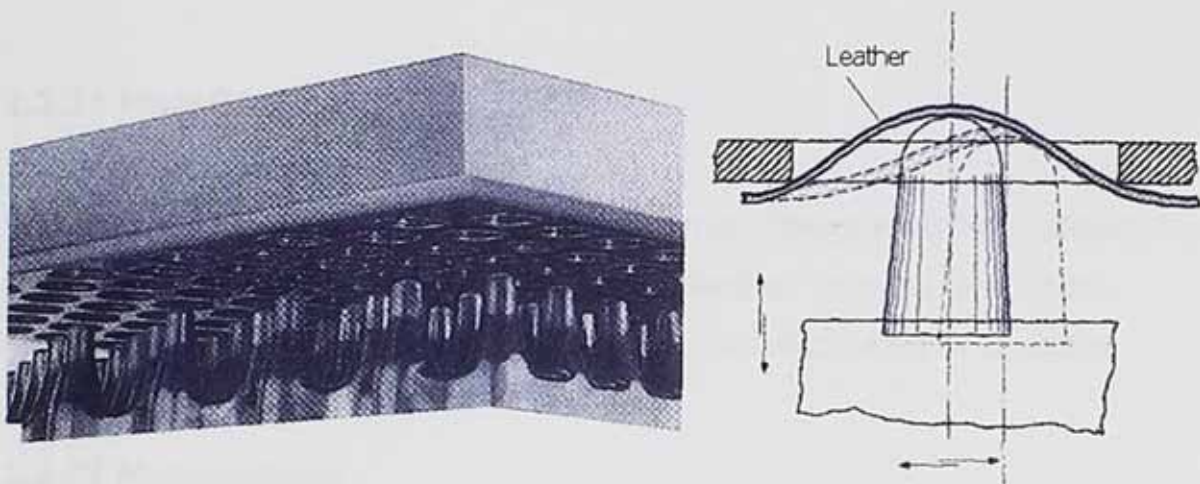


Fig 1.1.3 Upper hole tool plate and lower pin tool plate with effect of articulated staking pin system on leather ^[38]

1.2.19 Buffing and Brushing

The flesh surface is removed by mechanical abrasion to produce a suede effect or to reduce the thickness. In some cases the grain surface is buffed to produce a very fine nap, e.g. nubuck leathers. After buffing the leather is brushed to remove excess dust.

1.2.20 Finishing

Here various pigments, resins, binders, lacquers and dyes are applied by curtain-coater, pad, roller-coater and spray machines to give the leather its final colourful, scuff-resistant look and feel. Leather is often softened after finishing by milling in a milling drum for a few hours. If penetration of the finish is insufficient then hard leather will be produced, which results the formation of sharp edge creases on the surface of leather when folded grain inward. This property normally used for shoe upper is termed as coarse break. If penetration is sufficient then a microscopic creases or fine break will appear.

1.2.21 Final Grading

Leather is graded before dispatch to the customer. This grading may consider the colour intensity and uniformity, the feel of the leather, softness, and visual appearance, thickness, design effects and natural defects such as scratches.

1.2.22 Measurement

A considerable variety of machinery in this field has grown up over the years, ranging from mechanical (pinwheel system) to micro processing based measuring equipment (Image processing measurement). In pinwheel system leather is introduced via a feed table into the nip between transport roller and pinwheel, driving the pinwheels as it travels through the machine. The leather where it is present pushes the pins into the wheel, which ratchets the star wheel situated on the inside of the wheel by one tooth at a time. The pins are spaced at one inch horizontally as well as circumferentially around the wheel, which means that each pin can measure one square inch. It therefore takes 144 pins for the indicator to advance one square foot. The main purpose of the wheel is to sense the leather when it touches the circumferential surface of wheel. This is replaced by *photo*

electric cells and now the recent development has made the usage of *Camera* [39].

1.3 Leather as a Material for Shoes

A broad spectrum of materials and their combinations are used today in shoe manufacturing. Leathers, synthetics, rubber and textile materials are counted among the basic upper materials. Each material has its own specific character. They differ not only in their appearance but also in their physical qualities, their service life and different treatment needs. The material significantly influences the life of the footwear and in many cases dictates its use. PVC, PU, rubber, leatherette, polymers are materials which have a similar look as leather but their characteristics do not measure up to the qualities of natural leather as far as breathing, absorption, flexibility is concerned.

Leather is the most used natural material with ideal characteristics for footwear. Leather breathes, is soft, with very good absorption ability and is able to adjust to the individual shape of foot [40]. Leather, by virtue of its unique properties, has been used for shoe making for the following reasons.

1.3.1 Availability

Leather is the by product of meat industry. As long as meat is eaten, hides and skins will be available to produce leather.

1.3.2 Elasticity and Plasticity

It is an important requirement of the shoe that it should retain its original shape when it is not worn. This shape can only be maintained if the material to be used has plastic properties to some extent. Together with this it should be elastic as well to provide support comfort ease while walking and to allow it to regain its shape after deformation. The properties of elasticity and plasticity are important not only for shoe upper materials but also for soles and insoles. These are normally made from vegetable tanned leather.

1.3.3 Strength and Stretch

Materials used for shoe making should have enough strength that they should not reach the break point when stretched on a last or mould (*Section 1.4.3*). Leather can have both a very high tensile strength and adequate elongation to break depending upon the type of hide or skin it comes from, the method of tanning, finishing, its thickness (substance) and how it was dried.

1.3.4 Flexibility

Flexibility is an important property along with plasticity and elasticity. It means the ease with which the material may be bent. The bending behaviour of leather has been specifically associated with the term fullness. In practice leather is produced in many different thickness (substance) depending on the intended application. The forces required to bend leather are markedly dependent on its thickness. It is also observed that staking has a marked influence on the forces required to bend the leather with the un-staked leather requiring up to seven times as much force to produce a given amount of bending [41]. Leather can be produced in forms, which range from highly flexible to stiff. These properties of leather are achieved through different tanning processes and the selection of raw material e.g. kidskins are used for delicate shoe upper while heavy cattle hides are used for army boots.

1.3.5 Permeability to Air and Water Vapour

The ability of shoe materials to allow the passage of air, water and water vapour is one of the most important factors contributory to foot comfort. This is because the outer surface is subjected to varying conditions (cold, warm, rain, dry, wet grass and snow), whilst the inner surface is continuously in touch with a warm and perspiring part of human body (foot). Leather is permeable to both water and water vapour, the former being a particularly important property of vegetable

tanned insole leather, and the latter of chrome tanned upper leather. Insoles require to be water (and therefore perspiration) absorbent, on the other hand the sole and uppers should be waterproof or at least water resisting. Sole leather can be made waterproof (by waxes), upper leather can be made water repellent on its surface but at the same time permeable to air and water vapour.

1.3.6 Thermal Conductivity

Shoe materials should have a thermal conductivity such that during winter heat should not escape from the foot and during summer it should not easily flow into the shoe. Leather has a thermal conductivity value such that it is comfortable for both summer and winter.

1.3.7 Abrasion Resistance

Shoe materials should be resistant to abrasion. Rubber components have this ability more than leather and so have replaced leather soles to some extent.

1.3.8 Ease of Working

Shoe making involves the stretching of a flat material on a last or mould, which has a curved surface. It is necessary, therefore that the material should be capable of being easily cut and rejoined in different positions or attached to different materials (e.g. when a rubber sole is used), by threaded seam, via metallic attachment etc. Leather can be joined to itself or with other materials by any of these methods.

1.3.9 Maintenance

A shoe material should ideally have the property of being able to be repaired after deterioration due to wear and tear. Leather, unfortunately perhaps from some

aspects, lends itself to repair better than most other shoe materials due to its fibrous structure.

The following table lists the various types of shoe materials and their characteristics. The table is organized into three columns: Material, Characteristics, and Maintenance. The materials listed include leather, canvas, rubber, and synthetic materials. The characteristics describe the durability, flexibility, and breathability of each material. The maintenance section provides tips on how to care for each type of shoe to extend its lifespan.

Table 1: Characteristics and Maintenance of Various Shoe Materials

Material	Characteristics	Maintenance
Leather	Durable, flexible, and breathable.	Use leather conditioner, avoid water, and clean with a soft cloth.
Canvas	Lightweight and flexible.	Machine washable, avoid bleach, and air dry.
Rubber	Waterproof and durable.	Wipe clean with a damp cloth, avoid harsh chemicals.
Synthetic	Lightweight and flexible.	Machine washable, avoid bleach, and air dry.

1.4 Shoe Making

All the incoming deliveries of leather to the shoe manufacturer are examined for the quality, colour and any damage or flaws on its surface. Area measurements are also checked for any discrepancies. The area of purchased leather is reduced after taking into account the flaws and holes in the leather. Then the numbers of upper shoe sections, which can be cut from, the useable area are determined. Shoes are manufactured by joining these different upper sections cut from different parts of the skin. These sections are subject to different physical action depending upon the movement of feet. Therefore the quality and thickness requirement for each of the sections is different [42]. The most common shoe parts together with their quality and thickness requirements are given in table 1.4.1, while their shapes are shown in Figure 1.4.1

Table 1.4.1

Different sections of the shoe and their cutting location from skin/hide

PART/SECTION	REQUIREMENT	CLICK/CUT FROM
1. Vamps	High Thickness High Quality	Butt or Middle of Shank
2. Toe Caps	Low Thickness High Quality	Neck
3. Quarters	Low Thickness High Quality	Belly
4. Tongue	Low Thickness Low Quality	Belly or Shank
5. Back Strip	Low Thickness Low Quality	Neck, Shoulder or Belly

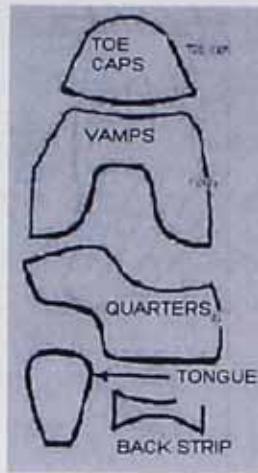


Figure 1.4.1 Common parts of the Shoe ^[42]

Although these pieces are selected from different parts of the hide, there should be no sudden change in quality when moving from one section of the shoe to the next and a pair of shoes must have the same quality i.e. both should wrinkle alike when they bend and develop the same "break" (*Section 1.1.20*) when they are worn [42]. The quality requirements for the various sections of the shoe are different, and it is impossible to write a definite specification for their properties until the type (e.g. dress shoe, work boot) and its style is defined.

However for any type of shoe manufacturing there are four main departments connected within a footwear company and the components follow a progressive route through each of these departments to produce the finished shoes. The departments are:

- Clicking
- Closing
- Lasting/ Making
- Finishing/ Shoe Room.

1.4.1 Clicking Department (or Cutting Department)

This is where operatives start to make the top part of the shoe (the upper). The clicking operative is issued with a number of skins of leather, mostly from cows, although leather can be made from almost all animal skins. By using metal press

knives he/she cuts out various shaped pieces (shown in Figure 1.4.1) that will eventually make up the upper. The size of each shape is normally clicked/cut larger than the required size for the shoe. This extra size for each shape is known as the lasting margin. This margin along the periphery of each shape is used to hold the each piece during the lasting operation and to interlock the different shapes to produce the shoe. Comparing with the associated labour cost in the cutting operation, the cost of upper material is relatively high. Therefore placing a number of specific shapes (See Figure 1.4.1) in order to minimise material waste is commonly encountered in the shoe making industry. This clicking operation is therefore a very skilled job.

The method of cutting the different sections of a shoe (listed in table 1.4.1) is normally followed by a systematic repetition of the arrangement. This is shown in Figure 1.4.2.

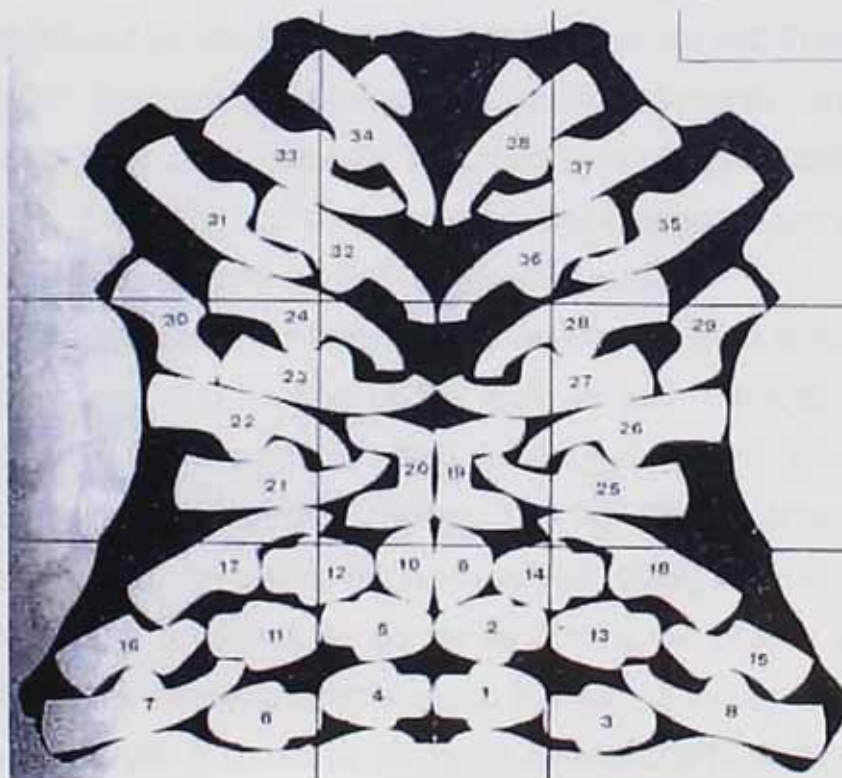


Figure 1.4.2 Typical location of cutting parts of a shoe from a hide/skin^[43]

In following this systematic repetition of an arrangement the cutter (clicker) must be fully aware of

- All types of common leather blemishes.
- Variability due to hide or skin location i.e. variation in the thickness of the leather [44]
- "Lines of Tightness" in the leather (see Figure 1.4.5 (a-d) later)
- Parts should be cut in a way that it should be less stretchy (tight) in the direction from toe to heel.

This systematic repetition of pattern cutting together with the human skills requirement is driven by the demand to find a layout of non-overlapping parts in a set area in order to maximise material utilisation. This in turn, places great emphasis on training and development of skilled operatives. It has also encouraged the development and application of computer aids both for assisting the training and the methods of cutting as these tend to place lower demand on operator skills and generally produce higher levels of out put. Therefore each year a seemingly ever-extending range of cutting systems are seen. Great achievements have been obtained in cutting system from Hand cutting, Swing arm presses, Manually operated travelling head presses, computer controlled travelling head presses and die-less (continuous) cutting.

A die-less system uses mechanical knives or high-pressure water jet instead of using pattern dies. The motion of the knife or path followed by the knife is controlled by the CAD (computer added design) system [44]. Usually CAD data is fed directly to the lay planning software. This lay planning is termed as nesting which is achieved by calculating the no-fit polygon (NFP) between any two shapes (*Appendix A*) [45]. It defines the border for placing two shapes so that they just touch with out the shapes overlapping and rotation. In Figure 1.4.3 the maximum utilisation of the hide is shown by fitting the different parts of the shoe upper with out considering the principle of lines of tightness as been shown in Figure 1.4.2.

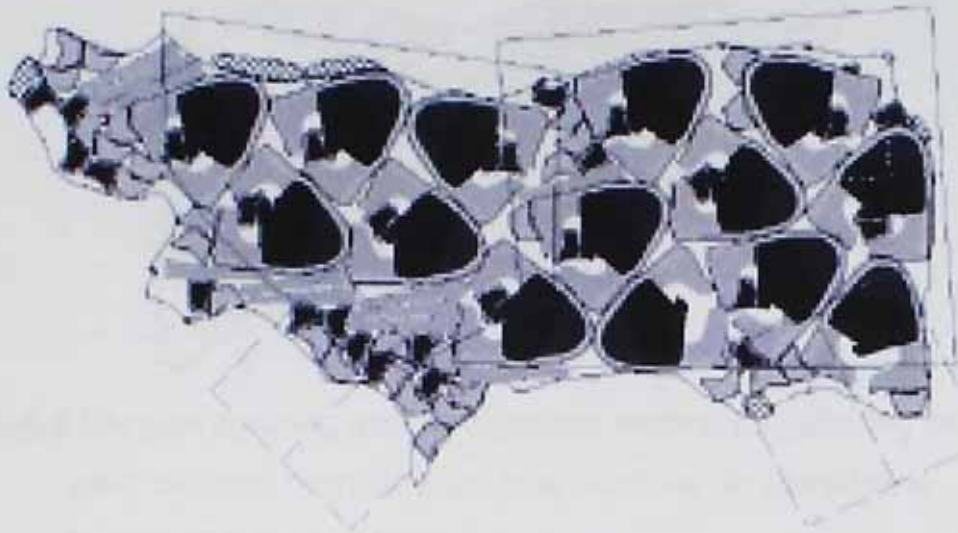


Figure 1.4.3 Nested result of shoe upper^[44]

The integration between Vision and CAD database has recently received an enormous amount of attention in vision research. Together with the introduction of angle dependent no-fit polygon method [46] some leather cutting systems incorporate an overhead camera for detecting the shapes of hides and flawed areas, previously marked by operatives, followed by automatic lay planning (nesting). Figure 1.4.4 [33], shows an example of a computer generated lay plan for a bovine leather half hide that takes into account the varying tightness and stretch characteristics around the hide the varying quality of the leather from area to area (including flaws) and the quality and directional requirements of the parts to be cut [44]. This tightness characteristic of leather is known as "*Lines of tightness*" by the shoe manufacturers and is explained in section 1.4.1.1

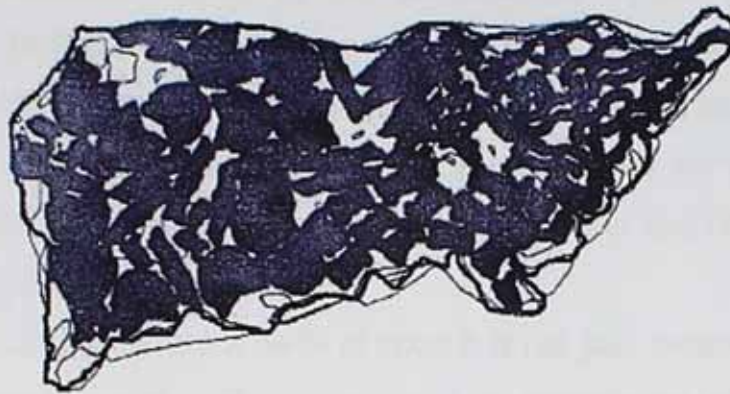


Figure 1.4.4 Lay plan by using genetic algorithm method for selecting different parts of shoes from different hide locations by considering hypothetical lines of tightness

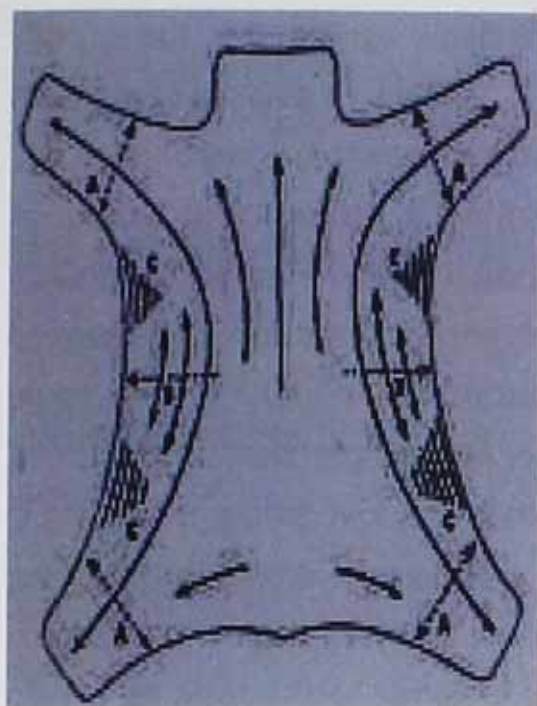
1.4.1.1 Lines of Tightness

The three-dimensional weave of collagen fibres in leather is not random (*Section 1.1.2*). Firstly the fibres tend to predominately lie at a certain angle (angle of weave) to the skin surface. Secondly, and of most importance to the shoemaker, fibres tend to run in preferred directions in respect of the animal's backbone [30]. The consequence is that leather stiffness varies with position and location [21]. Along these runs of preferred fibre orientation leather's strength is normally high and it has high modulus of elasticity [48], and its extensibility is less as majority of the bundles being aligned in this direction [44]. This stiffness variation is termed by the shoe maker as "Lines of Tightness in Leather".

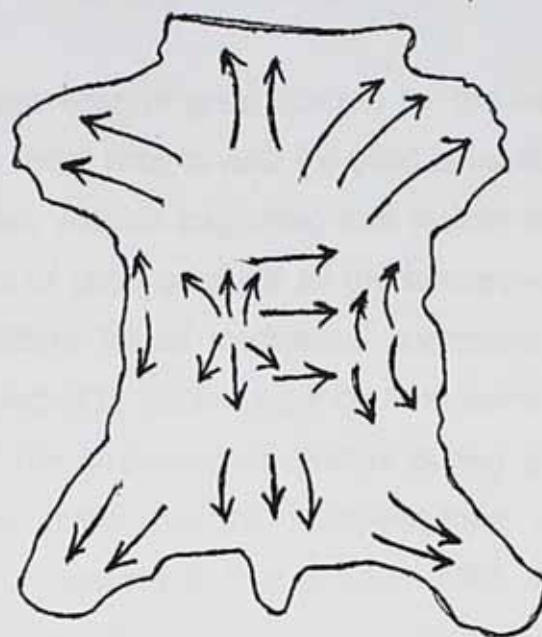
The configuration of the fibre bundles in the different layers also varies according to location in any individual skin. This variation in compactness of fibre bundles and their directional run along the skin plays an important role in determining the direction of lines of tightness. This directional run of fibres profoundly influences the physical properties of leather. Generally, the skin on the animal's back and butt will be most compact, with the corium fibres interweaving at about 45° to the surface. This area tends, therefore, to be the firmest and tightest or least stretchy and it has a fine break due to the compactness of the fibres. These properties

change in the shoulder region as the compactness of the fibres decreases (*Section 1.1.2*). In the belly and neck areas, the fibres have low angle of weave giving a much looser structure (few numbers of fibres aligned per unit area) and a coarser break. This variation in quality is the reason why vamps are cut from the butt areas and quarters and tongues from the shoulder and belly regions. This has also been illustrated in table 1.4.1.

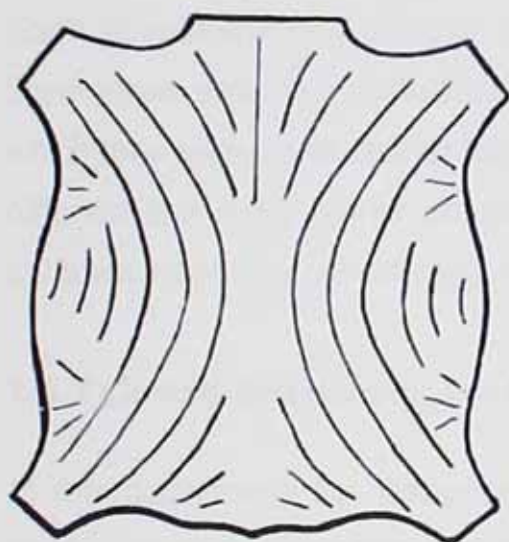
Therefore while cutting different parts of shoe it is not just general tightness that must be considered by cutter. They must have an appreciation of the direction of lines of tightness in the skin. The general rule for shoe upper is 'tight-to-toe' the toe-heel direction should be least stretchy [40]. So, by keeping this rule, cutters place the different shoe parts along the expected lines of tightness to get maximum quality and minimum waste of the material. However lines of tightness undoubtedly exist in leather there tends to be a disagreement about their location and intensity (i.e. degree of anisotropy). This is evidenced in Figure 1.4.5 which shows four diagrams (a, b, c, and d) from different sources illustrating the different suggestions about lines of tightness.



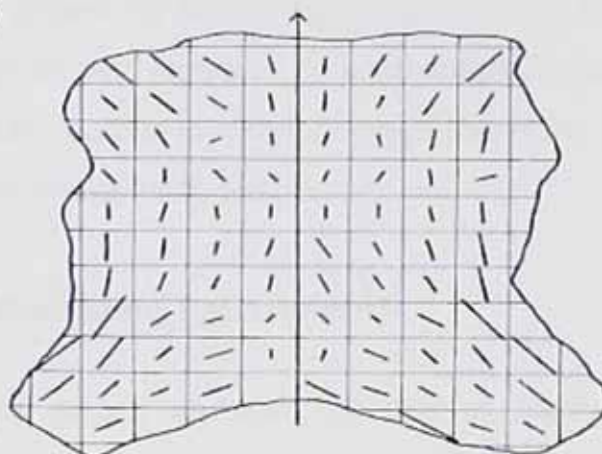
(a)



(b)



(c)



(d)

FIG 1.4.5 (a)-(d) (Diagrams showing lines of tightness) [17, 40, 42, 49]

1.4.1.2 Effects of Mechanical Processes on Lines of Tightness

As stated earlier (*Section 1.2.17, 1.2.18*) there are some mechanical processes which are applied during leather manufacturing. The pattern of lines of tightness

is very much influenced by these processes such as sammying, setting, staking, slicking out and drying, which impart a varying stretching action over the hide/skin to increase its area.

The determination of lines of tightness has been of great concern for the leather scientist since knowledge of the form of these lines is valid for good utilisation of leather and getting the best quality shoes. Maeser suggested that leather would be much easier to cut into uniform parts of good quality if all the tanners would agree on and follow a standardised pattern for all mechanical operations and particularly in stretching the skin for drying [43]. Recent work by Attenburrow on large leather pieces has revealed that the stretching of leather during drying process leads to the orientation of fibres in the direction of applied load, which consequently results in a high modulus of elasticity in that direction [48]. In the case of an un-stretched sample a greater tensile modulus was observed at lower test angles with respect to the back bone which is consistent with the finding that fibres lie predominantly along or at low angles to the backbone line.

Shoemakers assume a postulation pattern for lines of tightness (Figure 1.4.5 a-d), which they apply to all leather they receive. However because animal hides are all different and every tanner produces leather in different ways therefore lines of tightness must vary considerably from leather to leather.

1.4.2 Closing Department (or Machining Department)

In this department the component pieces are sewn together by highly skilled machinists to produce the completed upper. In the early stages the pieces are sewn together on what are called flat machines. In the latter stages the upper becomes three-dimensional and the machine used is called a post machine. This is where the sewing surface of the machine is elevated on a post to enable the operative to sew the three dimensional upper. They also complete various edge treatments to the leather to produce a more attractive look to the finished upper. Also, at this stage the eyelets are inserted to accommodate the laces in the finished shoes.

1.4.3 Lasting & Making Department

This transforms the flat leather in the closed upper into the three-dimensional shape of the shoe. It is perhaps the most fundamental of the shoe making operations. The shape is produced by stretching the upper over the shoe mould, called the last, and securing it to the underside of the insole. The most widely used operation of the lasting process consists of pulling over, wiping and attaching [50]. In pulling over the last the edge of the upper (lasting margin) is pulled down over the last by sets of pincers. The pincers are usually operated pneumatically or hydraulically and each one may be pre-set to apply a fixed force or to pull a fixed distance. The lasting operation attempts to ensure that the upper conforms to the shape of the last. This can occur due to the plastic behaviour of leather [24]. This plastic response may be reversed somewhat if the last is removed too soon after lasting. However, if leather is left in a stretched condition for sufficient time on a last, this will induce "set" [30]. During a controlled strain lasting operation, the difference between the stresses in different parts of the shoe upper are pronounced [51]. The highest value of stress is near the pincers where the leather will not be in contact with the last surface, until the lasting process is finished [52]. These stresses reduce over time due to the stress relaxation behaviour of the leather. The lasted uppers are passed through tunnels in which hot, moist air is blown on to the leather - a process which accelerates the stress relaxation [51].

However, it is important to use the correct temperature and humidity for the type of leather being set. This is a very critical operation from the standpoint of the thermal stability of the leather; however, a heat temperature of 120-130 °C may be used [51]. There is a common problem of grain cracking when lasting the shoe upper, as the strength of the grain layer of leather is lower than the underlying corium layer [53]. This can be alleviated by increasing moisture content, which increases the flexibility and crack resistance of the grain layer.

1.4.4 Finishing/Shoe Room

At this stage it depends on which materials have been used for the welt and sole to determine how it will be finished, i.e. leather or synthetic polymer. In the case of leather the sole edge and heel are trimmed and buffed to give them a smooth finish. They are then stained, polished and waxed to give them an attractive finish and to ensure the edge is waterproof. The bottom of the sole is often lightly buffed, stained and polished and various types of patterns are marked on the surface to give it a craft finished look. The "finished shoe" is ready to place the company brand name or manufacture's details.

CHAPTER 2

2 Fundamentals of Imaging System

The first part of the imaging system is the camera. The camera is responsible for capturing the light from the scene and converting it into an electrical signal. The camera consists of a lens, a shutter, and a sensor. The lens focuses the light onto the sensor, which converts the light into an electrical signal. The shutter controls the amount of light that reaches the sensor.

2.1 Introduction

The camera is the first part of the imaging system. It is responsible for capturing the light from the scene and converting it into an electrical signal. The camera consists of a lens, a shutter, and a sensor. The lens focuses the light onto the sensor, which converts the light into an electrical signal. The shutter controls the amount of light that reaches the sensor.

CHAPTER 2

The camera is the first part of the imaging system. It is responsible for capturing the light from the scene and converting it into an electrical signal.

- 1. Light enters the camera through the lens.
- 2. The lens focuses the light onto the sensor.
- 3. The sensor converts the light into an electrical signal.

The camera is the first part of the imaging system. It is responsible for capturing the light from the scene and converting it into an electrical signal. The camera consists of a lens, a shutter, and a sensor. The lens focuses the light onto the sensor, which converts the light into an electrical signal. The shutter controls the amount of light that reaches the sensor.

The camera is the first part of the imaging system. It is responsible for capturing the light from the scene and converting it into an electrical signal. The camera consists of a lens, a shutter, and a sensor. The lens focuses the light onto the sensor, which converts the light into an electrical signal. The shutter controls the amount of light that reaches the sensor.

The camera is the first part of the imaging system. It is responsible for capturing the light from the scene and converting it into an electrical signal. The camera consists of a lens, a shutter, and a sensor. The lens focuses the light onto the sensor, which converts the light into an electrical signal. The shutter controls the amount of light that reaches the sensor.

2 Fundamentals of Imaging System

In this work an imaging system is used to remotely measure strains imposed on leather samples. This chapter will describe the fundamentals of the imaging system, the representation of the images in the computer and the extraction of measurement information from the stored images.

2.1 Electronic Video Cameras

Video cameras convey images projected onto a sensor via a lens, to a machine capable of interpreting the information for storage, analysis and/or display. This can take the form of a simple monitor to display the image, a recording system such as tape to store the image, or a computer system, which can display, store and process the image.

The formation of image involves some physical processes

- Light reflected from a source (object)
- Incidence of light on the sensor
- Conversion of sensor output to electrical signals

Reflected light from an object is focussed onto a sensor via a lens. The sensor consists of an array of solid state elements called CCD's (Charged Couple Devices). The devices are activated for some short period of time, when each element records the intensity or brightness of the light that falls on it by accumulating a charge; the more light, the higher the charge [54]. The charge is subsequently converted to a varying voltage in order to interface with other devices. The array will therefore produce a 2-dimensional pattern, corresponding to the varying light intensity. This pattern can be represented as a function-image function $I = s[(x, y)]$

The most commonly used type of cameras are *analogue* and *digital cameras*. These are capable of producing both imaginary and moving images (continuous).

2.2 Digitisation

The camera can produce both stationary and moving images but for the processing, a stationary image is used. It is usual for video cameras that are capable of producing moving images to output the two-dimensional pattern sequentially, each line (row) of the array at a time. The output of such camera is filtered so that the sequential readout of adjacent pixels in a row forms a continually varying (analogue) signal [55]. To enable the computer to read these analogue signals it is necessary to convert it into digital form. This process of digitisation involves a sampling and quantisation phase.

2.2.1 Sampling

Sampling is done by measuring the signals at fixed time intervals as shown in Figure 2.1 and recording the value (to be subsequently quantised, see below).

The rate at which this happens is called the sample rate. Each sample corresponds to a small (most often square) area of the image known as a picture element (*pixel*). The level of the voltage represents the pixel intensity. Each line (row) of the original image is treated in this way so the result can be visualised as a two-dimensional array of pixel values.

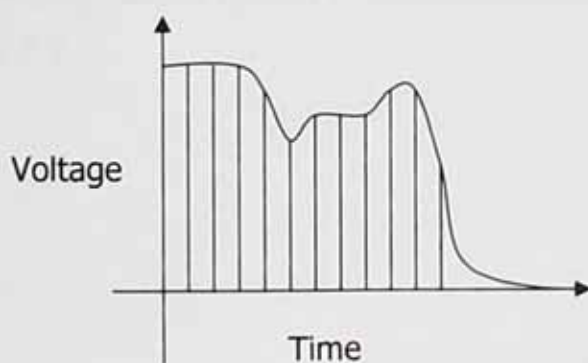


Fig 2.1 Light intensity converted to discrete data after sampling

2.2.2 Quantisation

Although the sensor output has been converted into sample points, the absolute voltage values at each point have to be represented by some numerical value in a computer.

Quantisation is the process of replacing the continuous values of the sampled image with a discrete set of quantisation levels. The number of quantisation levels employed governs the accuracy by which the image values are displayed. Conventionally L quantisation levels are defined by integers ranging from 0 to $L-1$, usually 0 corresponding to black, with intermediate levels representing various shades of grey.

All grey levels ranging from black to white colours are collectively referred to as *greyscale*. For convenience the number of quantisation levels is usually an integer power of two: $L=2^b$, so that the total " b " bits may be used to represent " L " different quantisation levels. The number of bits used to define a pixel value is called *bit depth*. The greater the bit depth the greater the number of quantisation levels and thus greater the number of tones that can be represented in the digital image [56]. An image represented by only 2 pixels with 0 representing black and 1 representing white is called a *binary image*.

Typically a bit depth of 8 bits is employed in digital imaging so that 256 possible grey levels ranging from 0 (black) to 255 (white) are used as pixel values. This is shown Figure 2.2

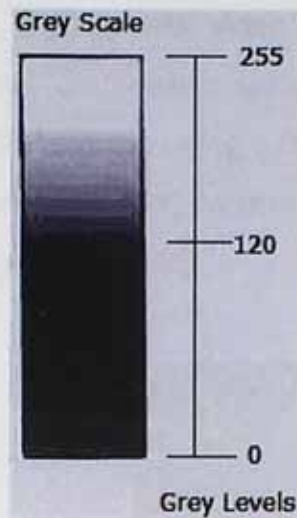


Fig 2.2 256 different grey levels constructed for 8 bit depth

This whole process of digital image formation is illustrated in Figure 2.3.

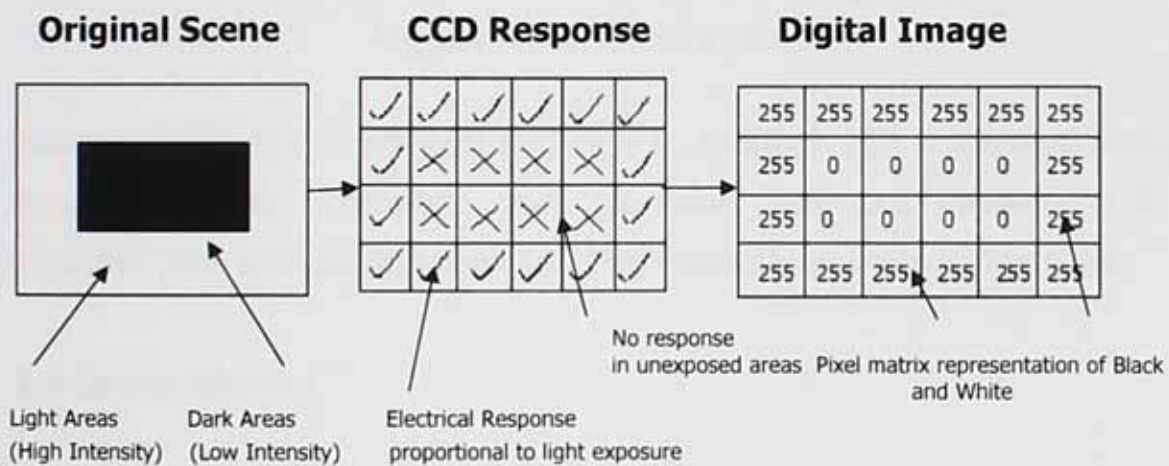


Fig 2.3 Digital Image formation

2.3 Analogue and Digital Cameras

The CCD sensor is an analogue device and the first generation CCD cameras were focused on backward compatibility being designed to have an analogue output. To read out these signals (varying light intensity) by computer for further processing and storing they should be converted into digital form. In modern cameras the output may be an analogue or digital depending on whether the

camera has an ADC (Analogue to Digital converter) and associated circuitry. In the case of an analogue camera, a composite video signal is an output, which is composed of synchronised signals and colour information [57]. These output signals are then converted to digital signals using a frame grabber. In the case of a digital camera the CCD together with ADC located inside the camera digitizes the output signals as shown in Figure 2.4 [58].

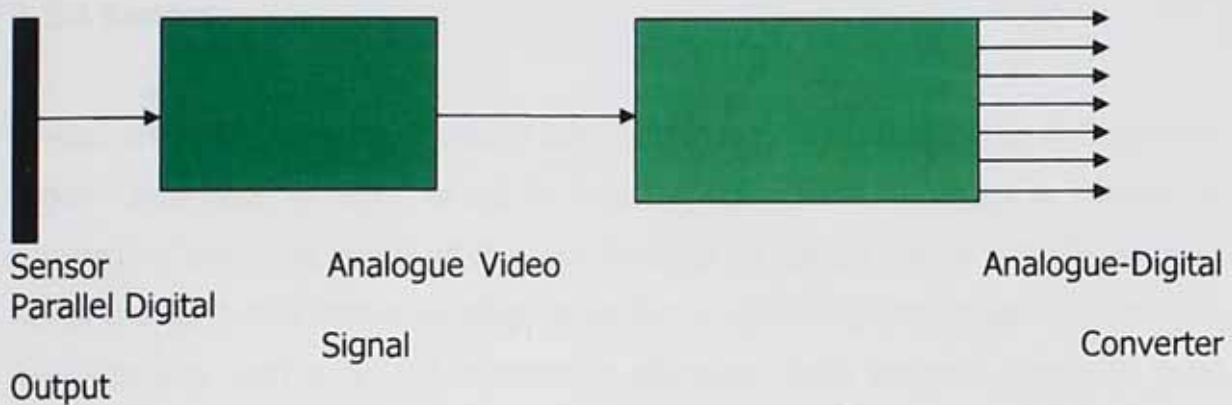


Fig 2.4 Digital Camera's function

Analogue cameras are low cost and easy to interface with a standard analogue acquisition device. Therefore, they can solve numerous applications at an attractive price and are commonly used for industrial and research purposes.

2.4 Image Storing

A digital image, as it is created by a digital camera and resides on digital storage medium like a hard drive, is simply an informational record of a grid of pixels - a map of specific tones at specific locations (BITMAP, TIFF, and PNG). It is common to refer the computer records as files, and thus digital images in this state, are commonly referred to as "digital image files," "image files," or even just "files."

When an image is displayed or output it takes on physical form as an image. Whether being displayed on a monitor or printed on paper, the physical image has spatial dimensions - width and height. The same digital image can assume many different physical sizes depending on the format used to store [59].

2.5 Camera Calibration

In order to use the imaging system to make measurements, the object has to be projected onto the digitised display (the screen), so the resolution of the imaging system has to be considered. The following parameters need to be considered while calibrating the camera to display an image on the computer screen.

2.5.1 Lenses

Lenses are made of glass or plastic and form images by refracting light. The most widely used type of lens, which is thick at the centre, is called a convex or converging lens. The centre of the lens is called its optical centre and the point at which the light rays converge after refraction is called its focal length. Lenses are manufactured with a limited number of standard focal lengths. Common focal length for lenses includes 6mm, 8mm, 12.5mm, 25mm and 50mm.

2.5.2 Field of View

When a scene is projected onto the camera sensor, some of the scene will fall on the sensor while the extremes of the scene will fall outside the sensor area. Clearly, the sensor cannot represent parts of the scene which do not fall on it. The field of view is that part of a scene which falls on the sensor and it can be adjusted (within limits) by changing the focal length of the lens or by changing the distance from the lens to the scene (working distance).

2.5.3 Basic Lens Calculations

Figure 2.5 shows the geometry of the situation. It shows (in one dimension) how the field of view is projected onto the whole height (or width) of the sensor, given a working distance "b" and a lens to sensor distance "a".

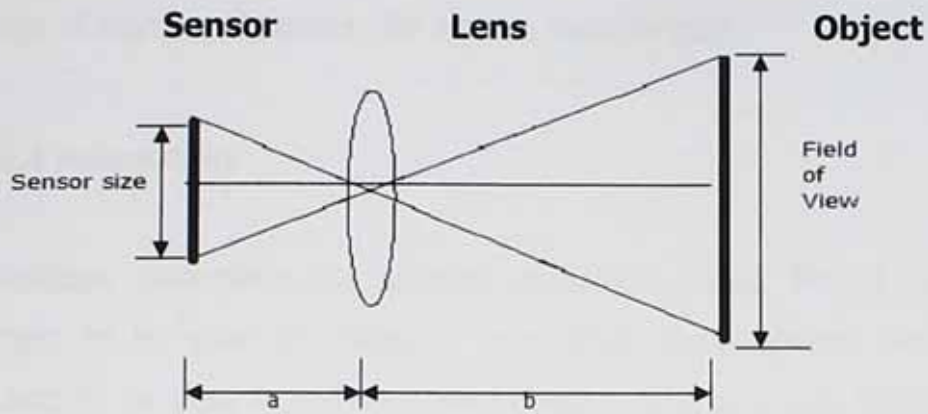


Fig 2.5 Image formation by using lens

The lens equation (Equation 2.1) relates the focal length "f" of a lens to the working distance "b" and the distance from the lens to the sensor "a". The focal length is the distance the sensor should be from the lens as the working distance approaches infinity (in practice when $b \gg f$).

$$\frac{1}{a} + \frac{1}{b} = \frac{1}{f} \quad \text{Equation (2.1)}$$

Generally the working distance is such that $b \gg f$ and therefore:

$$\frac{1}{a} \approx \frac{1}{f}$$

Inspection of Figure 2.5 then allows us to determine a simple relationship between the sensor size, the focal length, the working distance and the field of view. The light rays passing through the centre of the lens form two similar triangles. Therefore:

$$\frac{\text{focal length}}{\text{sensor size}} \approx \frac{\text{working distance}}{\text{field of view}} \quad \text{Equation (2.2)}$$

Provided that the lens can be focussed, the field of view can be matched with sensor size by varying the working distance (given a fixed focal length and sensor

size). The selection of the lens is dependant on its ability to focus over a suitable range of working distances (for a given focal length).

2.5.4 Resolution

Resolution determines the smallest resolvable detail. This is important for the system to be used to measure very small displacement, which requires the system to be able to differentiate between pixel and sub pixels (less than one pixel) i.e. if necessary the difference between, say, 1 mm and 1.1 mm for our measurements can be resolved.

The image sensor (or associated digitisation process) divides the image into an array of pixels. Each pixel represents a point on the image. If there are N_x pixels in the columns and N_y pixels in the rows of such an array, then the array can be considered as a 2-dimensional array of $N_x \times N_y$ pixels. The image is therefore divided into N_x points in the horizontal direction and N_y points in the vertical direction. The number of points N_x determines the horizontal resolution, while number of points N_y determines the vertical resolution. The greater the number of points, the more detail the sensor (or digitised image) can resolve.

Consider a pattern of lines shown in Figure 2.6, followed by spaces in a real image.



Figure 2.6 Pattern lines

In order to resolve this image the points must be close enough together to represent a line focused at one point and a space is focused at the adjacent point.

That is, twice as many points are needed (i.e. 22 points) as the number of lines (i.e. 11 lines) in our pattern.

Having made this decision the camera calibration is fixed. Each pixel spacing will correspond to half our chosen minimum distance and the field of view will be equal to the minimum resolvable distance multiplied by the number of points in our image divided by two. Figure 2.7 illustrated this in the vertical direction.

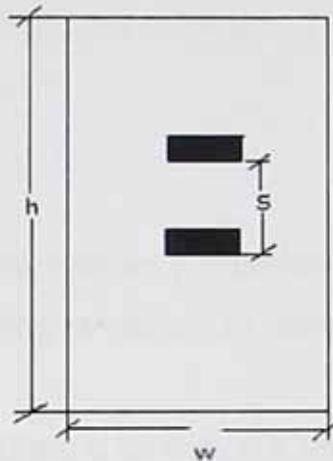


Fig 2.7 Relation between sensor size and resolution

$$h = [N_y \times s] / 2$$

Where h is the field of view in the vertical direction, N_y is the number of pixels in the vertical direction, and s is the spacing between the smallest detail. Similarly, for the horizontal direction:

$$w = [N_x \times s] / 2$$

2.5.5 Contrast

Resolution and contrast are closely related factors contributing to image quality. Contrast defines the differences in intensity values between the object under

inspection and the background. Better contrast can be achieved by proper lighting techniques. It does depend on the bit depth of the image (*Section 2.2.2*).

2.6 Processing the Acquired Data

The basic parameters for an imaging system required for making measurements by using image analysis techniques have been discussed. This section discusses the selection of the camera, lens, and software.

2.6.1 System Setup

A system has been set-up, which allows (i) controlled stretching of the leather (ii) acquisition of images during stretching of sample (iii) quantitative analysis of the images by computer.

The goal of this research project is to create a user-free system which could be used to determine the "Lines of Tightness" along the leather surface in a non-destructive way. There was a need to develop a system that could be employed as a computerized test and measurement system, which could be controlled from a computer desktop and could display test and measurement data collected by an external device on instrument-like panels on a computer screen.

A large variety of data collection instruments designed specifically for computerized control and operation have been developed and made commercially available in the field called Virtual Instrumentation (VI). It is defined as a combination of hardware and software with computer technologies to create a user defined system. It is possible with virtual instruments, to build measurement and automation systems that suit requirements exactly (user-defined) instead of being limited by traditional fixed-function instruments (vendor-defined).

It was decided to use this VI approach, which will support research on software development in order to achieve our ultimate aim of providing a strain map.

2.6.2 Software Selection and Development

A software package called "Lab VIEW" was obtained from National Instruments Inc. Lab VIEW is an integral part of virtual instrumentation because one of its best features is its front panel facility, which provides an easy-to-use application development environment. It offers features that make it easy to connect to a wide variety of hardware and other software.

2.6.2.1 Graphical Programming

Lab VIEW offers a graphical programming environment making it possible to design custom virtual instruments by creating a graphical user interface on the computer screen through which it is possible to operate the instrumentation program, control selected hardware, analyze acquired data and display results.

It is possible to customize front panels with knobs, buttons, dials, and graphs to emulate control panels of traditional instruments, create custom test panels, or visually represent the control and operation of processes. The similarity between standard flow charts and graphical programs shortens the learning curve associated with traditional, text-based languages.

The behaviour of the virtual instrument is determined by connecting icons together to create block diagrams, which are natural design notations. With graphical programming, systems can be developed more rapidly than with conventional programming languages, while retaining the power and flexibility needed to create a variety of applications.

2.6.2.2 Image Acquisition

National Instruments "IMAQ Vision builder" software is a tool for prototyping and testing image processing applications. It provides three types of image acquisitions: snap, grab and sequence. A *snap* acquires and displays a single image. A *grab* acquires and displays a continuous sequence of image which would

be useful when setting the camera, while the *sequence* function starts and stops a continuous acquisition of multiple images.

These images as acquired by vision builder will be digitized by a frame grabber in the case where an analogue camera is used (*Section 2.3*).

2.6.2.3 Software Development

The software development involved the production of a user-free system which could be easily used by a non-technical person to measure the strain distribution in leather with greater ease and efficiency. The software development starts by using *IMAQ Vision Builder*, which allows prototyping the application quickly without having to do any programming. To prototype the image processing application, an algorithm was build using the IMAQ Vision Builder scripting feature. The scripting feature records a series of image processing steps and the parameters that were specified for each of those steps [60]. This scripting feature records every step of the processing algorithm, e.g. open image, select edges, calibrate (convert pixel to real world co-ordinate), and calliper (measure distance between objects). After completing the algorithm for one image it can be used for other images. This feature allows batch processing. The most commonly used IMAQ Vision builder commands used for making measurements while writing scripts are discussed here.

2.6.2.3.1 IMAQ-BCG Look-up

Once an image has been captured and is ready for processing, the intention is to get a "better" image, which means a better distribution of the grey-level values. This process is termed as Image enhancing and is achieved by the BCG (Brightness, Contrast, and Gamma) function, which assigns a new value to each pixel. The default values for Brightness, Contrast and Gamma are 128, 45 and 1.0 respectively. This algorithm was used while enhancing the marked dots/lines on

the sample as compared with the background. In Figure 2.8, the default BCG function with an image and applied BCG function with a resulted image is shown.

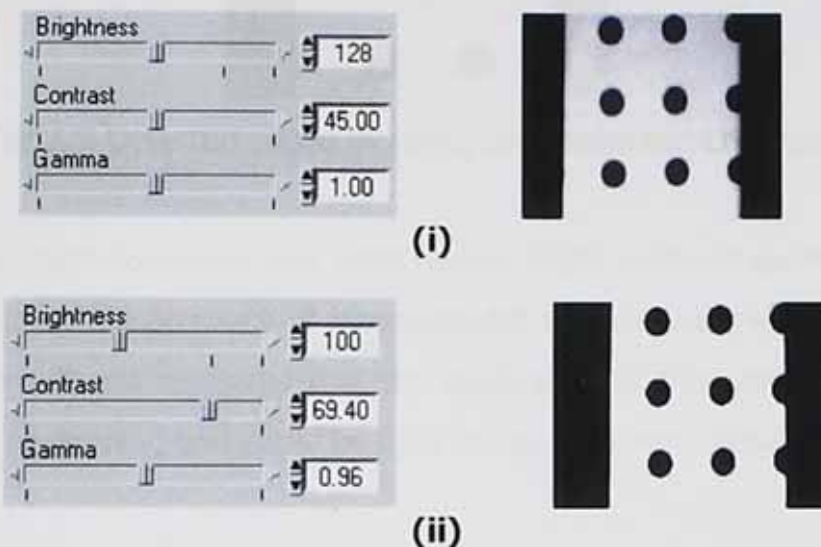


Fig 2.8 Default BCG function with resulted image (i) and applied BCG function with resulted image (ii)

2.6.2.3.2 IMAQ- Edge Detection

A digital image corresponds to a two-dimensional array of pixels (*Section 2.1*). The intensity of the pixels change across the whole image depending upon the reflected light from the object. The location of any point at which the intensity changes can be determined by using the "*edge detection*" command. It refers to the process of identifying and locating sharp discontinuities in an image. The discontinuities are abrupt changes in pixel intensity which characterize boundaries of objects in an image. The result of an edge detection operation is a set of points describing the locations of edges (x, y coordinate) identified in the image. It is used when measuring the separation between two lines before and after application of stroke on a sample.

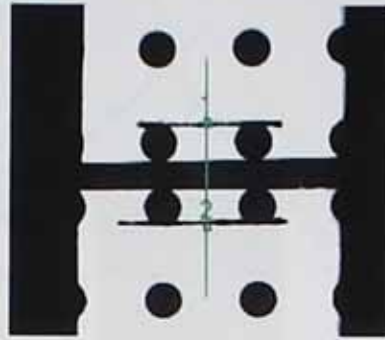


Fig 2.9 Detected edges by using edge detection command

The edge detection command was used for the initial series of experimental work while determining the accuracy of measurement system and measuring strain for a small region. It was observed that the application of this command for larger areas is time consuming and could be hard to use by a non-technical person.

2.6.2.3.3 IMAQ - Clamp

The separation between the marked lines can also be determined by using the clamp command. Its working principle is almost the same as that of edge detection command and is also used for grey-scaled images. This command is useful when any rotation of edges is expected within the region of interest. It measures the separation between two edges in a rectangular region by detecting points along the two edges then computing the distance between detected points (in pixels) and returns the largest or smallest distance. It can also produce results of detected edges in the form of a coordinate system.

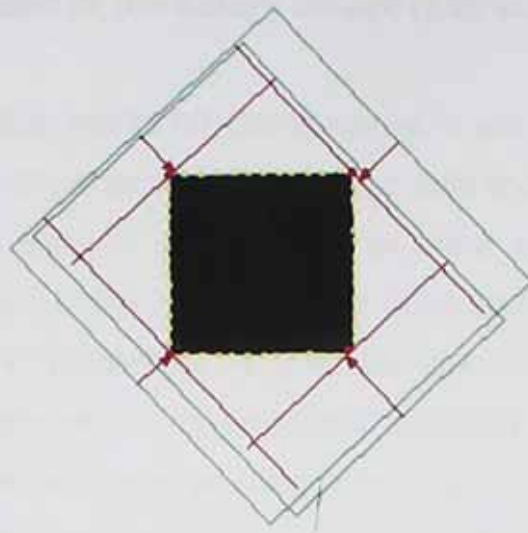


Fig 2.10 Detected edges by using clamp command

2.6.2.3.4 IMAQ - Thresholding

Clamp and edge detection commands are useful when working with small samples. The aim of this research project was to determine strain on larger pieces, therefore while working on large samples another technique was adopted by marking the sample with circular dots instead of drawing lines on it. The location of the dots (in terms of a coordinate system) is then determined after thresholding the whole image. Thresholding the grey-scale image will create a binary image, which separates the objects from the background. It specifies a region of values within which the pixel value is set to 1; all other values outside this region are set to 0. In the resulting image a pixel with a value of 1 are shown as red. In reality the image is binary, that is containing only pixel values 0 and 1. A threshold image is shown in Figure 2.9.



Fig 2.9 Image after applying threshold function

2.6.2.3.5 Improvement of the Binary Image (Extraction of Dots)

The thresholding function works on the image as a whole by processing pixels individually. Therefore together with the marked dots the resulting image would have some unwanted small or large marks. In order to extract the marks of interest only the *primary binary morphology* or *advanced binary morphology* was used. Advanced binary morphology is used for tasks such as removing small unwanted marks/regions, removing unwanted boundary regions blobs from an image, labelling blobs in an image, or filling holes in blobs.

The use of advanced binary morphology is shown in Figure 2.10, where marked circular dots were separated from boundary objects (unwanted region).

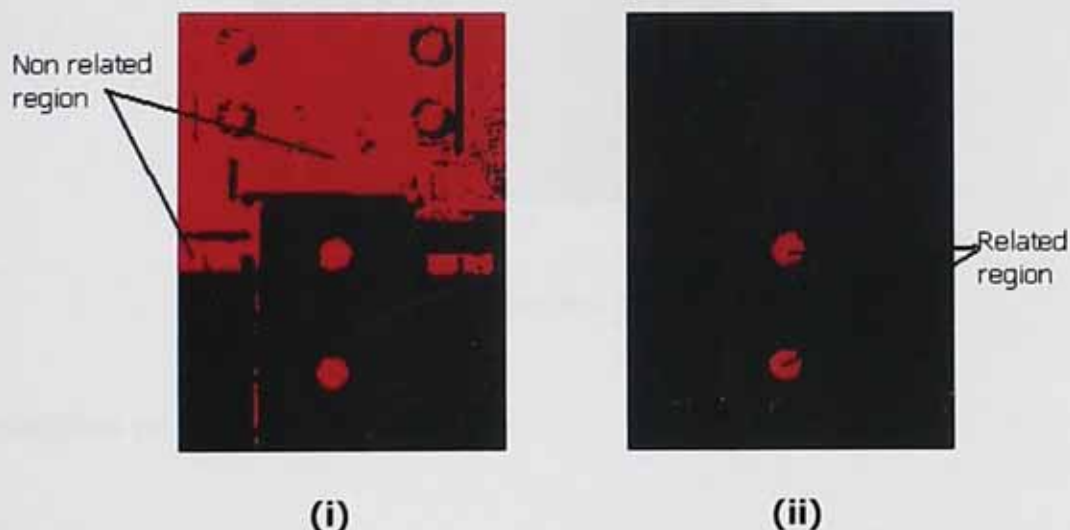


Fig 2.10 Resulting image before applying morphological function (i) and after applying advance morphological function (ii)

2.6.2.3.6 Calliper (Measuring Distance)

Once the coordinates of dots or edges are determined then the distance between them can be calculated by using the calliper command in terms of pixels or real world measurement (mm, cm) values.

2.7 Tensile Testing

The experimental work was carried out by using an uni-axial tensile machine supplied by Dartec Limited and biaxial tensile machine supplied by Deben limited. Both machines are available in the *material testing laboratory* at the British School of Leather Technology.

During the stretching the images were captured using digital camera. The system is shown in Figure 2.9.

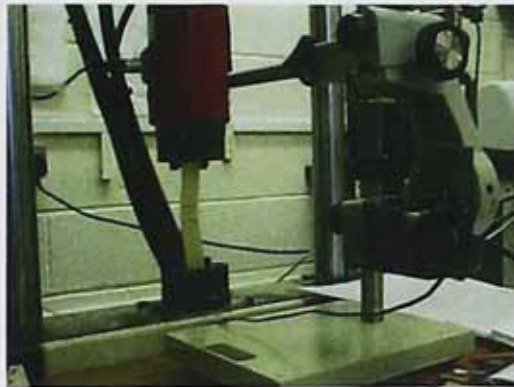


Figure 2.9 System set up

2.8 Selection of the Camera

One of the most fundamental questions in camera selection is what kind of signal is output. The main choice is between analogue or digital. It has been mentioned (*Section 2.5.3*) that two parameters out of four can be fixed while selecting the camera. By using an existing facility available in our laboratory two series of test will be performed.

In the first phase of the project a set of simple experiments will be carried out on an isotropic material (e.g. rubber) under uni-axial loading. The linear strain will be determined using a rectangular shaped piece (25 x 220mm) of the material. Therefore a camera needs to be selected whose sensor size should be sufficient

to give a field of view more than the sample size (25 x 220 mm), as it should be capable of capturing the whole sample even after it has been stretched.

In the second series, experiments will be performed on a biaxial machine, which can be used to stretch a sample having maximum dimensions of 250 x 250mm. Therefore a camera is needed which should be capable of extracting the image having a minimum Field Of View 250 x 250mm and maximum of about 300 x 300mm, as it is expected that up to 20% or more strain will be applied to the sample. The resolution can be determined by fixing the camera at any working distance.

Having discussed these parameters with the *National Instruments service engineer*, they suggested a CV A50 CCD camera (Specification Appendix B), with lenses having 12mm or 25mm focal length, which could be used for both machines.

3. Accuracy of Measurement

There is a limit to the accuracy of the measurement of any physical quantity. The accuracy of the measurement is defined as the closeness of the measured value to the true value.

3.1 Accuracy of Measurement

3.1.1 Accuracy

The accuracy of a measurement is the closeness of the measured value to the true value. It is a measure of the reliability of the measurement.

CHAPTER 3

3 Accuracy of Measurement

There is a need to determine the accuracy of measurements by using an image analysis technique before its application for the measurement of strain measurement in leather.

3.1 Accuracy of Image Processing Software

3.1.1 System Setup

It has been mentioned earlier (*section 2.8*) that a CVA50 CCD camera was used having sensor size of 6.4 x 4.8 mm (*Data Sheet-Appendix A*) with 12 mm lens for the first series of experimental work (uni-axial stretching). The minimum recommended working distance for this lens is 300mm. A sample size of 25 x 220 mm was used, as this would give us a gauge length of around 180 mm as shown in Figure 3.1.

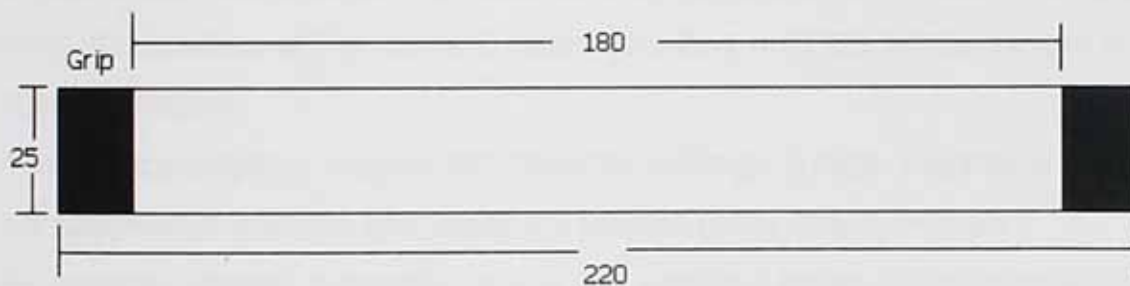


Fig 3.1 Sample dimensions used for uni-axial stretching

A strain of around 20% is applied to the sample, as the area of interest in measuring strain is the gauge length. Therefore, based on this gauge length, the working distance needs to be found for a field of view of 25 x 220 mm.

Using equation 2.2 (*Section 2.2.9*) with the following parameters, the approximate working distance is 412.5 mm.

$$\text{FOV} = 25 \times 220 \text{ mm}$$

$$\text{Sensor Size} = 6.4 \times 4.2 \text{ mm}$$

Focal Length = 12 mm

On the basis of these parameters, which will be used to measure the strain distribution, the accuracy of measurement will be determined.

3.1.2 Acquiring images

A PCI-1409 image acquisition board was used, which features a 10-bit analogue-to-digital converter (ADC) that converts video signals of CVA50 camera to digital formats. The NI-IMAQ 2.5 driver software configures through *measurement and automation explorer (MAX)* to acquire images and the IMAQ Vision Builder software processes images, both from *National Instruments*. IMAQ Vision Builder offers three types of image acquisitions:

- snap
- grab
- sequence.

A *snap* acquires and displays a single image.

A *grab* acquires and displays a continuous sequence, which is useful, for example when the position of the camera needs adjusting until the whole sample is in an imaging window.

A *sequence* acquires images according to settings (image acquisition rate) that are specified in advance and sends the images to the image browser.

An imaging window parameter allows the acquired image to be cropped so that irrelevant pixels are unnecessarily processed. Live images can also be acquired in IMAQ Vision Builder and transferred directly to the system memory.

With this integrated system a live view of the sample can be seen on the computer screen. If the whole sample cannot be reproduced on the screen the dimensions of imaging window needs to be changed. The dimensions of the imaging window should occupy the whole sample. These dimensions are integer values, which depict the number of pixels assigned to length and width of the whole image (field of view). Although the desired size of the imaging window was clear, the actual size of the imaging window was adjusted by trying different

width and height values until the whole field of view was obtained. This is necessary because the software seemed a little temperamental, such that adjusting the imaging window size has an affect on the acquisition stability. The dimensions of imaging window are allocated by *measurement and automation explorer*.

Once the whole sample is visible in the imaging window then an image can be snapped at any time and saved in multiple format e.g. TIFF, PNG, BMP etc for processing at any time.

3.1.3 Calibration Using a Grid

3.1.3.1 Placing Calibration Marks on the Sample

The process of calibrating a camera involves determining the intrinsic parameters, such as focal length, and extrinsic parameters, such as the position and orientation of the camera with respect to a coordinate frames. This process relies on the use of calibration patterns with known geometry.

The most commonly used calibration pattern is the grid pattern, consisting of black circular patterns with a white background to give strong features. The calibration process involves the extraction of pattern features (in pixels), and matching them or equating them with real world measurements (mm, cm). Once it has been achieved the intrinsic or extrinsic parameters of the camera cannot be changed, but the pattern can then be replaced by the sample. The accuracy of measurement by using image analysis software was evaluated by pasting the known pattern of grid on strips. These strips were then held by the upper and lower grips of tensile testing machine. The separation of the strips after application of each known value of stroke by tensile testing machine was measured by using the images. The grid is called the *calibration grid* and was supplied by *National Instruments*, having diameter of 4 mm and centre-to-centre distance of 1 cm. This is shown in Figure 3.2.

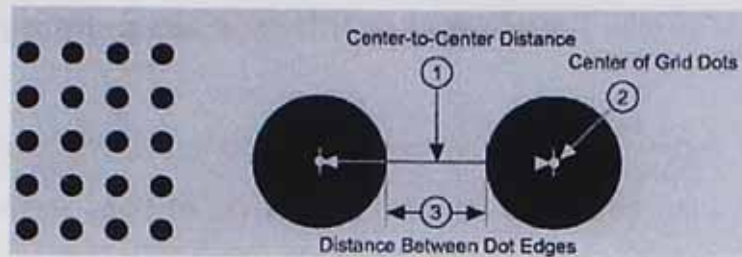


Fig 3.2 Grid used for calibration

National Instruments suggested that the diameter of the grid when measured by image analysis software should be 6 to 10 pixels [61]. Although the calculated working distance for a sample of 25 x 220 mm is approximately 415 mm, on placing the camera at a distance of 500 mm from sample, grids with diameter between 6 to 10 pixels were obtained. The same parameters as mentioned above (*Section 3.1.1*) were used to measure the separation of the strips. If the camera was positioned closer to the object, magnification can be increased by assigning more pixel values to the grid, but as the camera moves away (increase working distance) from the sample the assigned pixel values will be reduced. The test procedure was to hold these strips with jaws, drive the displacement rod (upper jaw) with a known value of stroke, and capture images at every applied stroke.

Another way of calibration is to mark some points of known dimensions (for example, two parallel lines with known gap) on the sample without affecting the actual parameter needed to be used for experimental work. The marked known distance can then be equated to the pixel values read by the software. A conversion factor could then be found. This conversion factor can then be used to make measurements on other areas of the sample. This method is time consuming and manual marking can lead to inaccurate data. Therefore, the technique of pasting the known grid pattern on the strips was adopted and the difference between them was measured during the image processing, after application of a measured stroke from the uni-axial tensile machine. Typical images used for calibration and for accuracy of measurement by using software are shown in *Appendix C*.

3.1.3.2 Programming the Acquisition Software

To measure the displacement between upper and lower strips tools from IMAQ Vision builder were used to create the analysis algorithm, which is called *script*. The script is normally written for the first set of images, and can then be used for other images to perform same analysis. It starts after a saved image is loaded and displayed on the screen. The script performs the following functions:

- a) It applies the function "IMAQ BCGLookup" (*Section 2.6.2.3.1*) to vary the amounts of brightness, contrast and gamma across the whole image. This is used to highlight details in the significant area, that is, it makes the grid marking stand out from the background. The image without applying BCG function and the resultant image after its application are shown in Figure 3.3.

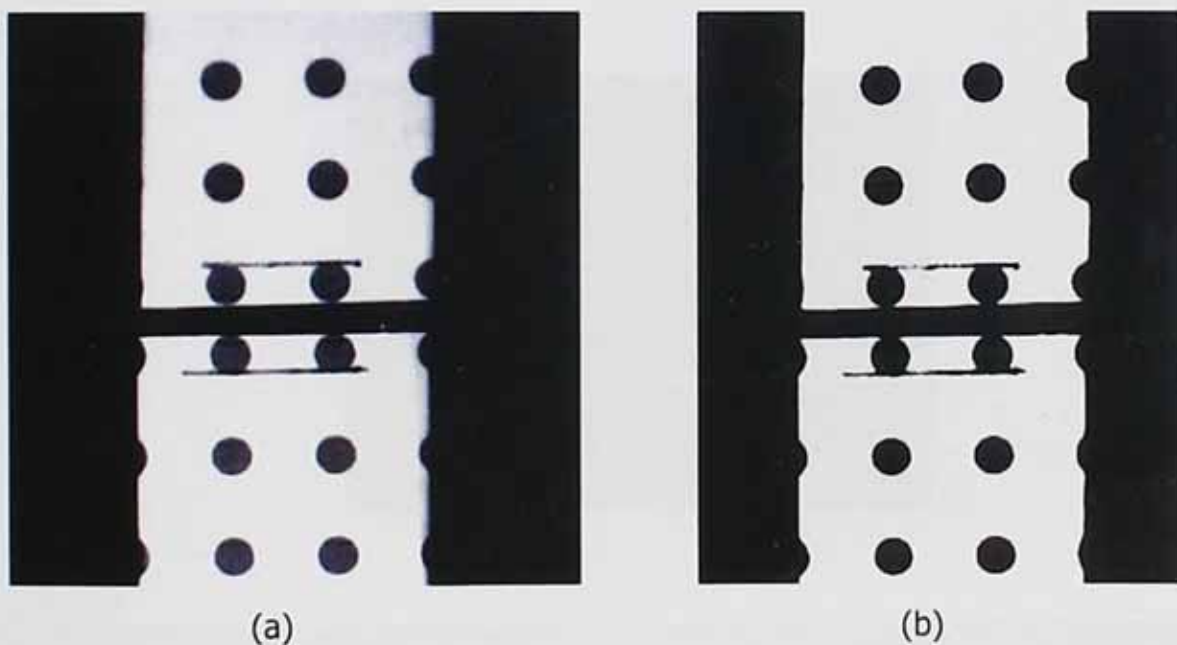


Fig 3.3(a, b) Effects of brightness, contrast and gamma function (a) Actual image (b) Image applying BCG function

- b) The grids can be isolated from the background by thresholding the whole image. This converts the image from greyscale to binary image. This

transformation allows *blob (binary large objects) analysis*, which aids the following automatic measurements.

- c) The script then eliminates the border objects so that only the circular grid marking of interest is left.
- d) The morphological operator "dilate" was then used to compensate for missing pixels and enhance the circular shape of the grid markings.
- e) Blob analysis was used to find the position and centres of the grid markings.
- f) Finally, a calliper (*Section 2.6.2.3.6*) function was applied to measure the distance between the blobs (grid markings) in pixels. The distances were transformed to millimetres by using the calibration command. The transformation was carried out by equating the known distance values between two dots (10 mm in our case) with the pixel values as calculated by the software.

The actual results of processed image after application of these steps are shown in Figure 3.4.



696x574 1/2

Results	1	2	3	4	5	6	7	8
Center X	395	303	397	306	403	311	404	313
Center Y	39	41	130	132	451	453	542	543
Radius	19	18	18	18	17	17	17	17

Fig 3.4 Image resulting after applying the script. The location of each dot is given by its coordinate values. The blobs are numbered from 1 to 8 starting from top right. Note that blob radius does not differ by more than 2 pixels

The calliper command was used to first measure the distance in pixels between dots 2, 4 (or any pair of dots on strip). This was then equated to actual distance between them i.e. 10 mm. Thus, the software measured transformed value (in millimetres) was used to measure the actual displacement (in mm) of the bottom lowest and top most dots on upper and lower strips respectively as shown in Figure 3.4, dots 4 and 6 or 3 and 5. Further to this, in order to avoid any distortion, the camera was placed in such a way that its centre coincided with the centre of the grid. After application of the complete stroke a change in the recorded diameter of the blobs at the extreme ends could have occurred due to a change in perspective which could lead to an error in determining their centres. Therefore in order to demonstrate that such an error was not occurring, it was confirmed that all blobs appearing on the imaging window had the same size. It can be seen that in Figure 3.4 the radius of each blob has an acceptable difference of only 1 to 2 pixels.

3.1.4 Measurement by Image Analysis Software

Our setup (using the CVA50 camera) consisted of following parameters.

- Lens 12 mm
- Working distance 500 mm
- Field of view (FOV) 288 x 570 pixels

By using this setup 15 images were captured after the application of every 5 mm stroke by the tensile testing machine. This separation between the strips was measured by using image analysis software. An approximately linear relation is obtained with a correlation factor of 0.99 and a residual of ± 0.01 mm as shown in Figures 3.5 and 3.6 respectively.

Image/Applied Stroke relation

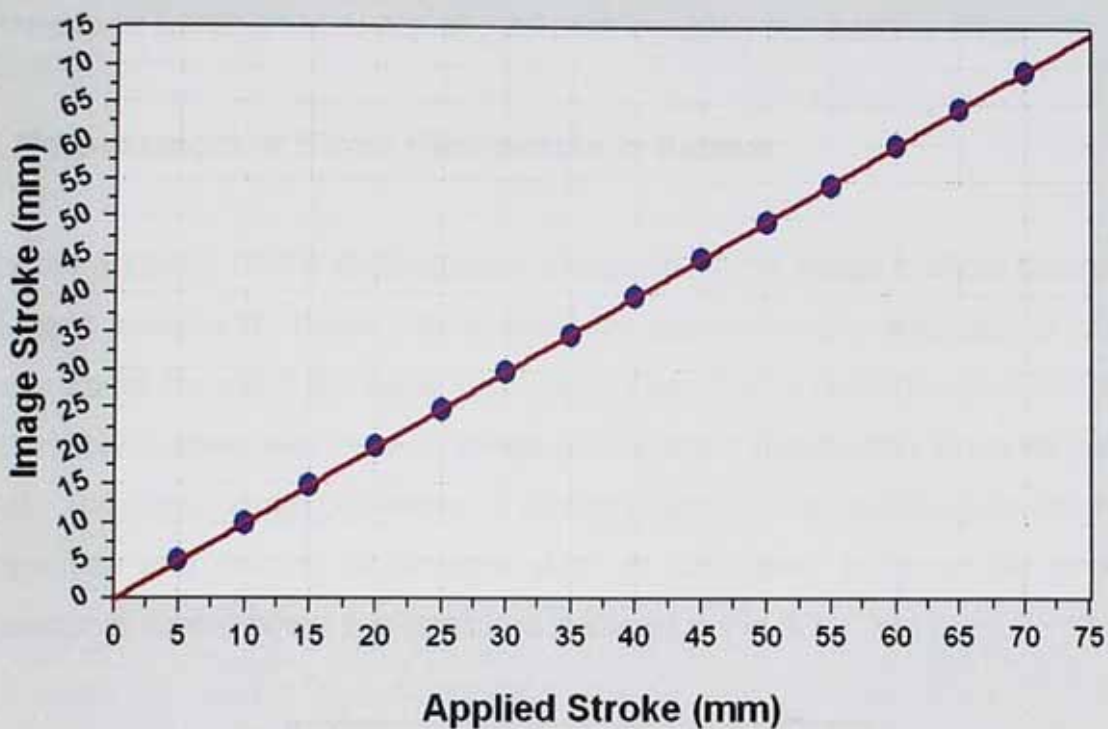


Fig 3.5 Relation between applied and image stroke measurement

Residuals

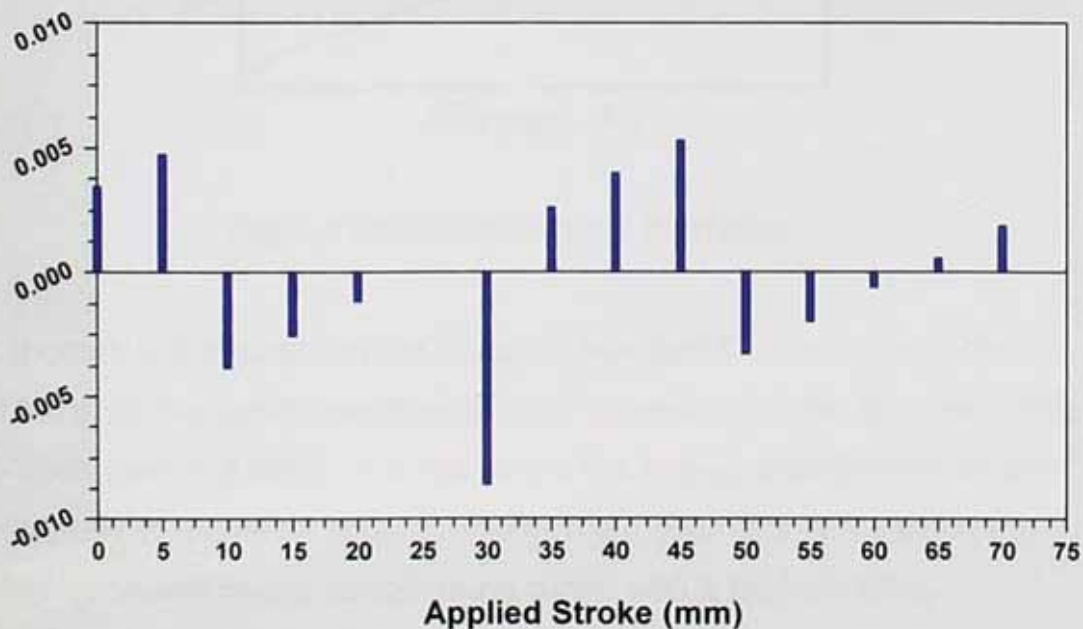


Fig 3.6 Residual measurement for image and applied stroke relation

The actual data and some images used for Figure 3.5 and 3.6 are shown in *Appendix C*. It can be concluded from the above graph that a stroke of 5 mm can be measured within an accuracy of $\pm 0.01\text{mm}$ by using our existing setup.

3.2 Measurement of Strain Distribution in Rubber

Once the accuracy of the displacement measured by the image analysis technique had been measured, there was a need to determine the accuracy of strain measurement by using the same technique. Therefore a homogeneous material, for example rubber, was used to measure the strain distribution along its gauge length. The stress strain behaviour of rubber is sensitive to variations in chemical composition and process parameters such as cure time. However the general behaviour of rubber when it is stretched is shown in Fig 3.7

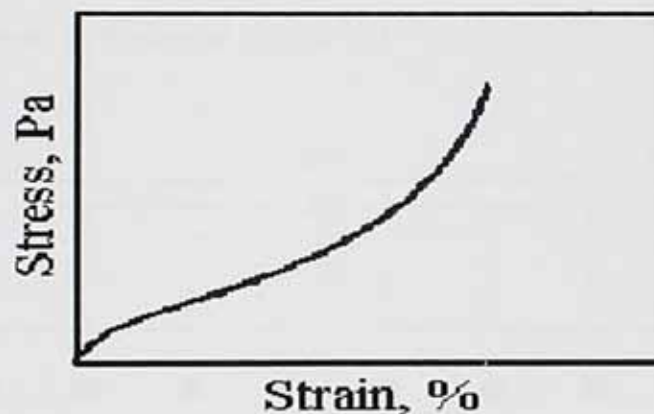


Fig 3.7 Stress-Strain curve for rubber

At first (bottom left of diagram) the rubber is reluctant to stretch under the applied force, so the curve rises steeply (large increase in stress to cause a little strain). Then there is a range of stress where the rubber extends more or less proportionately to the effort applied. Finally, the rubber gets very resistant to stretching, as shown by the steeply rising curve, until it finally breaks.

3.2.1 Experimental Set-up

In order to maintain consistency the calibration grid pattern was replaced with the actual sample while keeping the other parameters the same. To overcome the non-uniformity of light distribution and/or the surface material grain variation, a common approach used in machine vision inspection is to analyse a limited number of pixels within a defined neighbourhood. The methodology of thresholding the whole image was adopted after marking circular spots on the sample. The imperfect thresholding especially around the edge of circular spots may result in some error of locating the geometric centroids of the circular spots. Therefore the size of spots needs to be kept small to avoid the chances of error in locating its centroids [62]. In this experimental work, a rubber sample (220 x 25 mm) marked with equidistant dots of 4 mm diameter along its gauge length was used to detect the degree of strain distribution in the uni-axially stretched direction. The sample is shown in Figure 3.8.

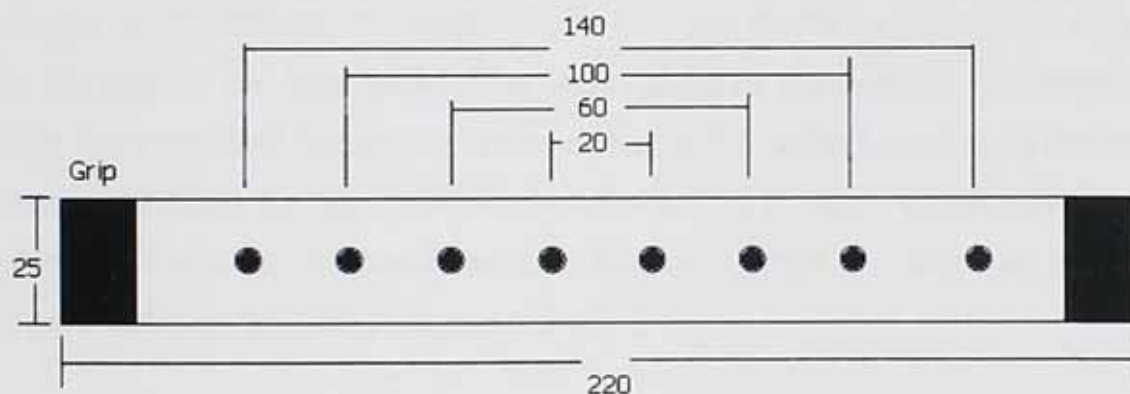


Fig 3.8 Rubber sample marked with spots along its gauge length used for uni-axial stretching. All dimensions are in mm

The sample is gripped at its ends on tensile testing machine and the CCD camera was positioned such that the whole sample can be viewed in the imaging window. In order to avoid perspective error, the camera was positioned with the sample

plane perpendicular to the camera axis and the centre of the camera matched with the centre of the sample.

As the camera was stationary during the test in the current equipment configuration, strains can be measured by the relative movement of the dots with reference to an image of un-deformed sample. To obtain the series of images at different strokes the sample was then uni-axially stretched with a load cell speed of 10 mm/sec. Both tensile testing and image analysis software were run in parallel on one computer. During this extension, the sample images were captured (by using the snap command of the software) after the application of each 5 mm of stroke.

Although the time difference between the application of stroke by one computer program while capturing images by the other computer program is negligible (< 2sec) the front panel has been built (*Section 2.6.2.1*) with the use of controls and indicators for future work, in order to avoid error in acquiring images after application of every 5 mm stroke. Controls simulate instrument-input devices and supply data to the block diagram of the Virtual Instrument (VI). Consecutive images were obtained at a fixed interval of 5 mm stroke by providing a skip table to the user on the front panel. This table describes the number of frames to skip after each acquired frame. The frame speed of the camera used is 25 frames/sec, thus in the table the frames to skip are multiple of 5, which is controlled by using graphical codes on the block diagram. The front panel and acquired images are shown in Figure 3.9 and 3.10 respectively.

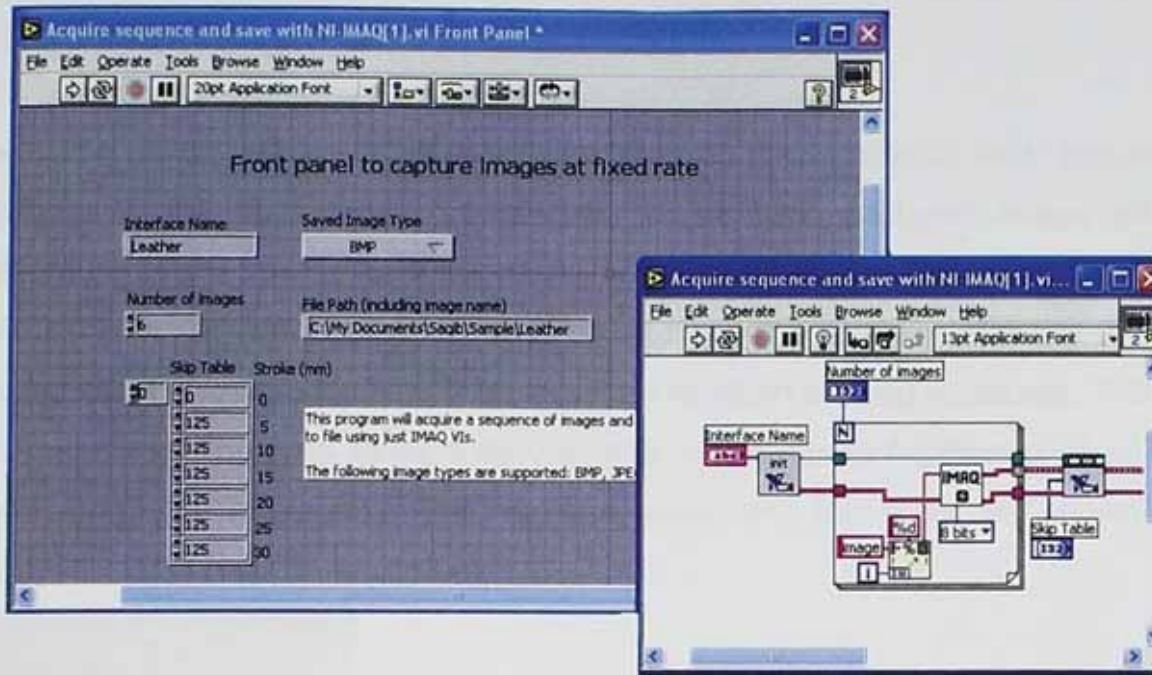


Fig 3.9 Front panel and Block diagram for continuous image capturing at different stroke rate

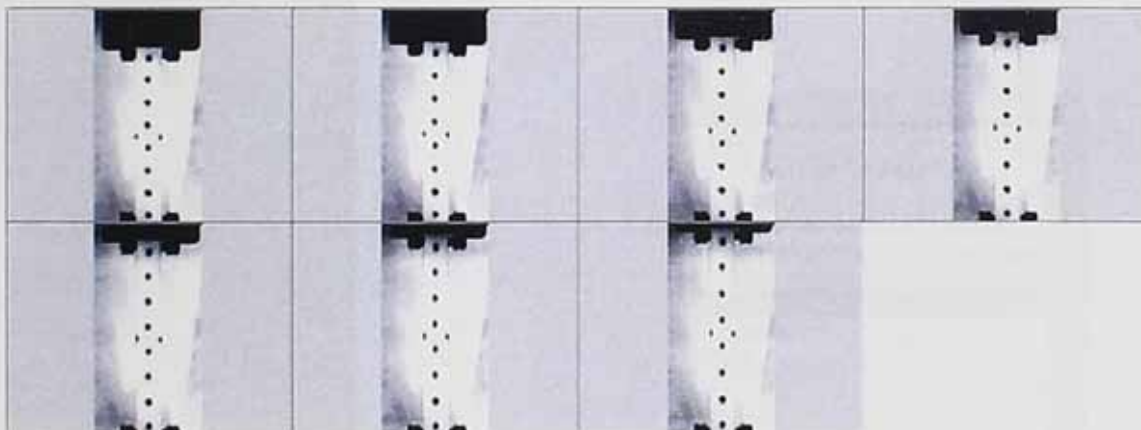


Fig 3.10 Images captured at different stroke

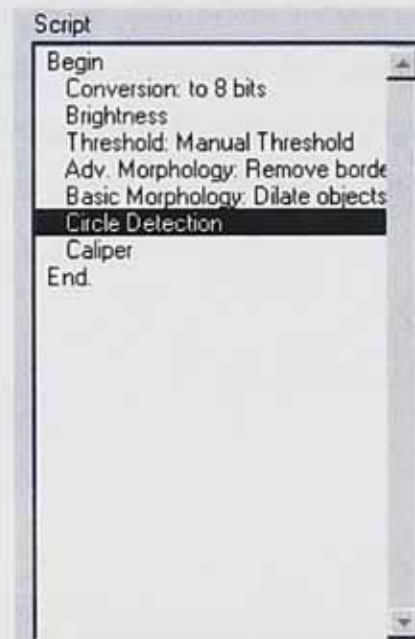
Subsequent images were captured at regular intervals under the control of an accurate timing facility. Images were saved to analyse later. The magnitude of the load after the application of each stroke is recorded automatically by the software used to operate the tensile testing machine.

3.2.2 Image Processing

Detection of the relative movement of the dots on the sample for each acquired image was the main region of interest. So for each captured image, after application of the stroke, all of the marked dots should be in an imaging window. The same script was applied as used to measure the accuracy (*Section 3.1.3*) except that the calibration step is unnecessary as strain is being measured. This is a dimensionless quantity so the measurements in either units (number of pixels or millimetres) are acceptable. The resultant image and the script are shown in Figure 3.11 (a) and (b) respectively.



(a)



(b)

Fig 3.10 Resultant image (a) and script (b)

After applying the script the location of each dot was determined. Then by using the calliper command the displacement between the dots before and after stretching the sample uni-axially is calculated. The whole sample was divided into four different sections A, B, C, and D with equivalent lengths of 140, 100, 60 and 20mm respectively as shown in Figure 3.11.

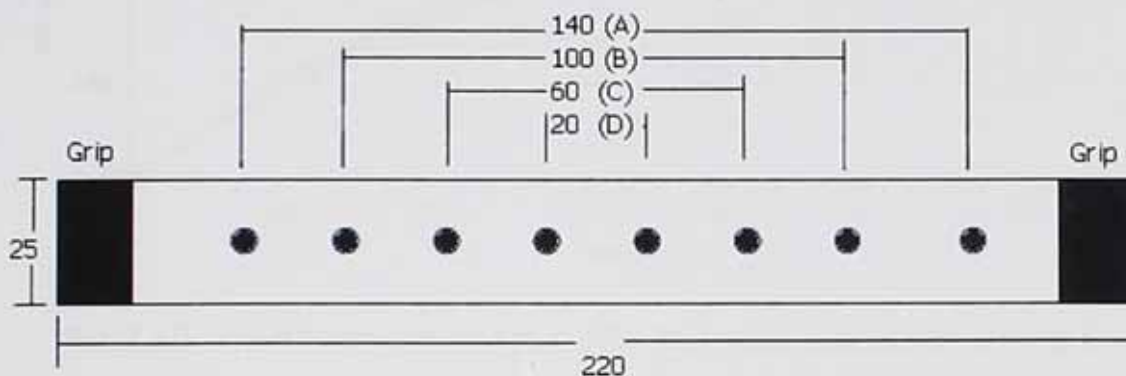


Fig 3.11 Rubber sample with different sections

The relative movement of marked dots on sample was used to determine the mean strain in each section (A, B, C, and D). When the strain values for each section were plotted against the applied load as measured by using image analysis technique the graph followed the same pattern as shown in Figure 3.7. Due to limited field of view it was not possible to obtain the full stroke length until sample breaks. The results are shown in Figure 3.12

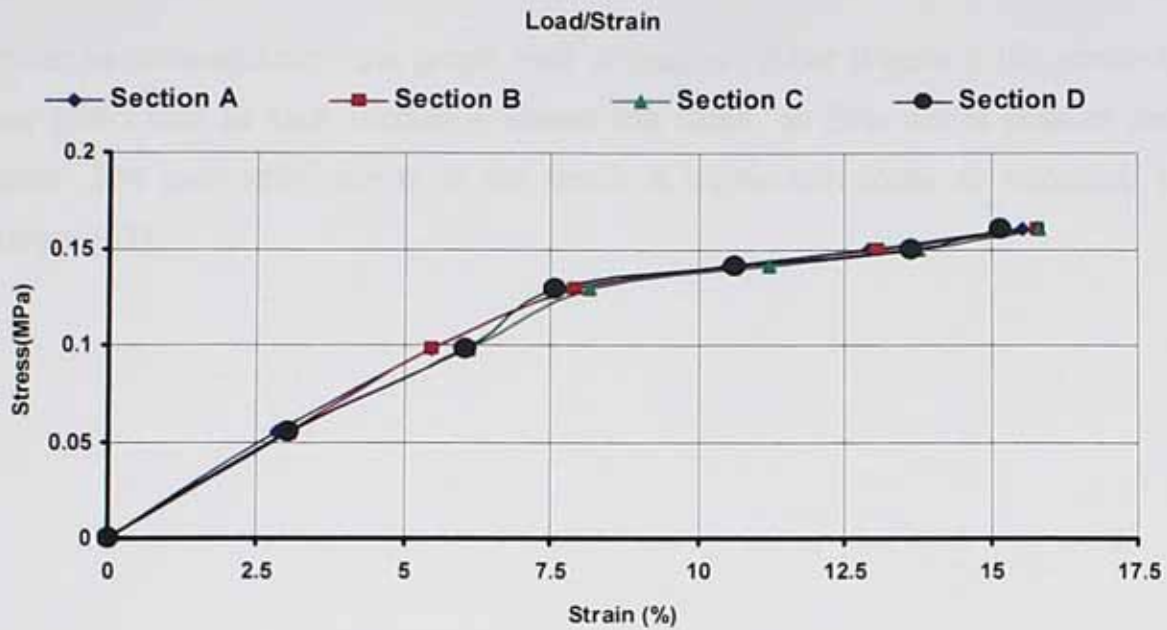


Fig 3.12 Strain measurement in rubber by image analysis at various loads

A uniform strain response was expected for rubber. When the best-fit polynomial function with 4th degree is applied, the result is shown in Figure 3.12, with a residual of ± 0.5 . This suggests that strain can be measured within an accuracy of $\pm 0.5\%$. The residual results are shown in Figure 3.13

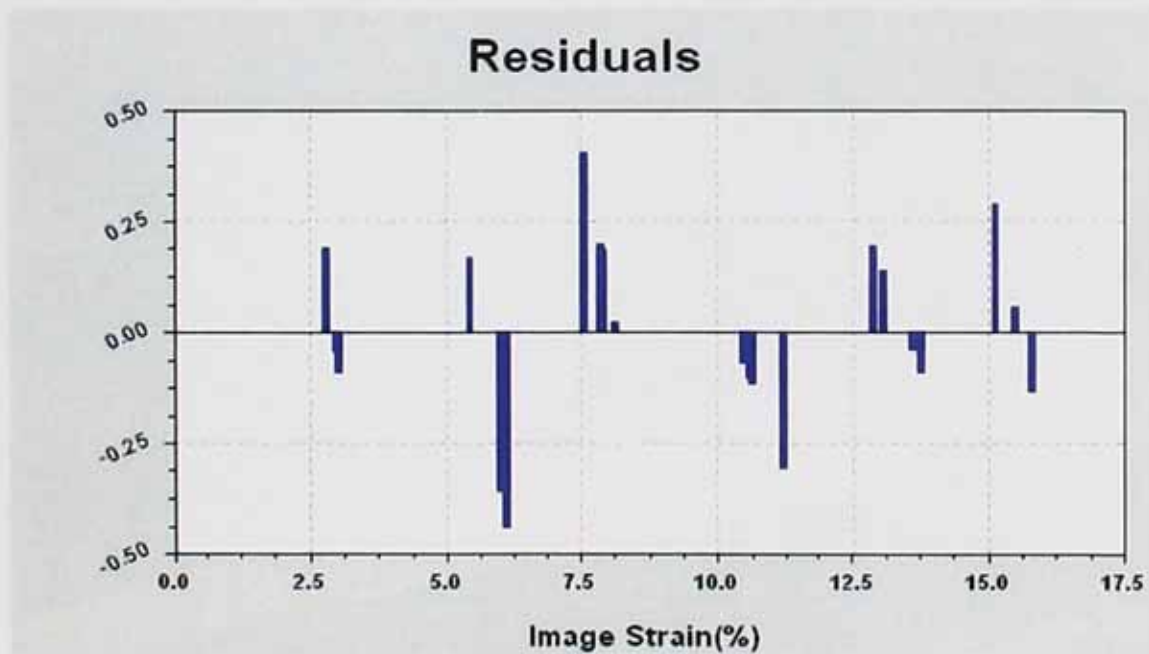


Fig 3.13 Accuracy of strain measurement by image analysis

It can be observed from the graph, that in case of rubber (Figure 3.12), strain for any given load in each section is almost the same, as data points overlap each other. The load-strain curve of the result is highly non-linear as expected for rubber [63].

4 Application of Large-Scale to Products Layer Functioning in Layer

The application of large-scale to products layer functioning in layer is a key concept in the study of large-scale to products layer functioning in layer.

The application of large-scale to products layer functioning in layer is a key concept in the study of large-scale to products layer functioning in layer.

The application of large-scale to products layer functioning in layer is a key concept in the study of large-scale to products layer functioning in layer.

CHAPTER 4

The application of large-scale to products layer functioning in layer is a key concept in the study of large-scale to products layer functioning in layer.

4.1 Introduction

The application of large-scale to products layer functioning in layer is a key concept in the study of large-scale to products layer functioning in layer.

4.2 Theoretical Framework

The application of large-scale to products layer functioning in layer is a key concept in the study of large-scale to products layer functioning in layer.

4 Application of Image Analysis to Evaluate Linear Stretching of Leather

The experimental procedure of applying the image analysis technique on whole hide/skin involved by first applying the technique on small pieces.

4.1 Determination of Stress-Strain Behaviour of Leather by Image Analysis

The stress-strain behaviour of leather as evaluated before [10] by using conventional method is verified by applying image analysis technique on small pieces.

4.1.1 Material

Hide obtained from a UK tannery was processed using the facility available in the BSLT tannery in accordance to a commonly used process for leather manufacturing (*Section 1.1*).

4.1.2 Experimental Procedure

Experimental work with a natural material is never easy because it is impossible to exactly repeat a test in a particular area, and direction, to evaluate the reliability of the test results. If samples were to be cut from another skin of the same kind and treated in the same way, it would be difficult to predict the differences in mechanical behaviour from the present results.

4.1.3 Sample Preparation

To obtain samples with straight edges, a cutting die having dimensions of 25 x 220 mm was placed vertically on the material and samples were cut using a

press. The approximate grip width of the tensile testing machine used was 30 mm, which produces a sample gauge length of 160 mm. This length is also termed *gauge length*. The location of the each sample on the material was obtained according to the official sampling method. Two samples were cut, one parallel and the other perpendicular to the backbone. Two parallel straight lines 20 mm apart from each other were drawn at the middle position of sample as shown in Figure 4.1

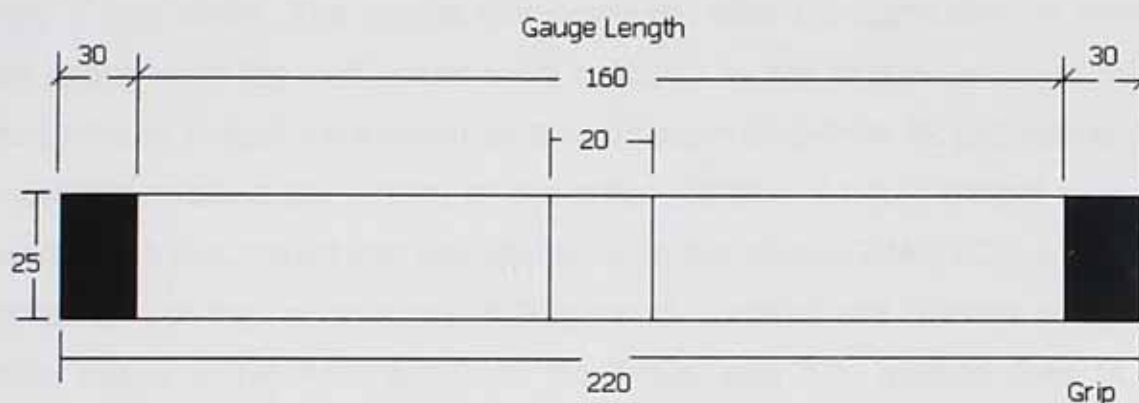


Fig 4.1 Leather sample for tensile testing

4.1.4 Methodology

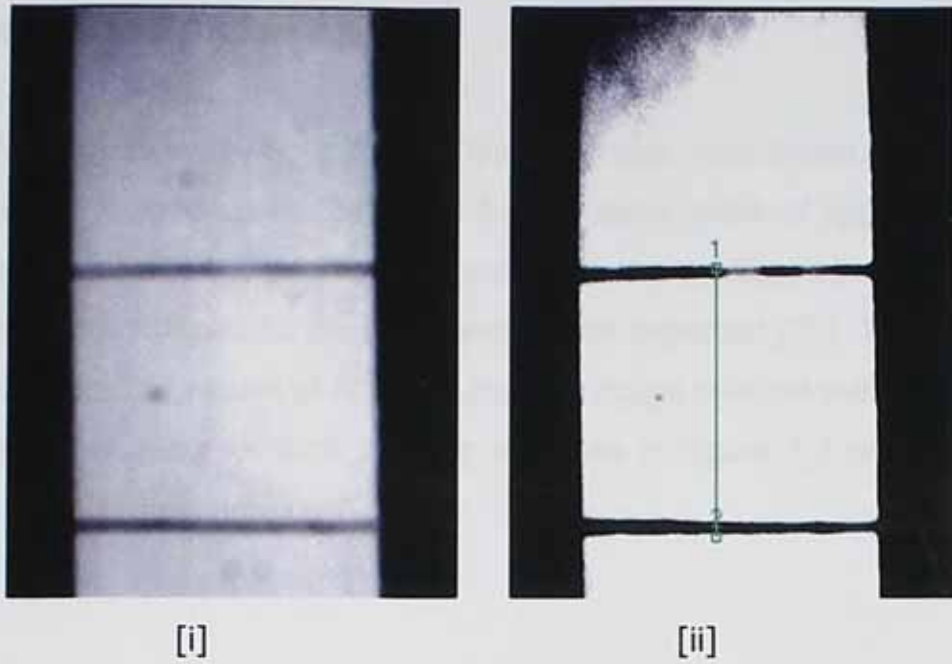
All uni-axial tests were performed on a Dartec Hydraulically Actuated Tensile testing machine at a stroke rate of 10 mm/sec. The machine was located in a conditioned room having a temperature of 20°C and a RH (Relative Humidity) of 65%, as required for the standard physical testing of leather.

Leather hide is a floppy and flimsy material. The success of applying the technique greatly depends on how it is presented to the camera. Even if the sample lies on a flat surface but not stretched, the image captured will have areas dominated by shadows and high reflections frequently resulting in lack detecting marked lines on it. Therefore it was necessary to maintain an initial tension in the sample. To achieve this the upper head of the machine with a load cell attached was moved until an approximate distance of 160 mm was obtained between the

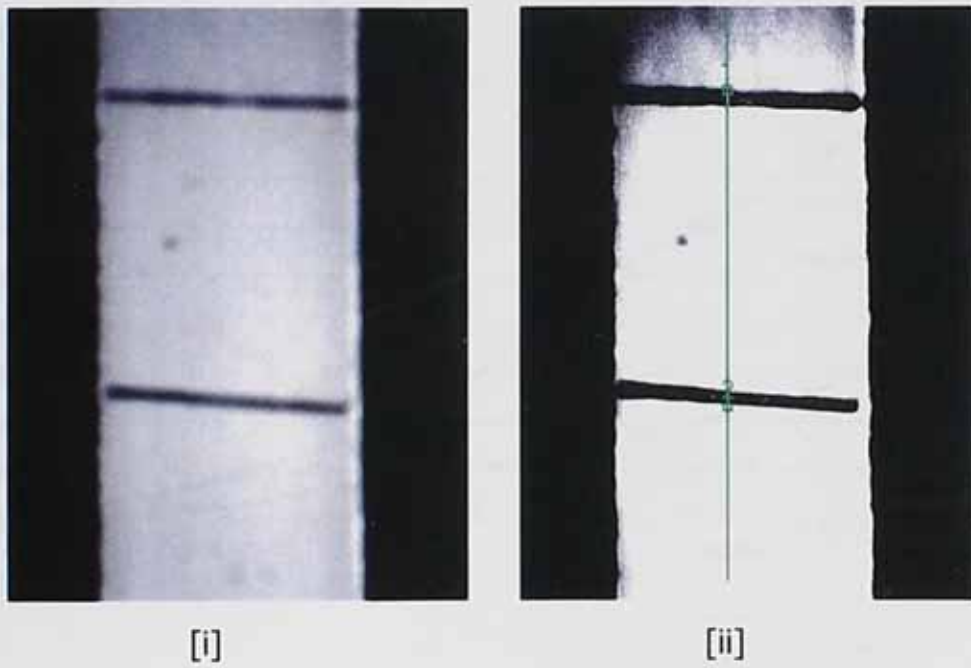
two jaws (gauge length of sample) with the load cell showing zero value at the start of every experiment.

The sample was gripped in the jaws and was straightened as much as possible, with a pre-tension value of almost zero, which is confirmed by Dartec software. The camera was positioned opposite to the sample to view the whole sample in the imaging window. It was felt necessary to capture images after the application of every 5 mm stroke and record the load value at this stroke. Both the Dartec and image analysis software were run in parallel in order to capture images after every 5 mm stroke. The images were captured after the application of every 5 mm stroke while the load values were captured by the tensile testing software. The captured images were saved on the computer hard-drive for processing. The processing involved the writing of the script (*Section 3.1.3.2*) started after the saved image was loaded and was displayed on the screen. IMAQ BCGLookup was applied by varying the amounts of Brightness, Contrast and Gamma across the whole image to highlight details of significant area e.g. marked lines at the expense of the sample surface. This would result in the form of sharp edges along the line thus allowing easy detecting of the pixel intensity changes as the drawn "*edge detecting line*" passes over the marked line. This edge detection technique (*Section 2.6.2.3.2*) was used to determine the separation between the lines after application of each stroke.

Images captured before and after stretching with and without edge detecting lines are shown in Figure 4.2 (a) and (b) respectively.



(a)



(b)

Fig 4.2 Images captured before and after stretching of the leather samples
 (a) before stretching [i] no edge detecting line [ii] with edge detecting
 line, (b) after stretching [i] no edge detecting line [ii] with edge
 detecting line

4.1.5 Results and Discussion

The overall stress-strain behaviour of both samples was drawn. Both samples follow the "J" shaped curve [24]. Also for the same value of applied strain the sample cut parallel to the backbone showed high stress values compared with the sample cut perpendicular to the backbone as was expected [25]. This agreement further validates the results of applying the new image analysis methodology. The stress-strain behaviour of both samples is shown in Figure 4.3 while the actual data are given in *Appendix D*.

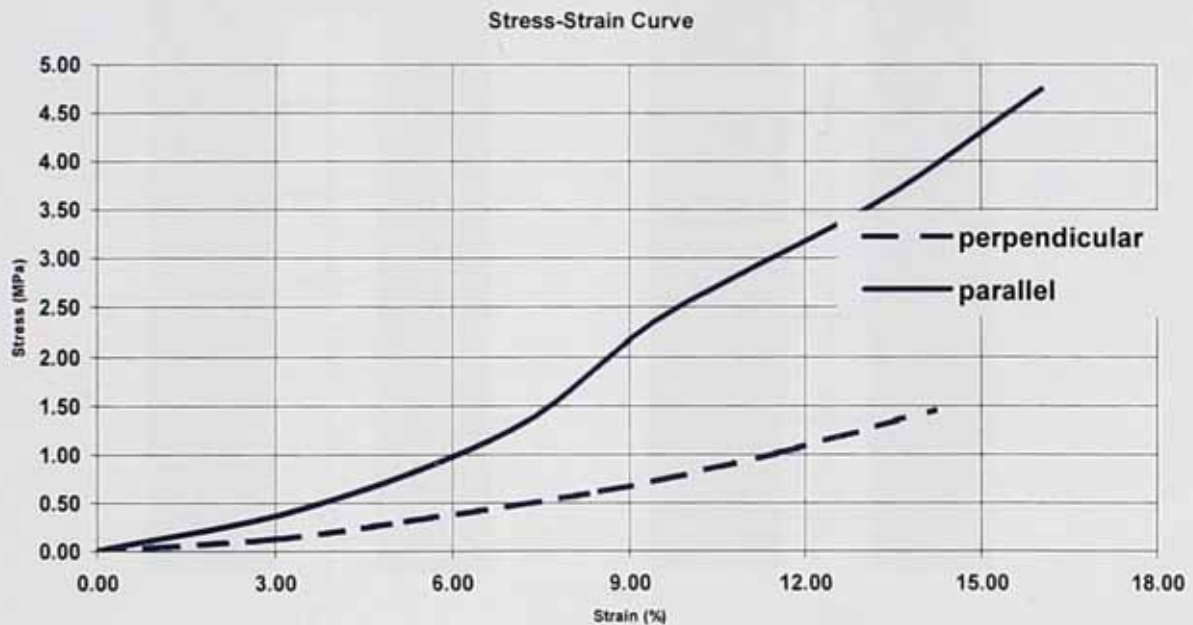


Fig 4.3 Stress-Strain data for leather samples where an image analysis technique has been used to measure strain

4.2 Measurement of Strain Distribution in Leather

The same edge detection methodology was used to evaluate the strain distribution along the whole length of the sample. For this series of experiments

the sample was marked with six lines along its length, thus dividing it into five almost equal regions. As it was necessary to get a larger area (field of view) in the imaging window so the camera was moved away from the sample until the whole sample length (plus some margin for stretching the sample) was visible in the imaging window. The actual images of the sample before and after stretching with the applied edge detection command activated are shown in Figure 4.4. The strain within each section was then measured by applying the same methodology. The results in Figure 4.5 show that the strain is different in each section. The curves are again highly non linear but concave to load axis giving a "J" shaped curve as expected.

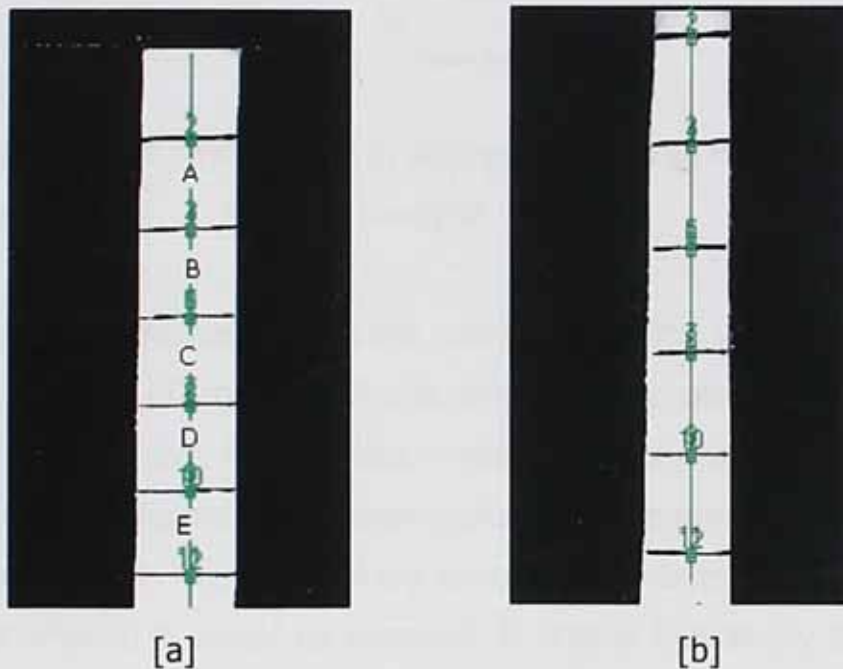


Fig 4.4 Images captured (a) before and (b) after stretching of the leather samples



Fig 4.5 Variability in strain values in different sections as measured by image analysis

In order to compare the results with the rubber sample the same methodology as was used for rubber (*Section 3.2.2*) was employed and also all the parameters (spot pattern, sample size, field of view, working distance) were kept the same. The curves drawn in Figure 4.6 (a) were generated by applying best-fit curve of a 4th degree polynomial. These curves are concave towards the strain axis and are effectively "J" shaped as would be expected. It is clear that at any given value of stress there are marked differences in strain in each of the regions. Thus it can be seen that at a stress of 1.75 MPa strain can be as low as 10.877% (section E) up to as high as 13.109% (section B). Differences in strain between the sections can be represented by calculating residuals. Figure 4.6(a) shows the data from each section at various values of overall applied strain (calculated from the jaw separation of the Dartec testing machine). These overall strain values were 2.5, 5.0, 7.5, 10.0, 12.5, 15.0, and 17.5%. Residuals are the difference between the strain in particular section and the overall applied strain. This shows quite clearly the variability as was expected [27], for leather with residuals varying from +10

to -10% (Figure 4.6 b) as compared with $\pm 0.5\%$ for rubber (Figure 3.13, Section 3.2.2). This variability is related to the heterogeneous fibre structure of leather.

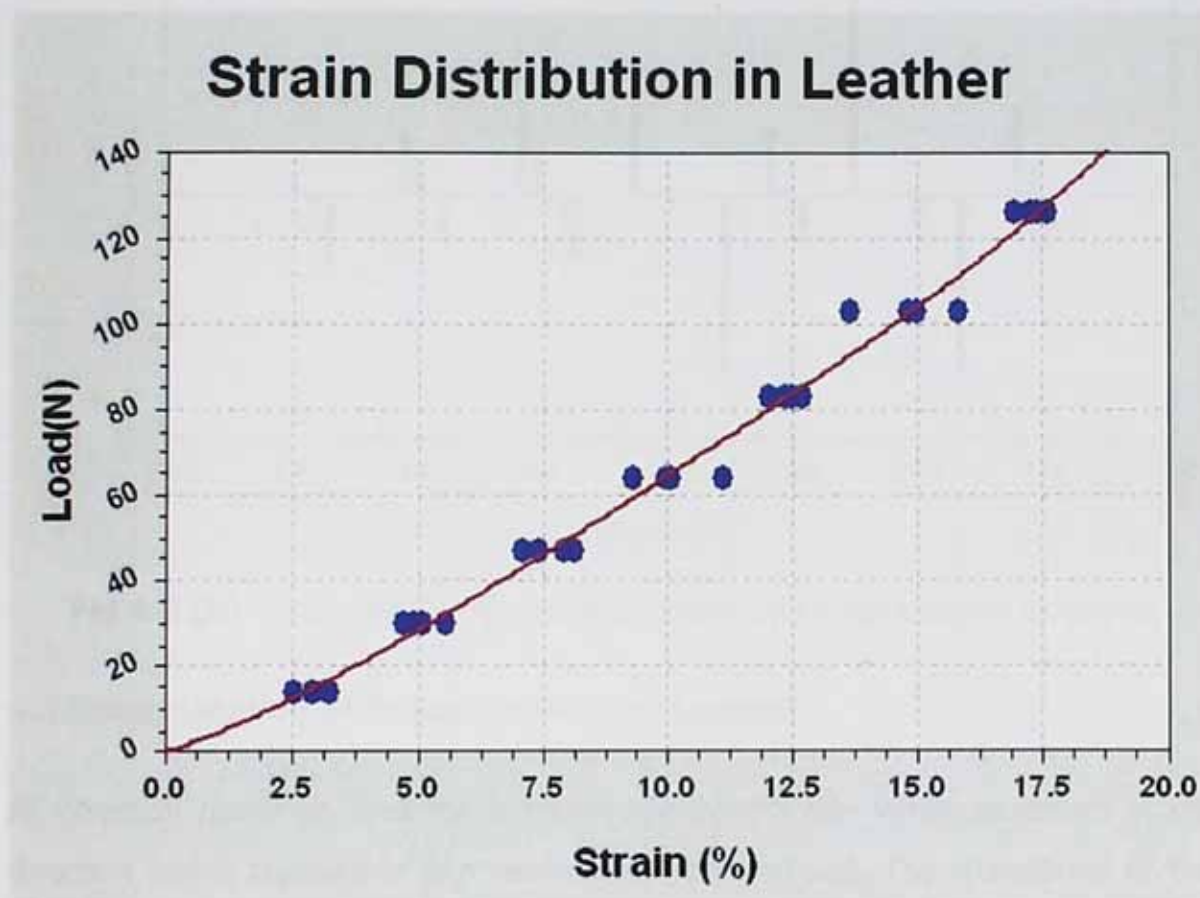


Fig 4.6(a) Strain measurement in leather by image analysis at various loads

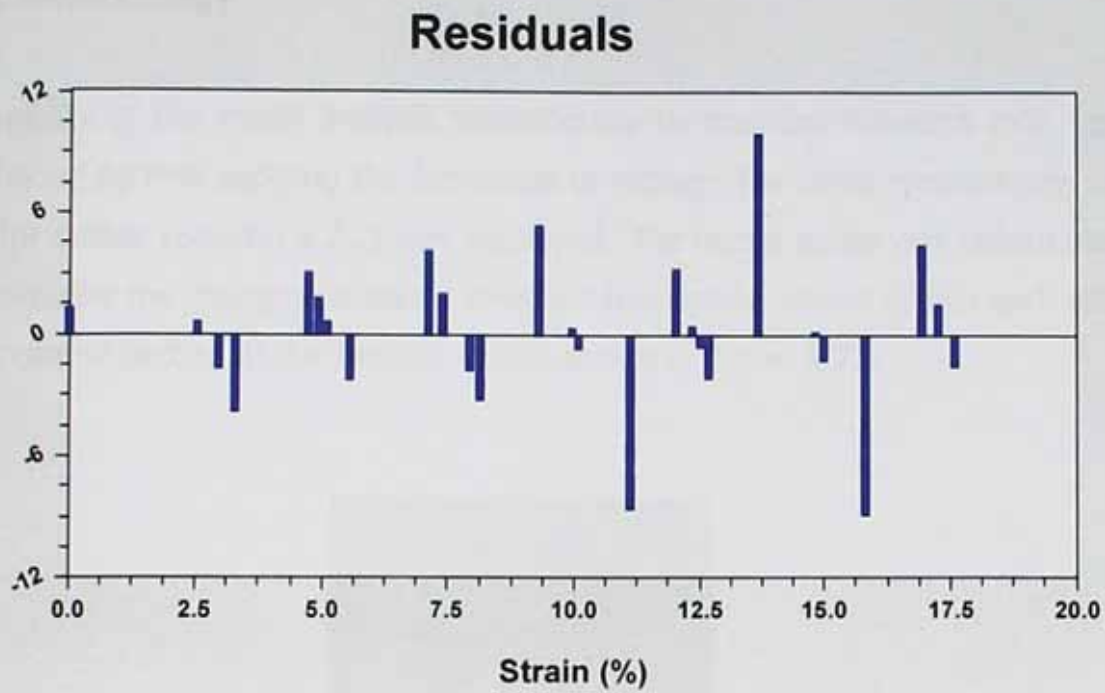


Fig 4.6 (b) Variability in strain measurement by image analysis in leather

4.3 Determination of Poisson's Ratio of Leather

All common materials undergo a transverse contraction when stretched in one direction and a transverse expansion when compressed. The magnitude of this transverse deformation is governed by a material property known as Poisson's ratio (*Poisson 1829*).

Poisson's ratio is defined as the negative of the transverse strain divided by the axial strain in the direction of stretching force.

$$\nu = -\left(\frac{\epsilon_l}{\epsilon}\right) \text{-----(4.1)}$$

where

ϵ_l , represents the lateral strain and

ϵ represents the axial strain

Poisson's ratios for various materials are, approximately 0.4 to 0.5 for rubbers and some soft biological tissues, 0.45 for lead, 0.33 for aluminium, 0.27 for common steels, 0.1 to 0.4 for cellular solids such as typical polymer foams, and nearly zero for cork [64].

4.3.1 Methodology

The validity of the image analysis methodology to measure Poisson's ratio was determined by first applying the technique to rubber. The same methodology as used for rubber (*Section 3.2.2*) was employed. The lateral strain was determined by measuring the changing distance between two circular marks drawn each side of the central section of the sample. This is shown in Figure 4.7.



Fig 4.7 Showing a captured image of a rubber sample. The change in separation of two circular marks 5 and 6 was used to determine the lateral strain

The value of Poisson's ratio found was 0.41 ± 0.04 (*Appendix D*). Theoretically for rubber a Poisson's ratio of 0.5 is expected but due to processing methods used to make rubber typically lower values are obtained [64].

The measurement of the lateral dimensions of leather when it is stretched uniaxially is of great concern, as leather being a viscoelastic material [35] will relax and tend to regain its original shape to some extent. Furthermore some dimensional measurements on leather e.g. thickness require the application of a specific standard pressure (500 gm/cm^2). It is therefore almost impossible with leather to measure the width of the sample (lateral dimension) manually when it is stretched, as the application of more or less pressure on the free ends by a measuring device (e.g. Vernier callipers) will lead to discrepancy in the results. If images of the deformed sample are used to measure the lateral strain then the chances of error caused by delay or applying more or less pressure will almost be zero. As images are captured immediately after the application of each stroke, the sample will have no time to relax. The variation of strain along the length of a stretched leather sample has been previously confirmed by using an image analysis technique (*Section 4.2*). Some variation may also be expected in the lateral strain at each section along the gauge length and consequently the Poisson's ratio may be expected to be different for each section.

Leather samples having dimension of $25 \times 220 \text{ mm}$, were cut out from the butt, belly and neck regions in the direction of parallel and perpendicular to the backbone. Samples were marked with two horizontal parallel lines separated by a distance of 20 mm at the centre. These samples were then uni-axially stretched on the tensile testing machine and images were captured after application of every 5 mm stroke. As stated earlier (*Section 2.8*) due to the constrained field of view a strain of around 18 to 20% was applied to each sample.

When measuring the axial strain in rubber, two parallel lines drawn on the sample remained normal to the axial strain as shown in Figure 4.8a. Interestingly for leather these lines which were initially normal to the sample edges became inclined when axial strain was applied as shown in Figure 4.8b. This meant that the application of the edge detection (*Section 4.2*) methodology was no longer

useful for measuring the Poisson's ratio exactly for the middle section. As the fibres will tend to re-align in the direction of applied strain [24] the marked horizontal lines on the surface of the sample will no longer be parallel but will be distorted, following the re-alignment of fibres, after the application of the stroke. In case of rubber, which is homogeneous and isotropic, these lines will remain parallel to each other.

Almost the same steps of script that were used for edge detection were used to measure the separation of the marked lines and for the reduction in width. The *vertical clamp* and *horizontal clamp* commands (Section 2.6.2.3.5.) of *Imaq Vision Builder* were used. The vertical clamp gave the minimum separation between the two lines after application of the stroke to give a measured of the direct strain while the horizontal clamp gave the minimum width and thus measured the lateral strain.



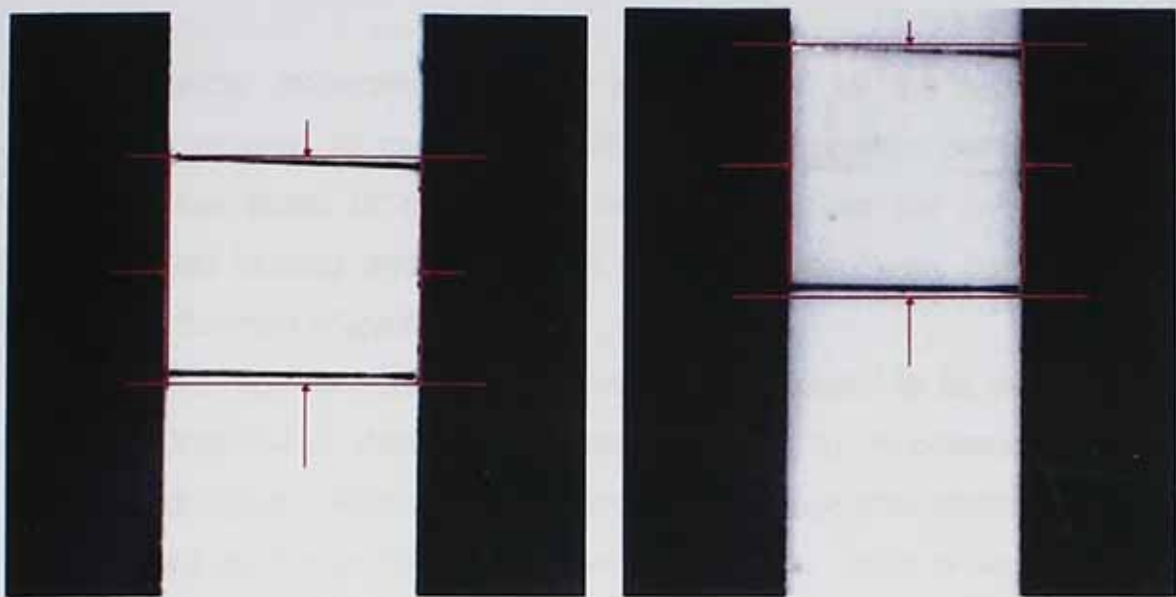


Fig 4.8 (a) Marked lines on the rubber surface, it can be seen that the lines remain parallel after application of the stroke.

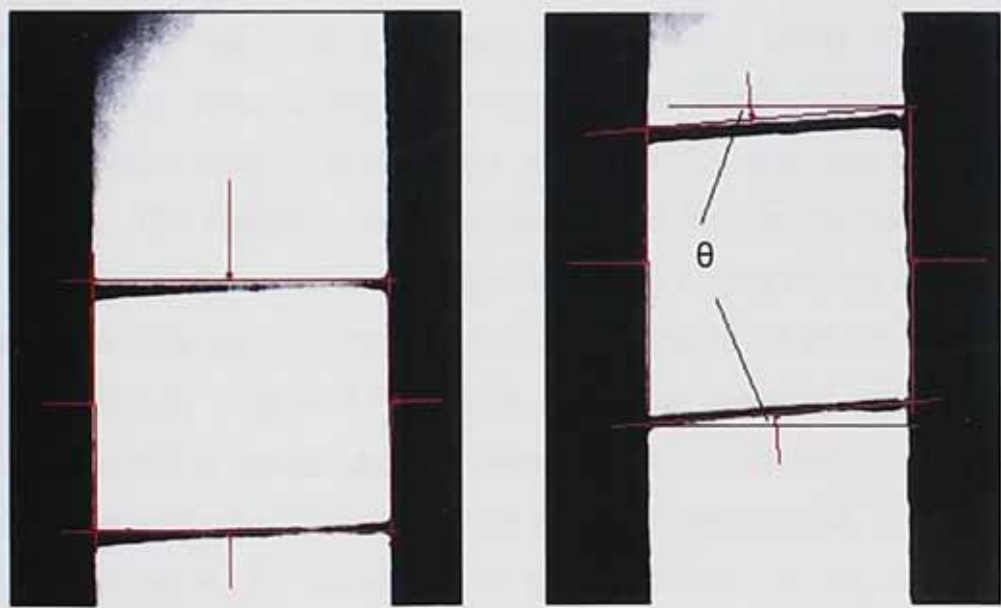


Fig 4.8 (b) Marked lines on leather surface, it can be seen that the lines have become inclined at an angle θ after application of stroke

4.3.2 Results and Discussion

The mechanical properties of leather are governed by the geometry of and interaction between its constituent collagen fibres. Leather behaves elastically only at a low stress or deformation level, beyond this the collagen network becomes load bearing and there is an increasing viscoelastic behaviour (*strain becomes a function of load and time*).

The Poisson's ratio for leather may therefore be expected to be time dependent and could increase or decrease with time [65] due to viscoelasticity. A control panel was designed (*Section 3.2.1*) to acquire the image after application of every 5 mm stroke by the tensile testing machine, for this series of work the tensile testing software (*Dartec*) and the Imaq Vision Builder were run in parallel on the same computer to bring the time difference between application of stroke and to capture the image to almost zero. Since the same image was used to measure lateral and direct strain, this eliminates any time delay between the two measurements (as would occur of, say, callipers were used). This is the first investigation that uses a two-dimensional strain measurement using image analysis for leather when it is stretched uni-axially thus enabling a calculation of Poisson's ratio. The Poisson's ratio was determined for samples taken from three different regions, but for this present discussion the results for the butt region will be used, since they are expected to be most representative of the whole leather. It has been shown (*Figure 4.3*) that for the same value of applied strain the sample cut parallel to the backbone showed high stress values compared with the sample cut perpendicular to the backbone as was expected [25]. Almost the same behaviour is observed for lateral strain, as can be seen in *Figure 4.9* that the value of the lateral strain for parallel direction is higher than the perpendicular direction. This is been shown in *Figure 4.9*, in which right hand side of the graph shows axial strain and the left hand side shows lateral strain.

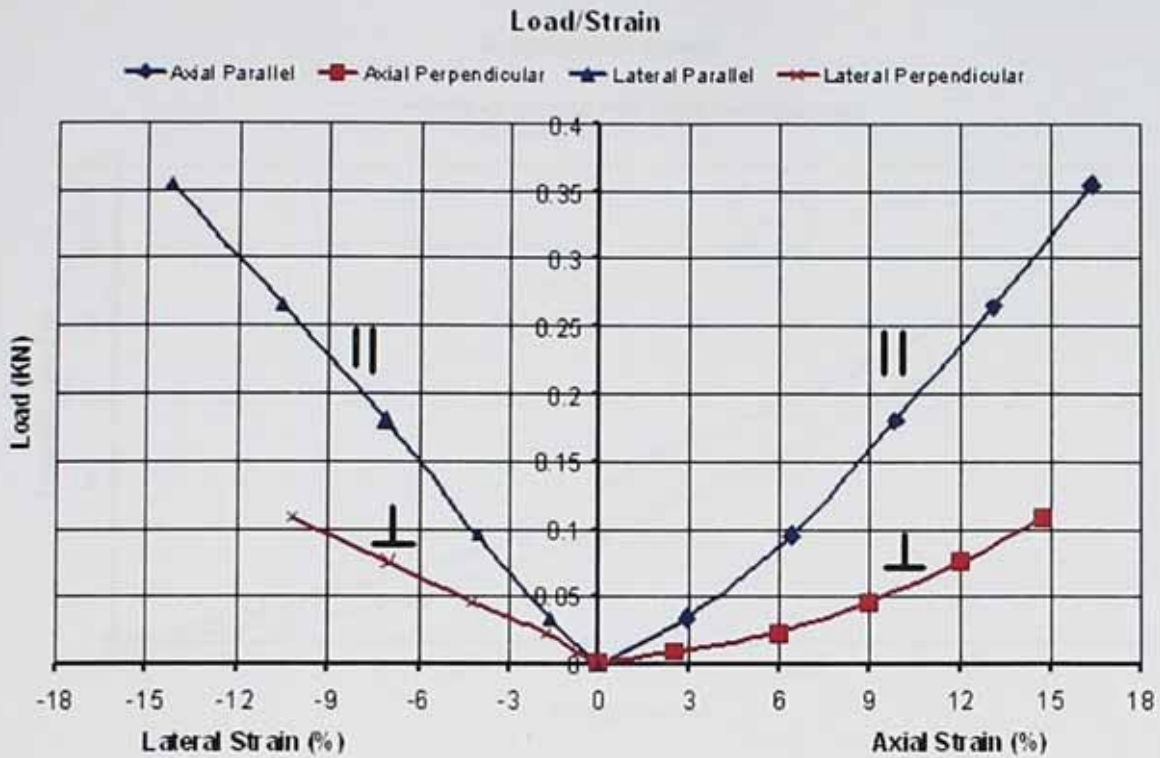


Fig 4.9 Axial and Lateral stress-strain curves for parallel and perpendicular directions of samples taken from the butt region

It can be observed from the graph (Figure 4.9) that curves on the right side are "J" shaped while curves on the left hand side show an almost a linear relation between load and lateral strain for both directions.

If the values of lateral strain are plotted positively along the Y-axis and direct strain values along the X-axis of a graph then the gradient of the line will give the Poisson's ratio. Figure 4.10 shows such a plot of lateral strain against axial strain. It is seen that the curve still has a "J" shape with the higher value of slope (Poisson's ratio) in the parallel direction as compared to perpendicular. A possible reason for this difference is the directional runs of the fibres, which may affect the lateral strain values, as these values are higher in samples having majority of fibres align parallel to the backbone or in other words large amount of necking has observed at the middle of the samples taken along the parallel direction.

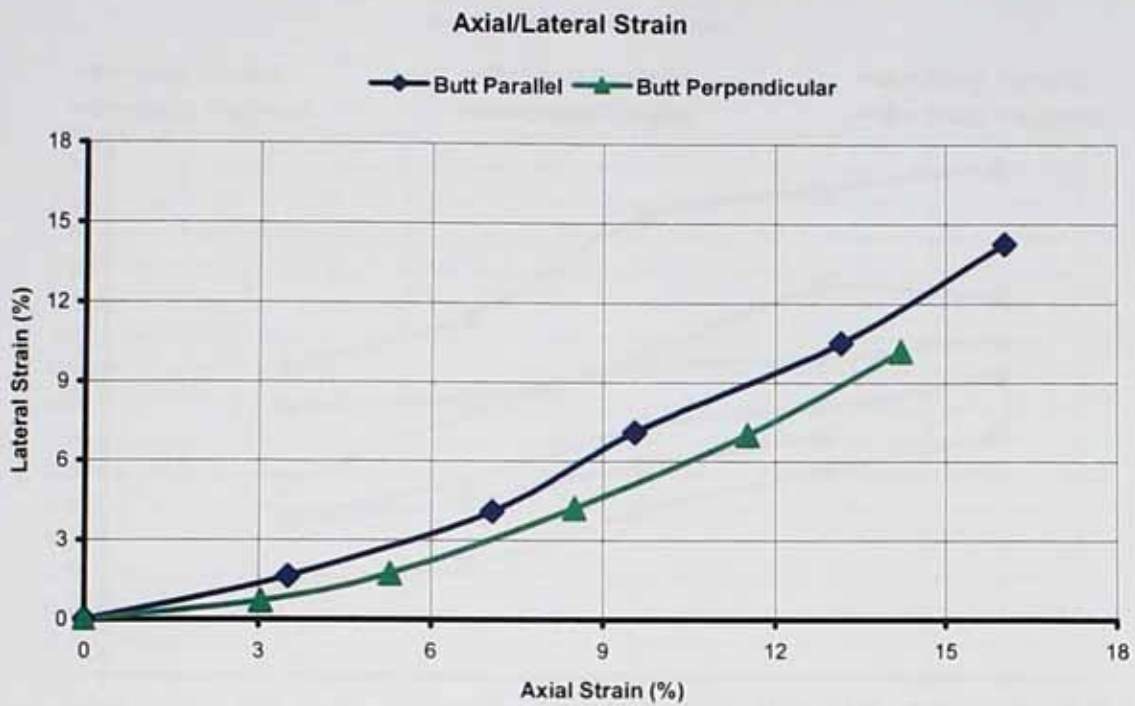


Fig 4.10 Lateral strain plotted against axial strain for parallel and perpendicular directions with respect to backbone of the butt region

Figure 4.11 shows the variation of Poisson's ratio with applied direct axial strain (termed as nominal strain because the direct axial strain value will be different for each region). This shows that the differences between the regions are *a)* dependent on the orientation of the test sample to the backbone *b)* dependent on applied strain.

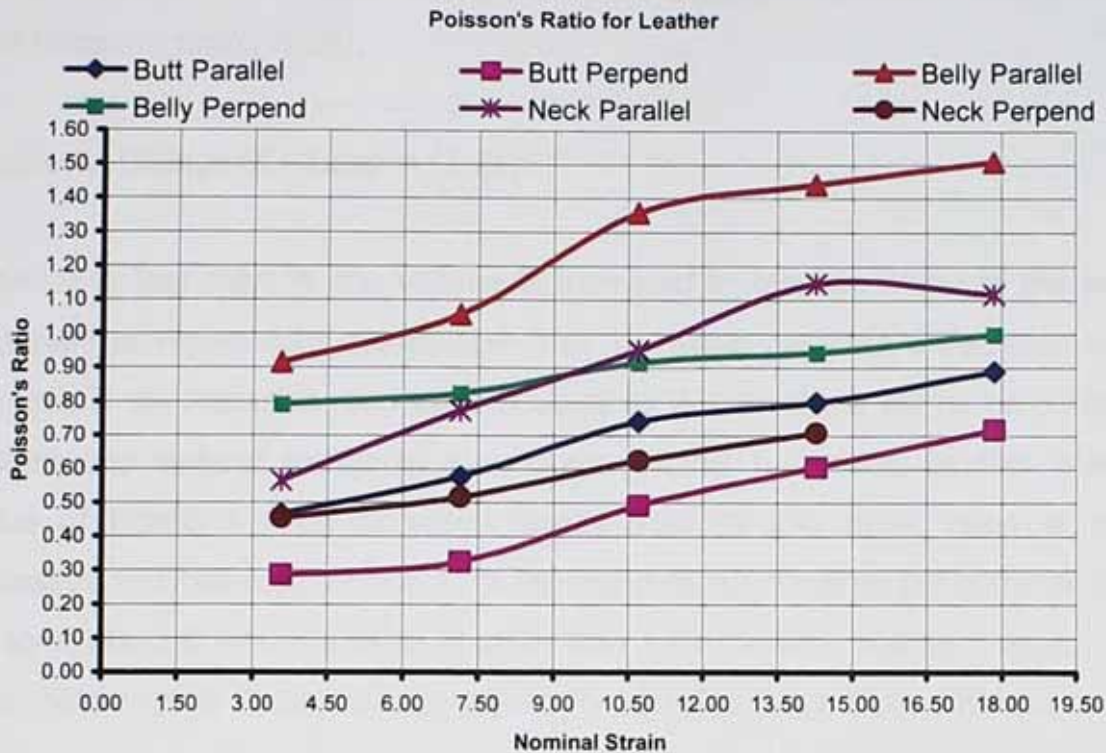


Fig 4.11 Poisson's ratio plotted against nominal direct strain for different regions of leather

A possible reason for region-to-region variability is variability in the compactness of fibre packing (*Section 1.1.2*) and also variability in tow fibres, which join together to form a 3-D network. Higher values of lateral strain are observed in the belly region (2.847 to 24.499) as compared to butt region (1.631 to 14.238). Consequently the Poisson's ratio values for the belly region are higher (lateral strain being a numerator). Also, as the compactness of weave is high at the butt region as compared to other regions, the fibres have less inter-fibre space to squeeze against each other in this region giving a higher value of lateral strain as compare to other regions. The increasing gradient of the curves implies that Poisson's ratio increases with strain and this is apparent in Figure 4.11. As nominal strain increases from 3.5% to 18% Poisson's ratio can increase by up to double its low strain value. The possible reason for the increase in Poisson's ratio values as applied strain increases is due to the open porous structure of leather. This porosity caused a decrease in the volume of the sample which resulted in a

increase in its Poisson's ratio value due to the relationship between volume change and Poisson's ratio (ν)[66].

Fractional Change of volume $\approx (1-2\nu)$

When ν is less than $\frac{1}{2}$ the volume is increased in tension. Many of the values observed in Figure 4.11 are greater than $\frac{1}{2}$, which replicate a decrease in the volume. If the Poisson's ratio value is equal to $\frac{1}{2}$ then there will be no change in volume and material elongates at constant volume. It can also be seen that the value of Poisson's ratio increases rapidly from its low strain value as strain increases, but between 12 and 15% the curve bends towards the nominal strain. At some stage it attains a value of more than 1 for the belly and neck regions.

This difference in Poisson's ratio values for samples taken from different regions of the hide was also observed when determined the Poisson's ratio at different sections of the leather sample along its gauge length as shown in Figure 4.4. Although the values were found to be strain dependent, this difference in values was not large - the minimum value was 0.718 (Section A) and maximum 1.033 (Section E).

4.4 Poisson's Ratio and the Lines of Tightness

It was observed experimentally that Poisson's ratio is different for each region of leather (butt, belly, and neck) also samples tested parallel and perpendicular to the backbone direction give different results for each direction. Higher values of Poisson's ratio have observed in samples taken parallel to the backbone direction. It has been found in other anisotropic, natural (knee joint) and man-made (composites) materials that Poisson's ratio does depend on the fibres orientation [67,68,69].

In a further series of experiments the Poisson's ratio at different angles with respect to the backbone direction was measured. The material used for this experimental work was chrome tanned bovine wet blue hide obtained from a UK

tannery. The term *wet blue* refers to a hide that has been fully preserved and tanned using chromium salts, to leave a material essentially comprising of a non-biodegradable cross-linked collagen network [21].

Two treatments were performed on the wet blue samples before drying. One was drying without stretching to produce a sample referred to as the *control* and the other was drying whilst the sample was stretched to produce samples, which will be referred to as the *dried under strain*. To obtain the *dried under strain* samples a tensometer made by *Hounsfield* was used. The existing grips of the tensometer were not big enough to hold the samples of the size required. Therefore new grips were prepared using the workshop facility in *British School of Leather Technology*. The modified apparatus is shown schematically in Figure 4.12.

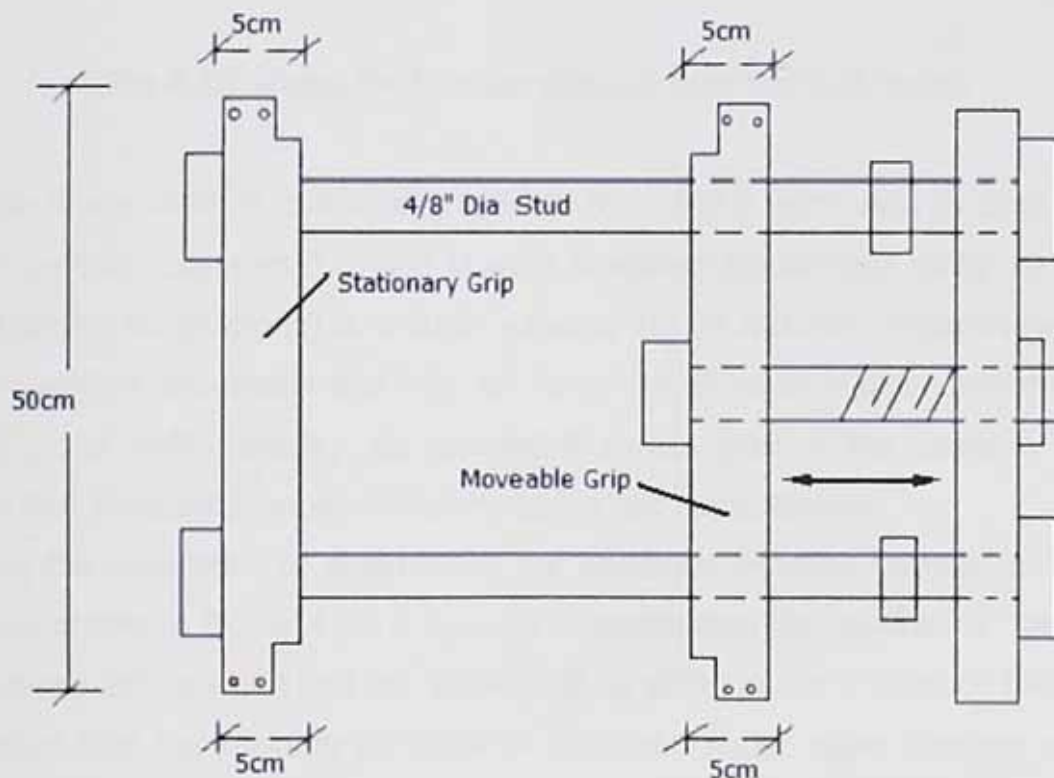


Fig 4.12 Schematic diagram of the Uni-axial stretcher based on a Hounsfield Machine with modified grips

4.4.1 Experimental Setup and Methodology

In order to get consistency in the results a large rectangular piece of leather was taken from the butt region and was then further divided into four smaller rectangular samples as shown in Figure 4.13.

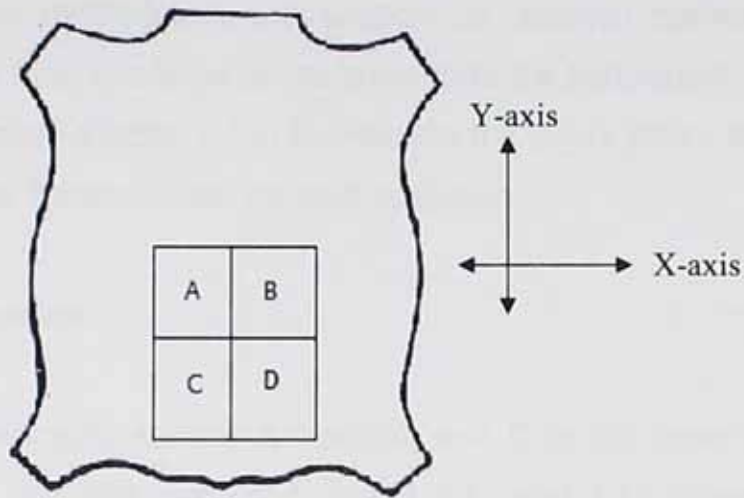


Fig 4.13 Shows the four samples cut from the Butt region

Sample A was used as control sample while B, C, and D were used as dried under strain samples. Samples B, C and D were stretched sequentially along their long axis (parallel to backbone) by a strain value of 10, 20 and 30% respectively using the Hounsfield tensometer and then left to dry for 48 hours in a conditioned room at 22°C and 65% humidity. On removal from the grips of the machine it was found that the stretch imparted before drying had been retained.

Due to the application of strain along the backbone direction (parallel to the Y-axis) as shown in Figure 4.13, it is to be expected that the majority of fibres will align along this axis and that the leather will be stiffer in this Y direction [30]. It is expected that the majority of fibres in the dried under strain samples will be aligned along the Y-axis, therefore these samples can be considered as having an increasingly strong line of tightness running along the Y-axis as the applied strain increases from 0 to 30%.

Five rectangular shaped specimens (25 x 220 mm) were cut from each of the four large pieces (A, B, C, D), either at angles of 0, 30, 45, 60, 90° or 0, 45, 60, 75,

90° to the Y-axis in clockwise direction with 0° measuring parallel to it. Two series of experiments were carried out, in one the Poisson's ratio at fixed load was measured and on the other a fixed stroke or strain was applied instead of fixed load. The direction of the applied load and the applied strain for both cases was along the Y-axis and same methodology was adapted to obtained control and dried under strain samples form two large pieces taken form the butt region. Same methodology was used (*Section 4.3.1*) to measure the direct strain, lateral strain and consequently the Poisson's ratio for each specimen.

4.4.2 Results and Discussion

In the first series of experiments sample A (control) and C (dried under 20% strain) obtained from the first hide was used. Figure 4.14 and 4.15 shows the graph of Poisson's ratio against the angle to the backbone for control and dried under strain samples respectively.

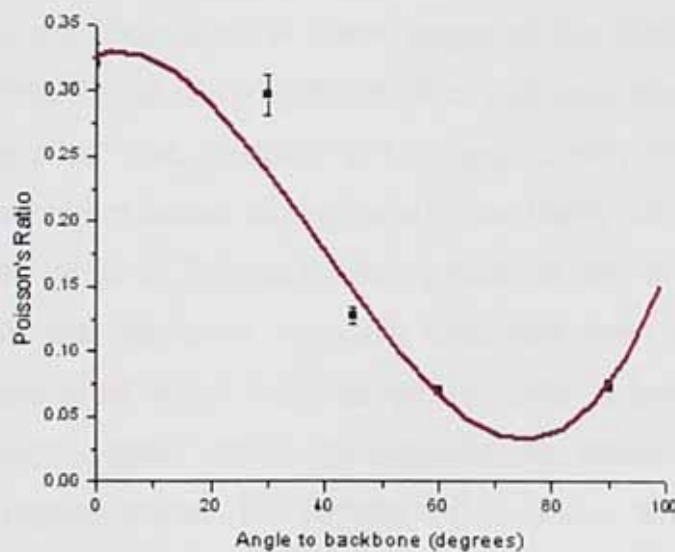


Fig 4.14 Poisson's ratio for the control sample at different angles to the backbone at an applied axial strain of 3.13%

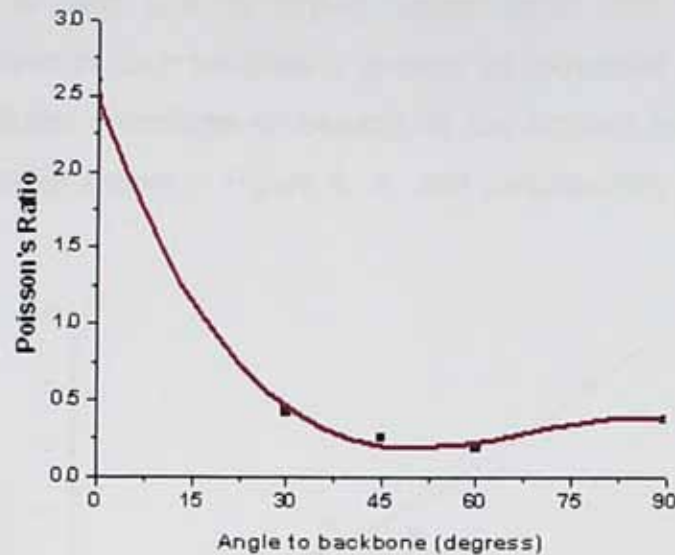


Fig 4.15 Poisson's ratio for the dried under strain (20%) samples at different angles to the backbone at an applied axial strain of 3.13%

It can be seen in both graphs that at low angles to the backbone the Poisson's ratio is relatively high but it falls rapidly as the angle increases. The possible reason may be, as the fibres align at lower angles to the backbone direction [7] and have low contribution in carrying the applied load just after its application as they carried the applied load gradually [24]. Consequently the fibres along the loading axis had low strain values as compare to the fibres orthogonal to it, which results in an acute drop in Poisson's ratio values at the lower angles. Large difference between the values of Poisson's ratio has been observed for both control ($\nu=0.32$) and dried under strain sample ($\nu=2.48$) at lowest angle and also that there was much greater difference between the Poisson's ratios at 0° to those values at higher angles for sample dried under strain. However this difference in values was low in dried under strain sample where the curve becomes almost parallel to the X-axis at higher angles. The possible reason of this lower anisotropy is due to the smaller spaces between fibres when samples dried under strain. This also contribute in lower axial strain values of these samples as compare to the control sample which results in higher Poisson's ratio of these sample (dried under strain) as axial strain being in the denominator. A possible

reason for this is that due to drying under strain the compactness and straightness of fibres in such samples is greater as compared to control sample. Therefore more fibres contribute to bearing of the applied load, leading to low direct strain values as shown in Figure 4.16, and consequently the high Poisson's ratio.

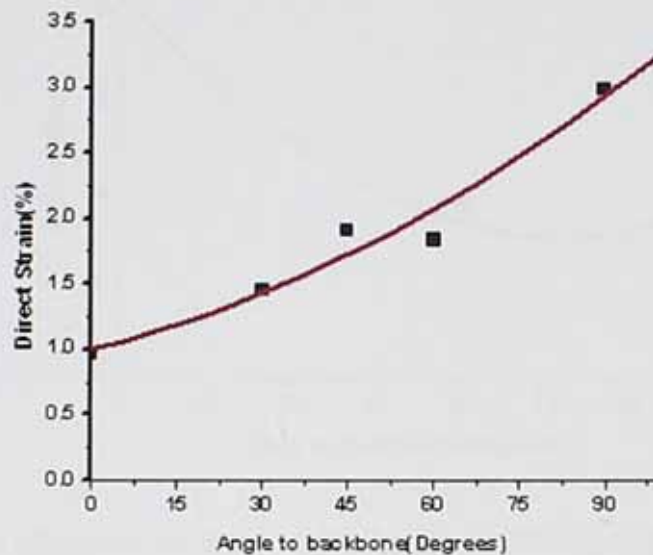


Fig 4.16 Strain observed in dried under strain samples at different angle to the backbone at an applied strain of 3.13%

It can also be observed from the results for the control and dried under strain samples that the Poisson's ratio significantly depends on sample orientation as observed in other materials [70,71]. A possible reason for this is that the fibres are expected to be oriented along the backbone direction and applied strain direction will carry less load as the angle of the fibre to the loading direction increases. Therefore a higher value of Poisson's ratio is observed at 0° for both samples, as most of the fibres are aligned at this angle. It may also be observed that the both curves almost have the same shape except higher values of Poisson's ratio for dried under strain sample. When stress against fibre orientation curve is drawn almost same pattern is observed as observed in wood [71] and uni-directionally reinforced composites [72]. The result shows that to produce same strain for different fibres orientation along the loading axis. A higher value

of load is required for sample having fibres orientation parallel to the loading axis and lowest for samples having fibres orientation orthogonal to the loading axis. The results of stress against fibre orientation are shown in Figure 4.17.

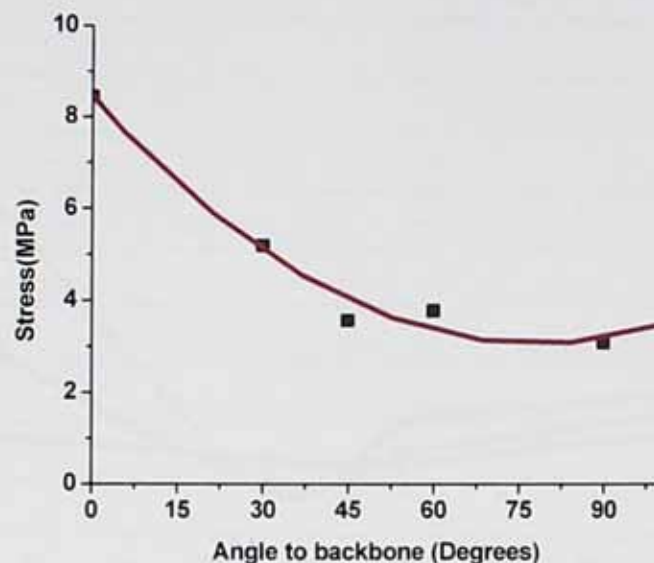


Fig 4.17 Stress observed in dried under strain (20%) samples at different angle to the backbone at an applied strain of 3.13%

In a second series of experiment another hide was used and measurements of the Poisson's ratio values were made at constant load. When the Poisson's ratio values for specimens taken from samples B, C, and D (dried under strain) measured at constant load are compared higher values are observed in sample with a higher applied strain value i.e. 30% and the same dependence of Poisson's ratio on angle was determined with lower angles tending to give greater values. The results are shown in Figure 4.18.

It can be concluded from data for both control and dried under strain samples that a higher value of Poisson's ratio is obtained when the direction of applied load or strain is the same as that of a line of tightness.

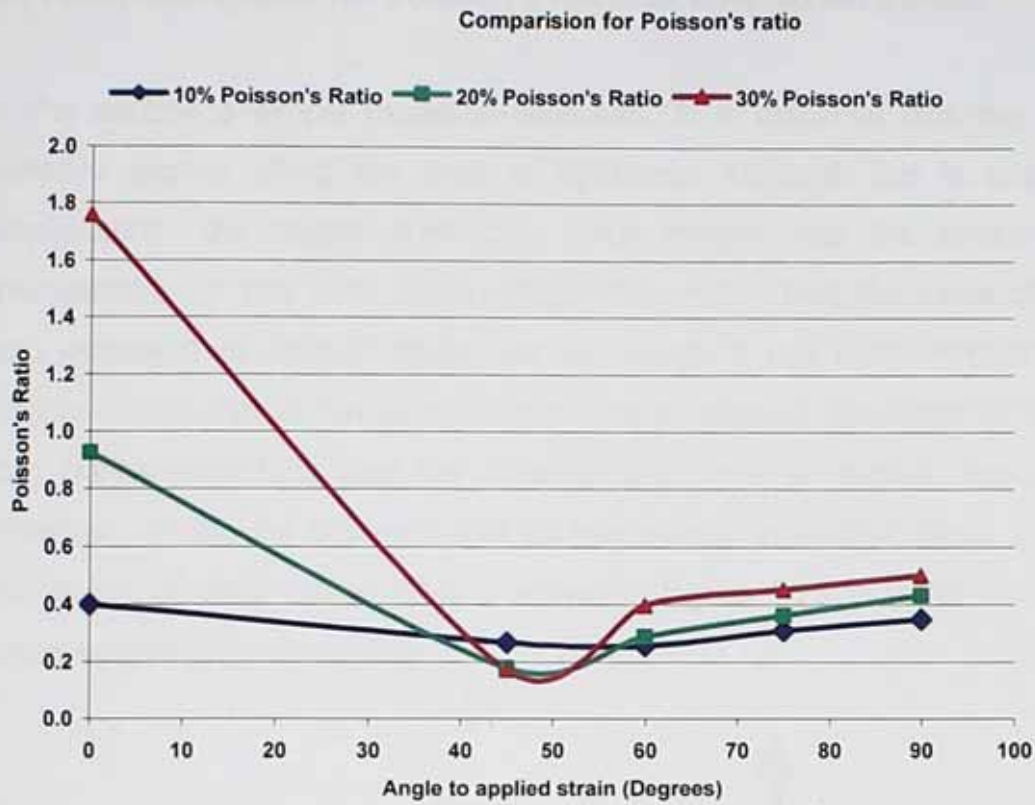


Fig 4.18 Poisson's ratio for leather sample cut at different angles to the applied strain axis, dried under strain (10, 20, or 30%)

4.5 Analytical Model for Poisson's Ratio at Low Strain Values

In this section a simple model is proposed. It is assumed that the fibres are perfectly aligned along the lines of tightness. Although this is a gross over simplification, the model does give some insight into the reasons for the observations. It has been observed (*Section 4.3.2*) that the value of Poisson's ratio increased as applied strain was increased. It has been mentioned earlier (*Section 1.1.3*) that at low strains there is no increase in the length of constituent fibre during stretching and the stress-strain curve of leather shows a linear behaviour. It can be assumed that at low strains inter-fibre shear is the main mechanism of deformation. This is shown in Figure 4.19 in which the length ab remains same after stretching.

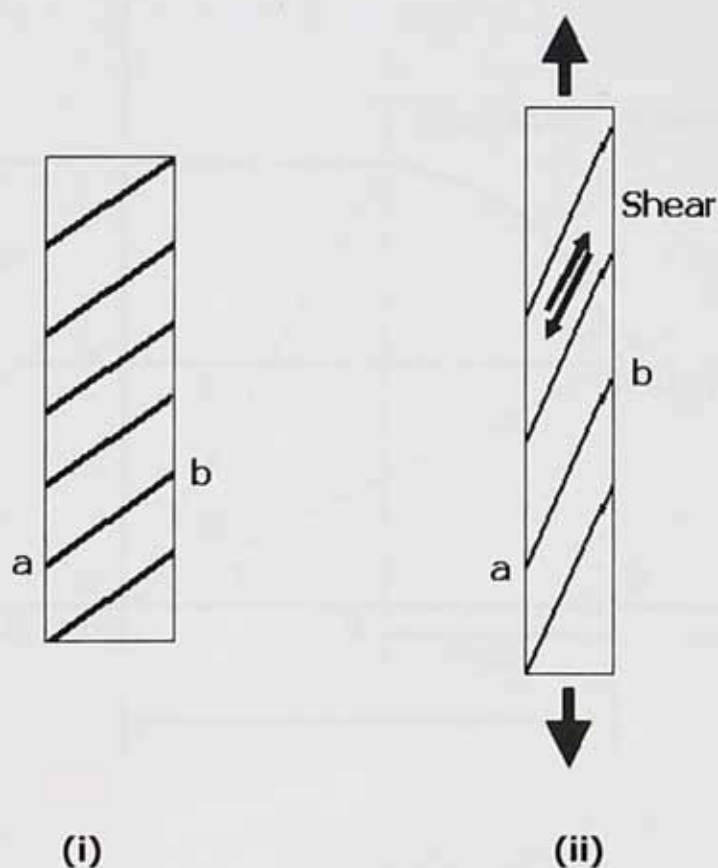


Fig 4.19 Fibres orientation (i) before stretching (ii) after stretching, ab represents a fibre lying along a line of tightness

Consider a rectangular shaped slab of material which is represented by rectangle "abcd" with height "v" and width "u" as shown in Figure 4.20. If a force "F" is applied along the y-axis, and assuming no translational or rotational motion of the rectangle of material, then due to the application of the force its height will be increase by an amount of $\partial v/\partial y$ and width will be decrease by an amount of $\partial u/\partial x$. The deformed rectangle "agfe" will then have a height of $(v + \partial v/\partial y)$ and the width of $(u - \partial u/\partial x)$.

If the diagonal (ac) of the rectangle before application of force is represented as OP and after application of force as OQ , then from the geometry of the Figure the coordinates of point P will be (u,v) and that of Q will be $(u - \partial u/\partial x, v + \partial v/\partial y)$.

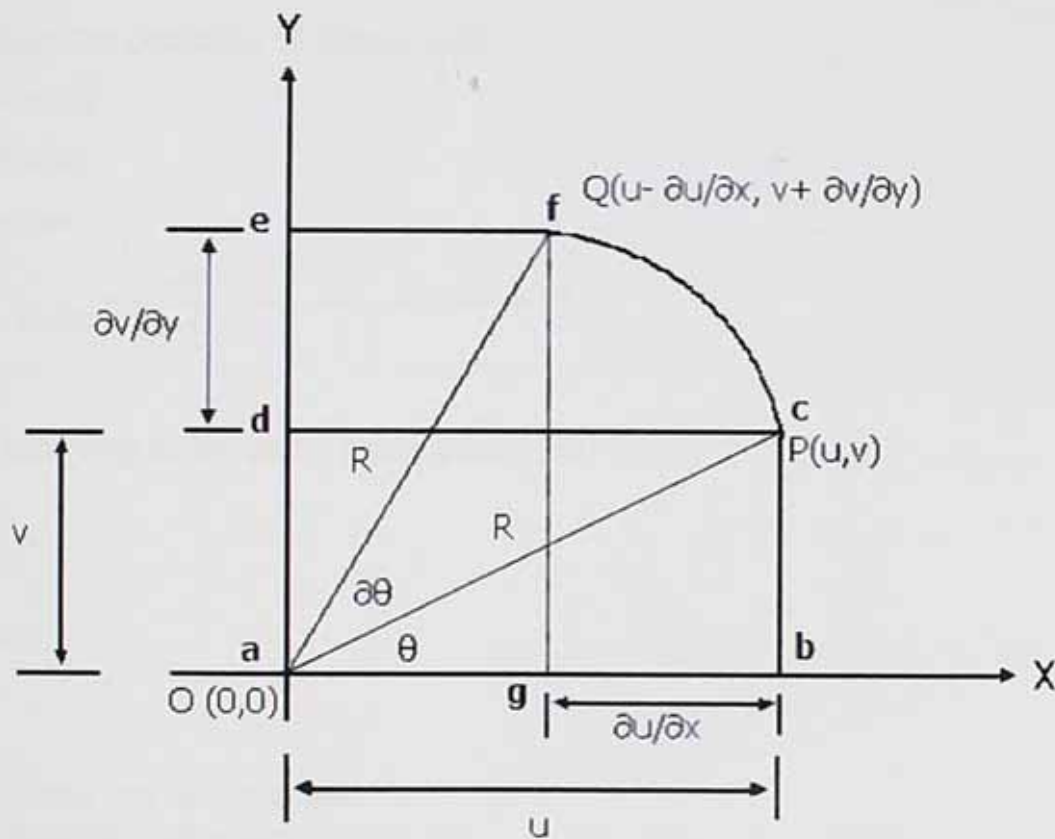


Fig 4.20 Analytical representation of direct and lateral strain

If the inclination of OP along the x -axis is θ , OQ will then have the inclination $(\theta + \partial\theta)$ following application of the load. If it is assumed OP and OQ are both equal

to R (due to shearing of fibres), then the arc subtended by R lies on the circumference of a circle with centre at the origin O (0, 0). It should then satisfy the equation of circle i.e.

$$X^2 + Y^2 = R^2 \longrightarrow (4.1)$$

Solving equation 4.1 for points P (u, v) and Q (u - $\partial u/\partial x$, v + $\partial v/\partial y$).

$$u^2 + v^2 = R^2 \longrightarrow (4.2)$$

$$(u - \partial u/\partial x)^2 + (v + \partial v/\partial y)^2 = R^2 \longrightarrow (4.3)$$

Expanding equation 4.3 and subtracting it from 4.2 then by neglecting the higher order terms the following relationship can be obtained.

$$2u\partial u/\partial x - 2v\partial v/\partial y = 0$$

$$\frac{\partial v/\partial y}{\partial u/\partial x} = u/v$$

But from the geometry of Figure 4.20

$$u = R \cos \theta$$

$$v = R \sin \theta$$

Therefore

$$\frac{\partial v/\partial y}{\partial u/\partial x} = \frac{\cos \theta}{\sin \theta} \longrightarrow (4.4)$$

Also according to the plane strain theory [73]

$$\frac{\partial u}{\partial x} = \epsilon_x$$

$$\frac{\partial v}{\partial y} = \epsilon_y$$

Where

ϵ_x = Strain in x direction and

ϵ_y = Strain in y direction

Therefore equation 4.4 can be written as

$$\frac{\epsilon_y}{\epsilon_x} = \cot \theta$$

Also Poisson's ratio (ν) is given by

$$\nu = \left(\frac{\epsilon_y}{\epsilon_x} \right)$$

$$\therefore \nu = \text{Cot}\theta \longrightarrow (4.5)$$

In Figure 4.21, the results obtained by using equation 4.5 and those obtained from dried under strain (20%) sample are shown.

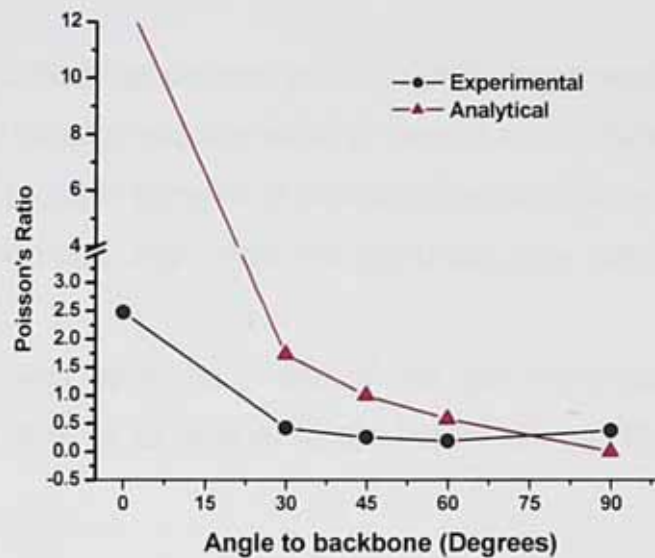


Fig 4.21 Comparison of analytical and experimental data for dried under strain (20%) samples

Analytically the value of Poisson's ratio in equation 4.5, at lower values of angle i.e. 0 degrees, will be unrealistic which are experimentally not possible. As the material is stretched and fibres come into alignment, the thickness and spacing of the fibres themselves will affect the extent to which the fibres can reorient. Alternatively, factors which limit deformations perpendicular to the plane of hide (3D network of collagen fibres) would result in behaviour grossly different from our simplified model. The complexity of leathers due to its fibrous structure and the simplicity of the theory mean that a close agreement of the mathematical and experimental data is not found. However the theory accounts for observed trends of higher Poisson's ratio values at low angle to line of tightness and lower values of Poisson's ratio at higher angle. The theory assumes perfect fibre alignment

along a line of tightness, which in practice this does not occur [48]. However it is interesting to work from Figure 4.17 that as the strain under which the leather is dried increases Poisson's ratio increases. The possible reason is the more perfect alignment expected at higher applied strain implies a close correspondence with the theoretical analysis as is observed.

4.6 Auxetic Behaviour of Leather

Auxetic materials exhibit the unusual property of having a negative Poisson's ratio. That is, they expand laterally while in tension and contract laterally when in compression. The possible benefits of auxetic behaviour did not begin to receive serious consideration until 1987, with the manufacture of the first synthetic, auxetic foam [74].

Auxetic behaviour was observed in one of the specimens cut from uncontrolled sample, stretched 30% of its original length before drying. The results are shown in Figure 4.22.

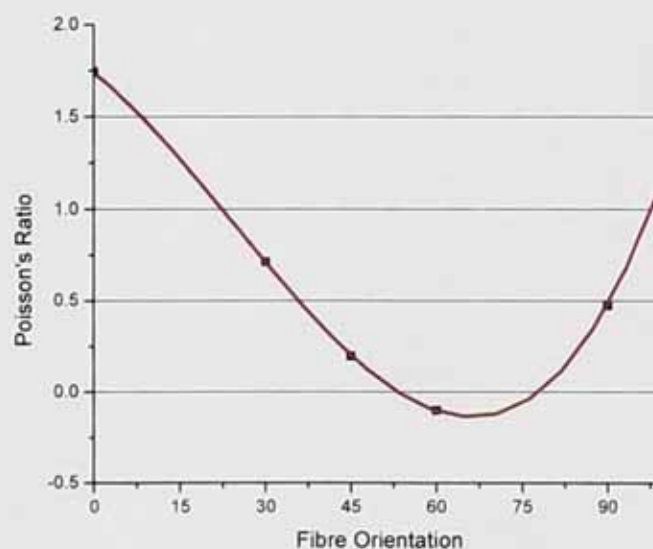


Fig 4.22 Auxetic behaviour of leather

As leather is a natural material, experimental work with it is never easy because it is impossible to exactly repeat a test in a particular area, and direction. If samples were to be cut from another skin of the same kind and treated in the same way, it would be difficult to predict the differences in mechanical behaviour from the present results.

4.7 Conclusion

It can be concluded from experimental work on linear stretching of leather, that along the lines of tightness, Poisson's ratio values are high while strain values are very low. Therefore in order to determine these lines along the whole surface of hide/skin there are two possible ways. One is by measuring the Poisson's ratio and the other is by measuring the lowest strain values.

5 Bi-Axial Stretching of Leather

The validity of techniques to determine the lines of tightness has been investigated by applying the technique on small pieces (*Section 4.5.2*). There was a need to apply the technique on larger pieces to further check the application on a whole hide/skin. Therefore a new series of experimental procedures were performed on large rectangular shape pieces by using a bi-axial tensile machine supplied by Deben UK. This machine consists of four sets of five sliding grips, which are 90° to each other as shown in Figure 5.1.

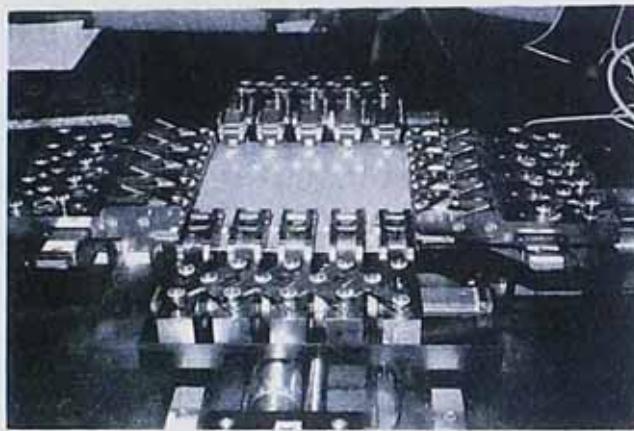


Fig 5.1 Biaxial testing machine

Two sets of grips on each of the orthogonal axes (X and Y) can be controlled by a stepping motor, which is connected to the computer by transducers to measure both load and extension along each axis. Each set of grips is mounted on a slider and linked together by a concertina formation of links in order to allow a controlled lateral movement of the grips to accommodate an extension of the sample in this direction. When all the grips are positioned as close as possible to each other it can hold a sample having dimensions of 145 x 145 mm and similarly when they are apart from each other it can hold a sample having maximum dimensions of 220 x 220 mm.

The interest was to stretch the maximum rectangular sample to achieve more information about line of tightness within the sample. Therefore for the whole series of this experimental work a sample was used having dimensions of 220 x 220 mm which gave a gauge length of 180 mm.

5.1 Determination of Lines of Tightness of Leather for Large Pieces

Three different methods, based on the findings described earlier (*Chapter 4*) were investigated.

5.2 Method 1: Lateral Contraction Method

It was concluded from the experiments previously described (*Section 4.5.2*) that along the directional runs of fibres (*lines of tightness*) the value of Poisson's ratio is higher. Based on this technique the Poisson's ratio was determined in different parts of a piece of leather. This method is termed the Lateral Contraction Method thereafter.

5.2.1 Material

Skin obtained from a UK tannery was processed using the facility available in the BSLT tannery in accordance to a commonly used process for leather manufacturing (*Section 1.1*).

5.2.2 Sample Preparation

To obtain samples with straight edges, a cutting die having dimensions of 220 x 220 mm was placed vertically on the material and a sample was cut from the butt area of the hide using a press. An array of 25 circular spots having diameter of 5mm and centre-to-centre distance of 30mm was then stamped on the central portion of sample. This is shown in Figure 5.2.

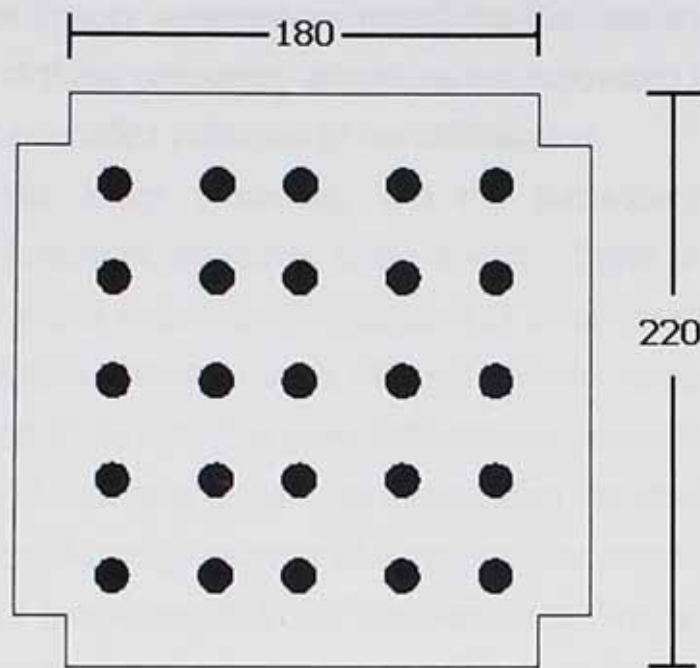


Fig 5.2 Array of spots used on large pieces of leather

5.2.3 Methodology

The same methodology (*Section 4.3.1*) was used as that for small pieces, by isolating the marked spots from the background and then determining their location. There was a need to divide the whole surface area of the samples into smaller areas and thus calculating the direct and lateral strain for each area to measure the Poisson's ratio. As deformation over large areas is being characterised in a uni-axial loading case, a large extension yields a substantial change of the transverse dimensions. This substantial change in lateral dimensions was used to determine the lateral deformation and consequently the Poisson's ratio for each location.

To calculate the lateral and direct strain values for each location over the whole surface a new technique known as "*The Photonical, Pure Grid Method*" [75] was adopted to determine the location of the grids spots in each consecutive image

captured after application of stroke. This technique has been successfully applied to measure local deformation in larger areas [76]. The methodology involved the processing of two images separately by measuring the location of grid spots and then the results of these processing operations are subtracted from each other in order to obtain a quantified indication of the deformation.

The speed of the image processing and the subsequent computation of deformation characteristics are related to the number of grid spots applied on the surface. From previous experiments (*Section 4.2*) it has been shown that it is possible to characterise the strain at six different sections along a gauge length of 160 mm and width of 25 mm. The same methodology was adopted (*Section 3.2*) for current series of experimental work by thresholding the whole image.

An array of grid spots having diameter of 5 mm and the centre-to-centre distance of 30 mm along a gauge length of 180 mm was used. The grid method is then applied by dividing the whole square array of spots into 16 triangles as shown in Figure 5.3.

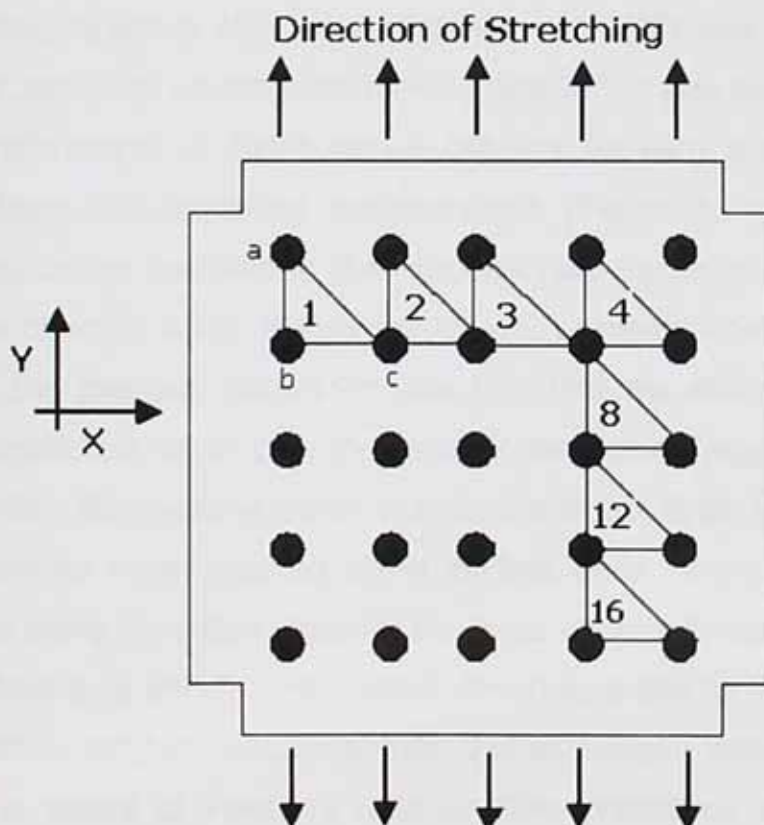


Fig 5.3 Schematic diagram of the triangles used to determine direct and lateral strain by Grid Method

When sample appeared on the imaging window, the upper left most corner of the sample is considered as the origin. The location of each dot in terms of coordinates is determined after thresholding the image. By using the coordinate value direct strain was calculated using displacement measurements for spots "a" and "b" and lateral strain using spots "b" and "c" located as vertices of triangle 1 in Figure 5.3. The same procedure is applied for each deformed and un-deformed triangle before and after the application of stroke. This gave Poisson's ratio values at all 16 locations over the surface.

5.2.4 Results and Discussion

Previously described experimental work (*Section 4.5.2*) showed that the value of Poisson's ratio decreases as fibre orientation with respect to the stretching axis is increased. A higher value of Poisson's ratio was observed if the fibres are predominately oriented along the stretching axis (0°) and a lower value was observed if fibres are oriented between 60 and 90° . It was also observed that the Poisson's ratio profile or distribution is different for each region (*Section 4.3.2*). However from our modelling approximation (Figure 4.21) a range of fibre orientations can be assigned to the Poisson's ratio values in order to predict the actual fibre direction within the sample. It was observed from recent work in this study and the previous studies on skin [77] that the Poisson's ratio values of smaller samples are lower than the values obtained for large sample taken from the same hide. The possible reason may be the lateral strain values, which for the smaller samples were obtained along its free ends having partially entangled loose fibres along the edges while for the large samples it was measured over the whole surface thus affecting the lateral dimensions due to fibres recruitment. It was also observed both experimentally and analytically that there was a sharp decrease in values of Poisson's ratio as fibre orientation increases along the loading axis. These values then start increasing with a small difference and showed very low positive gradient. The Poisson's ratio distribution with respect to

the fibres orientation allowed the hide to be divided into three regions. In the first region the Poisson's ratio has the highest values. In the second region the Poisson's ratio starts to decrease sharply. Finally, in the third region the Poisson's ratio starts to increase with a low gradient.

The total percentage decrease between highest and lowest values of Poisson's ratio of the whole sample was calculated. This total percentage was then further divided into three intervals thus assigning each value to the three ranges of $0-10^{\circ}$, $15-50^{\circ}$ and $55-90^{\circ}$.

In Table 5.1 the calculated range of Poisson's ratio values with corresponding range of fibre orientation for sample stretched perpendicular to the backbone at an applied stroke of 60 mm are shown and in Figure 5.4 the expected preferential fibre orientation based on Poisson's ratio values at different region are drawn manually.

It was observed that the difference between lowest and highest value of Poisson's ratio was very low along the whole region of the sample. Almost the same results were obtained for a smaller sample when determining the Poisson's ratio values along its gauge length (*Section 4.3.2*). This small difference in values of may be overcome if a larger area of hide is stretched. However, using the results of previous experiments on small samples taken from butt, belly and neck regions, the lowest Poisson's ratio value for the belly region (0.914) was higher than the highest value of the butt region (0.888). This would result in a great discrepancy while allocating the calculated range of Poisson's ratio values for each level of fibre orientation i.e. due to the higher value assigned to low fibre orientation the expected lines of tightness for butt region will always be perpendicular to the loading axis which is actually not possible.

Table 5.1 Preferential fibre orientation for different values of Poisson's ratio

Poisson's Ratio Values (Experimental)	Percentage	Calculated Values of Poisson's Ratio	Intervals
1.13 (Max)	15.93%	1.130 → 1.069	0-10°
		1.069 → 1.059	15-50°
0.95 (Min)		1.059 → 0.964	55-90°

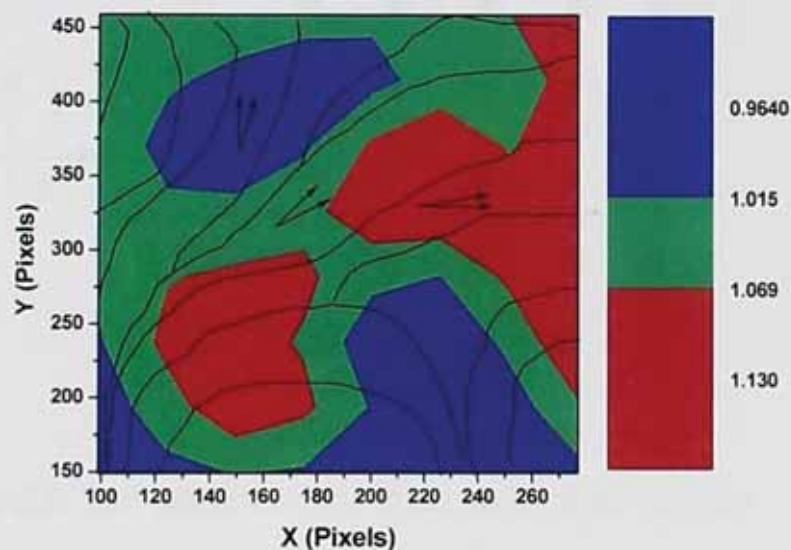


Fig 5.4 The expected lines of tightness based on the local Poisson's ratio values

5.3 Method 2: Uni-Axial Constraint Method

A new methodology was investigated using the biaxial testing machine on a control and dried under strain sample. The control sample was chrome tanned finished shoe upper, while wet blue was used as before for drying under strain. The wet blue sample was marked with equidistant parallel lines in the backbone direction before drying under strain. The sample was then stretched around 20% of its original length in the backbone direction by using the set up and

methodology used for uni-axial stretching (*Section 4.4.1*) of small samples. The marked lines were parallel to the Y-axis and considered to be known direction *Lines of Tightness* in the sample. Four samples having dimension of 220 x 220 mm were taken at angles of 0, 30, 45, 60 and 90° along the lines of tightness. All the samples were then marked with an array of spots and images were captured before and after application of load. In Figure 5.5 actual image of sample having lines of tightness at 90° to the Y-axis has shown.

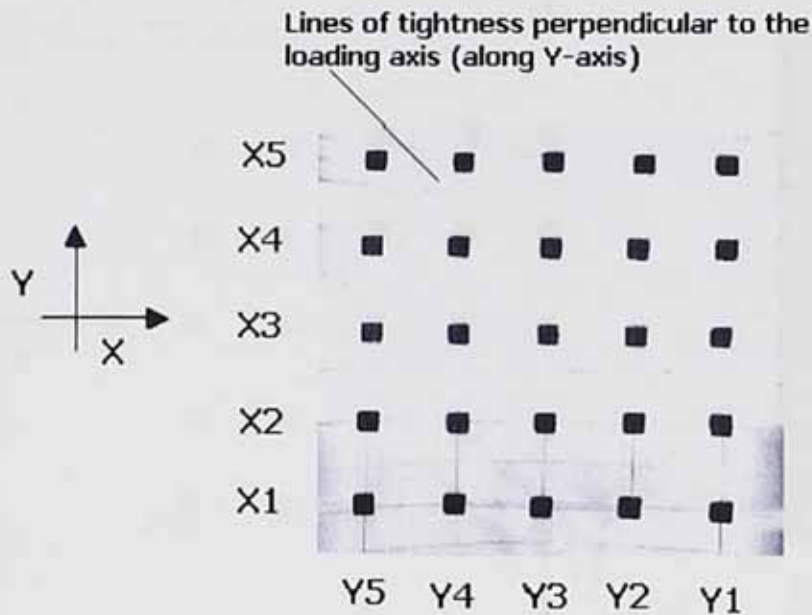


Fig 5.5 Spot pattern on the dried under strain sample

The sample was located in the biaxial testing machine with each of its five grips covering each edge at position X1 to X5 and Y1 to Y5 along X and Y-axis respectively. Strain was measured at an applied load of 100N along Y and X-axis for different orientation of known lines of tightness i.e. 0, 30, 45, 60 and 90°. The sample was stretched in Y direction to measure ϵ_y by actuating one grip each time i.e. grip Y1 to Y5 while the grips in X direction were stationary. This would result in $\epsilon_{yx}=0$ (Strain in X direction while applying load in Y direction). This strain value was measured by locating (*Section 3.2.2*) marked spots along each active grip. Instead of thresholding the whole image, the spots located along the direction of active grip (Y1) were selected, which was region of interest. This

reduced the computational time to find the location of spots, as when a window size enlarges, the computational time increase. Figure 5.6(a) shows the actual image of the sample after application of load by using grip along Y1 direction while all grips along X-axis direction kept stationary and Figure 5.6(b) shows the image to locate the position of the spots after thresholding.

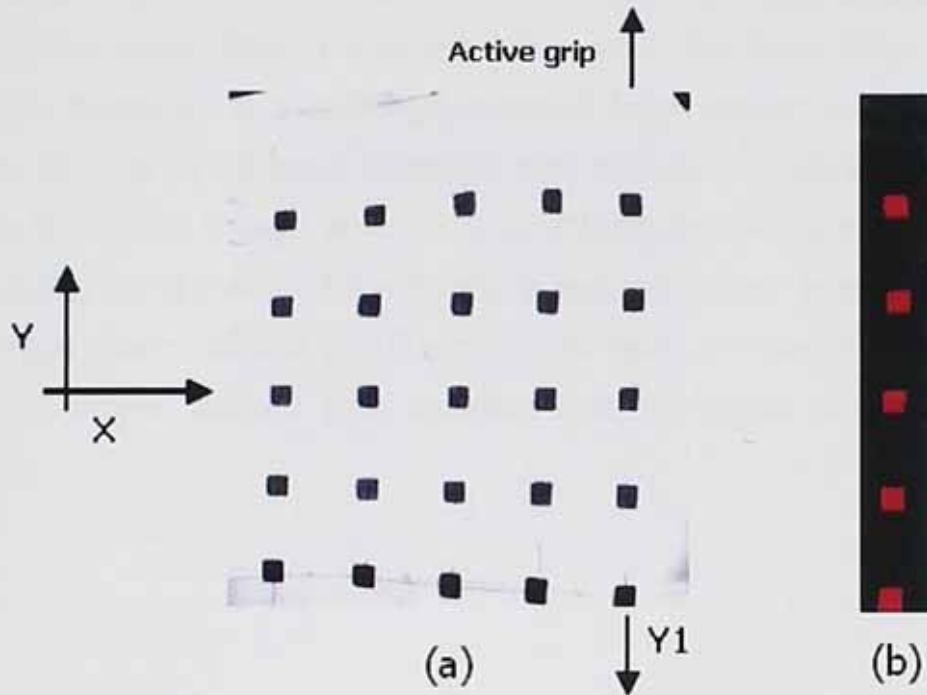


Fig 5.6 Sample stretched along Y-axis by using grip Y1 (a) Extracted spots along the Y1 axis after thresholding the image used to locate the position of spots (b).

Similarly the sample was stretched in X direction by actuating each grip individually to measure ϵ_x . This would give biaxial strain values at sixteen different locations with respect to the direction of lines of tightness.

5.3.1 Results and Discussion

It was observed from earlier experimental work on uni-axially stretched samples (*Section 4.5.2*) that the strain value will increase as the angle between applied load and the direction of lines of tightness increases. Almost the same behaviour was observed for large samples stretched while constrained laterally. Relatively small values of strain were observed when both the direction of applied load (Y-axis) and the known lines of tightness are parallel. The strain value increases as the angle measured in a clockwise direction from applied load to the known direction of lines of tightness increases and achieves its maximum value when both are orthogonal to each other i.e. lines of tightness are parallel to X-axis while load is acting along Y-axis. This relationship between known lines of tightness and the average strain value of all 16 locations for both X-Y directions has shown in Figure 5.7 where marked lines between dots represents the known lines of tightness.

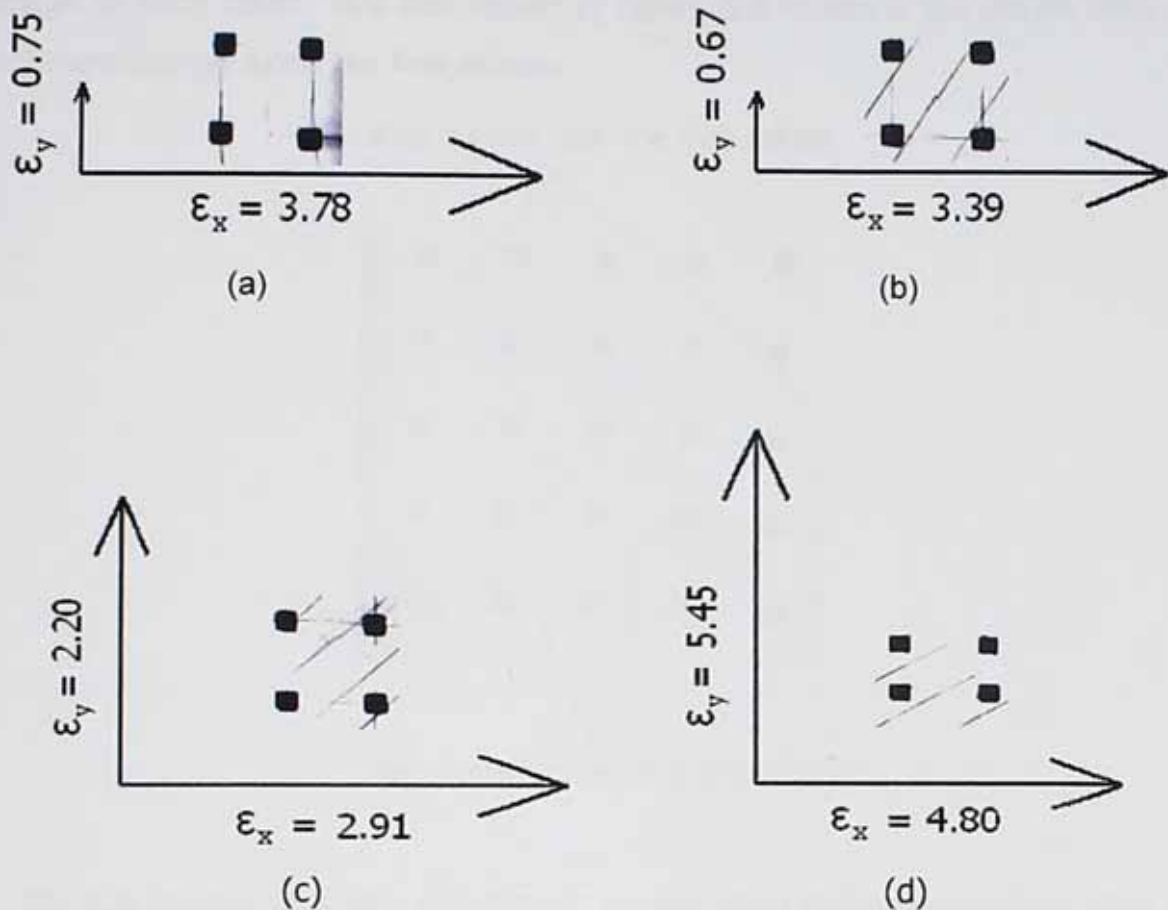


Fig 5.7 Biaxial strain values of sample having lines of tightness oriented at 0 and 90° (a) 30° (b) 45° (c) and 60° (d) measured along Y-axis.

To represent the strain value of 0° and 90° samples, the same sample was used i.e. Fig 5.7(a). In which ϵ_y denotes the strain value when both direction of applied load and known lines of tightness are parallel to each other (0°) and ϵ_x was considered when the direction of applied load and known lines of tightness are perpendicular to each other (90°) i.e. when sample was stretched along the X-axis.

The possible reason for ϵ_y (0.75) for 0° being slightly higher when compared with ϵ_y (0.67) at 30° would appear to be due to a Poisson's ratio effect. Because of this the known lines of tightness actually followed a curved pattern near the free edges where as they were almost parallel at the centre when the samples were

dried under strain. The curves along the free edges on each side were same image of each other. This has shown in Figure 5.8 in which the drawn lines of tightness curved along the free edges.

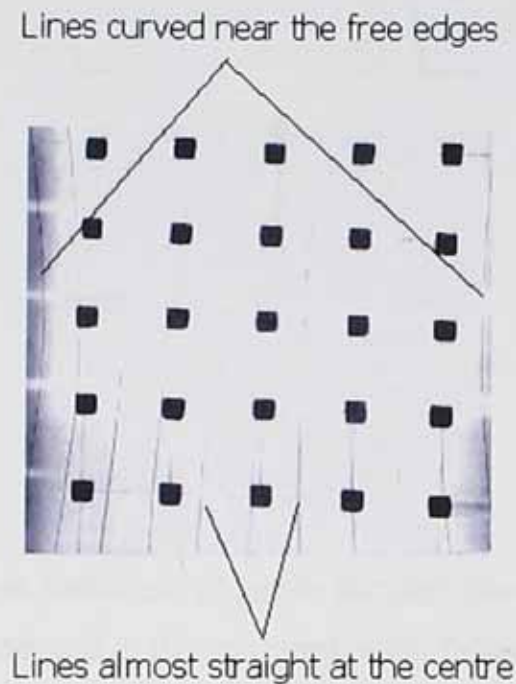


Fig 5.8 Sample with lines of tightness curved along its free ends when dried under strain

The actual strain values for all locations across the whole sample of all different orientations are shown in Figure 5.9 (a) to (d) in which the direction of induced lines of tightness has shown by bold arrow. It was observed that at some points mostly in the 0° and 30° samples the strain values in one direction are very low to represent in vector form as compared to other direction. The possible reason for this is the presence of lines of tightness along the direction of constraint. Also in the 45° samples the majority of strain values for both directions are equal to each other but in 60° sample the majority ϵ_y values are slightly higher as compare to ϵ_x values.

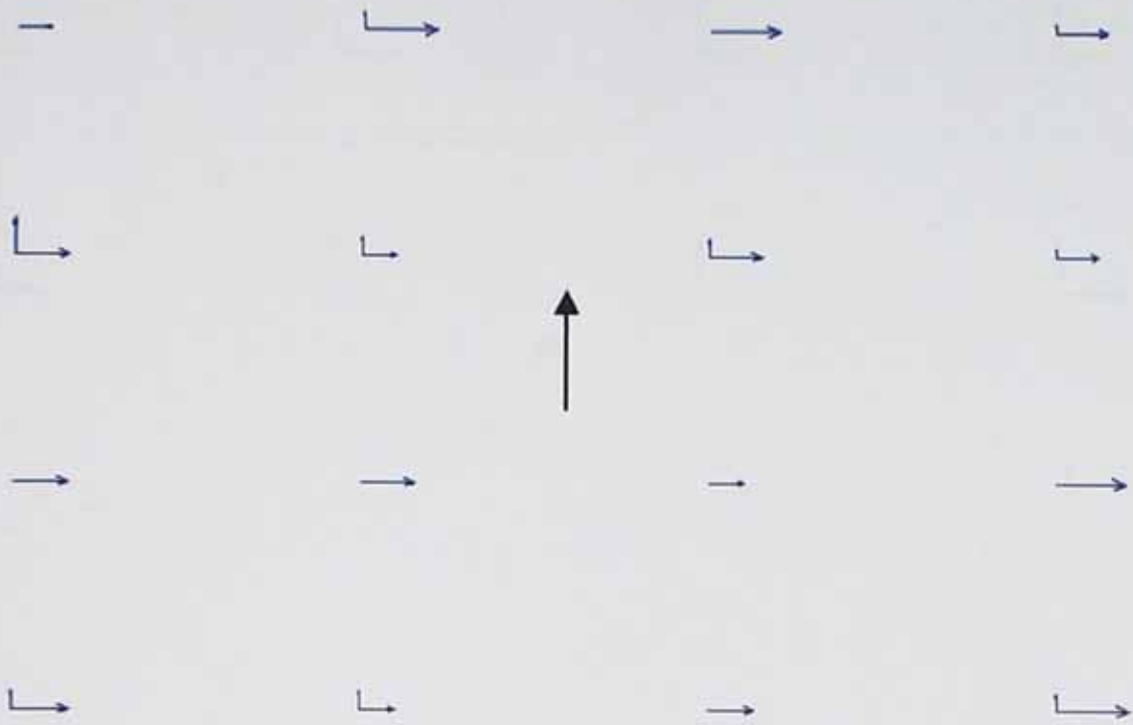


Fig 5.9(a) Anisotropic behaviour of larger samples having lines of tightness oriented at 0° measured along Y-axis.

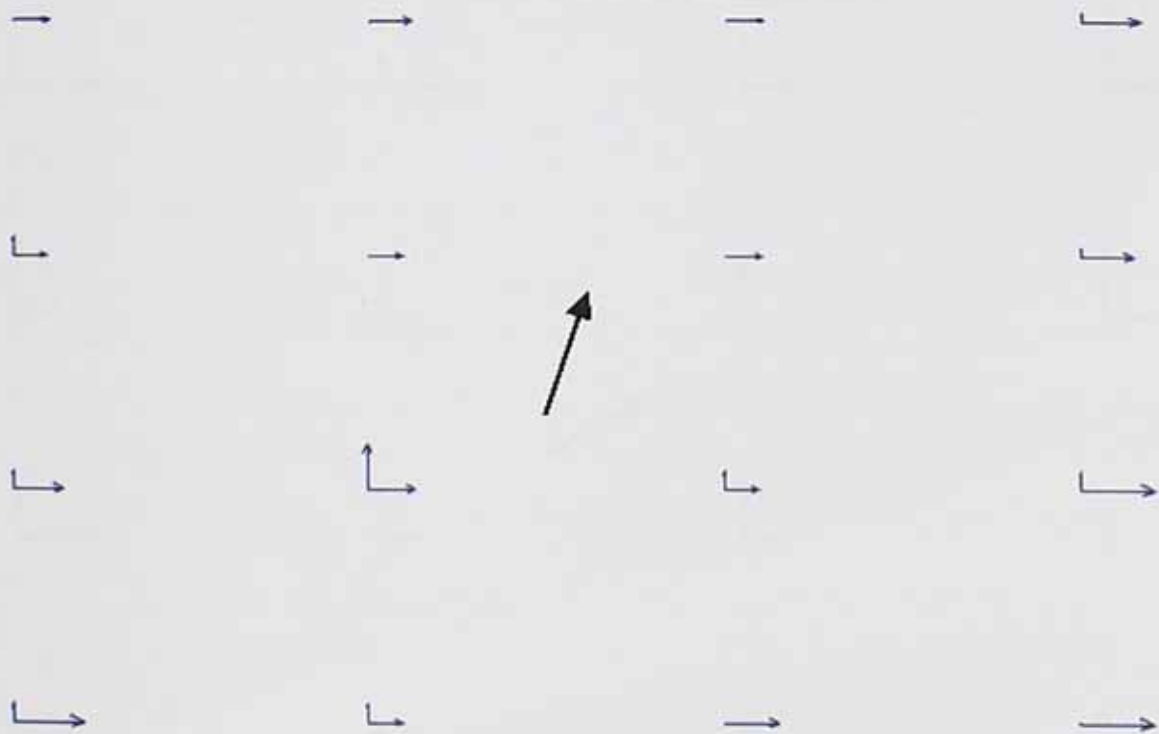


Fig 5.9(b) Anisotropy behaviour of larger samples having lines of tightness oriented at 30° measured along Y-axis.

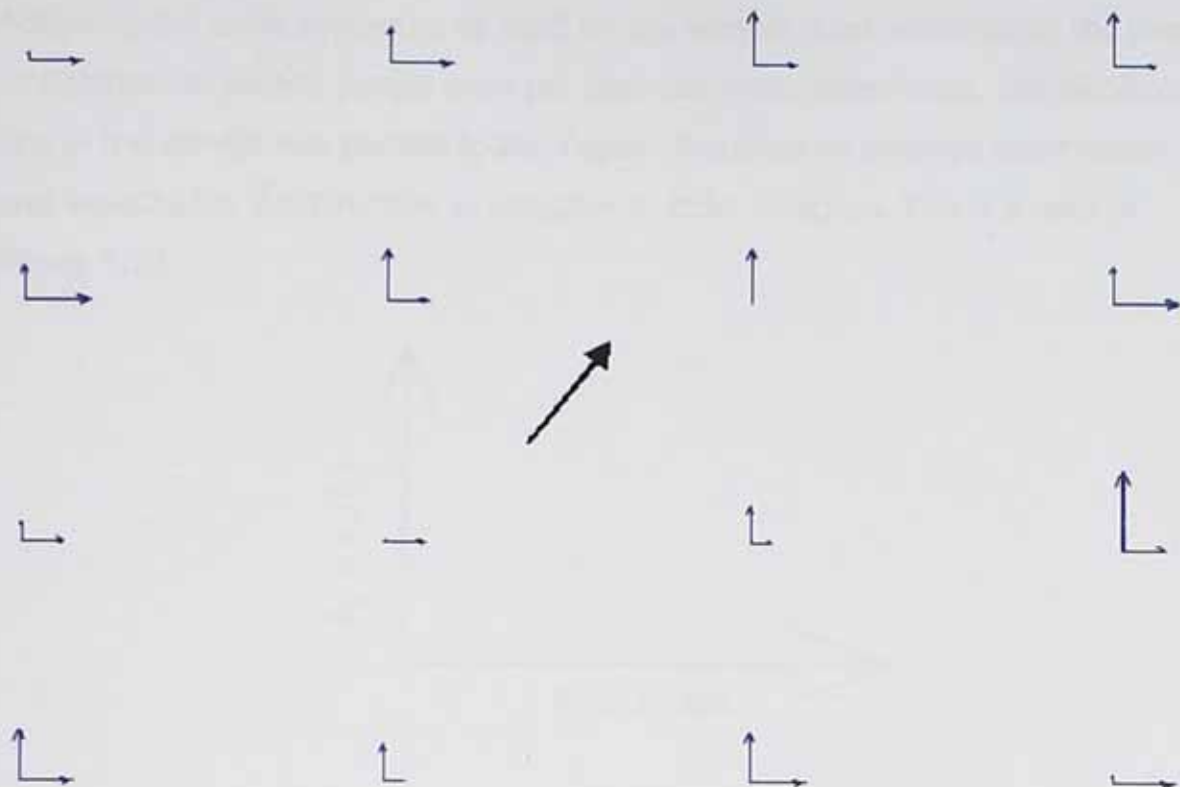


Fig 5.9(c) Anisotropy behaviour of larger samples having lines of tightness oriented at 45° measured along Y-axis

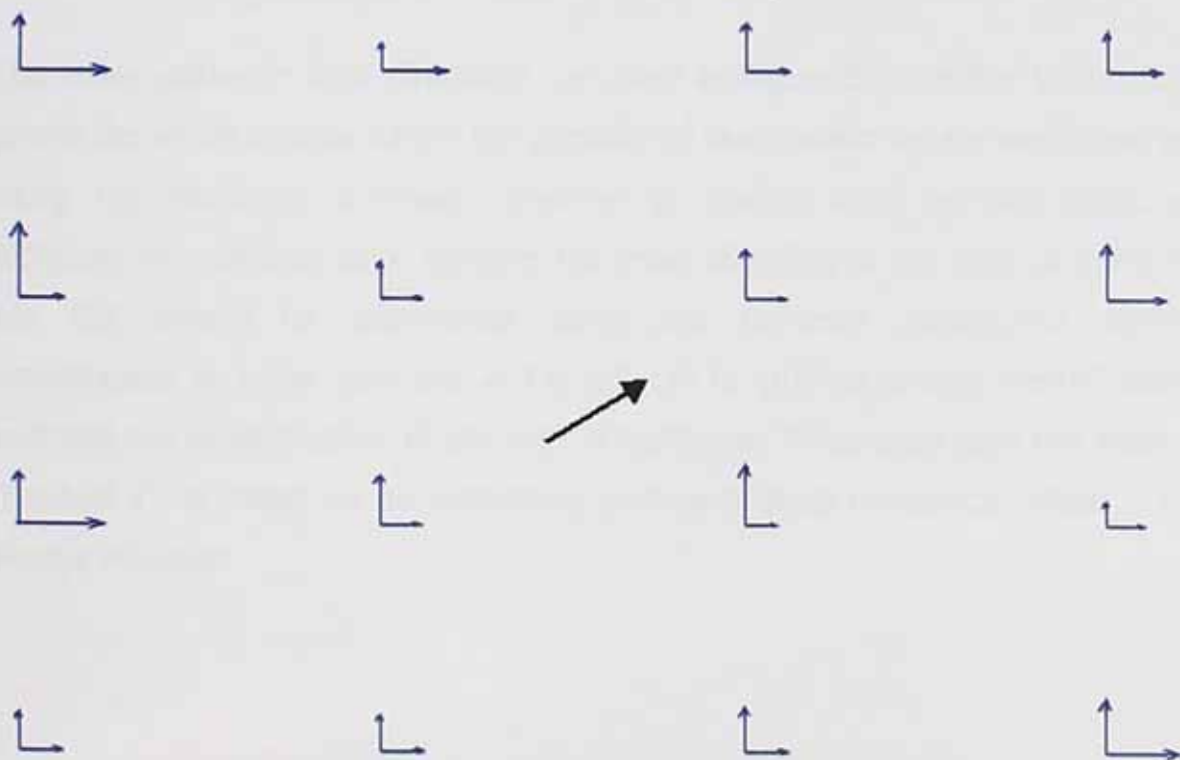


Fig 5.9(d) Anisotropy behaviour of larger samples having lines of tightness oriented at 60° measured along Y-axis.

Following the same procedure as used for the sample dried under strain the lines of tightness in control sample (non-pre strained) were determined. The backbone line of the sample was parallel to the Y-axis. Therefore an average lower strain was expected in this direction as compare to other direction. This is shown in Figure 5.10.

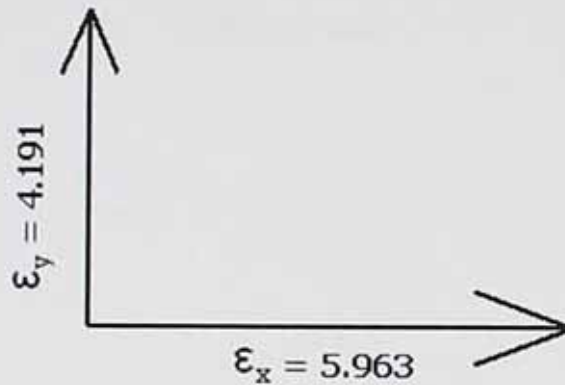


Fig 5.10 Average strain value of control sample having backbone parallel to Y-axis

The strain values in both directions are given in Figure 5.11 at the 16 locations across the whole sample where the majority of lower strain values were observed along the backbone direction (direction of loading axis) as was expected. Although for relatively large samples the exact direction of the lines of tightness can not always be determined using this uni-axial constrained method nevertheless at some locations in Fig 5.9 (a) to (d) the smaller vector values indicates the exact location of the lines of tightness. To be clear then this method (method 2), is based on an estimation of lines of least resistance, which is not always accurate.

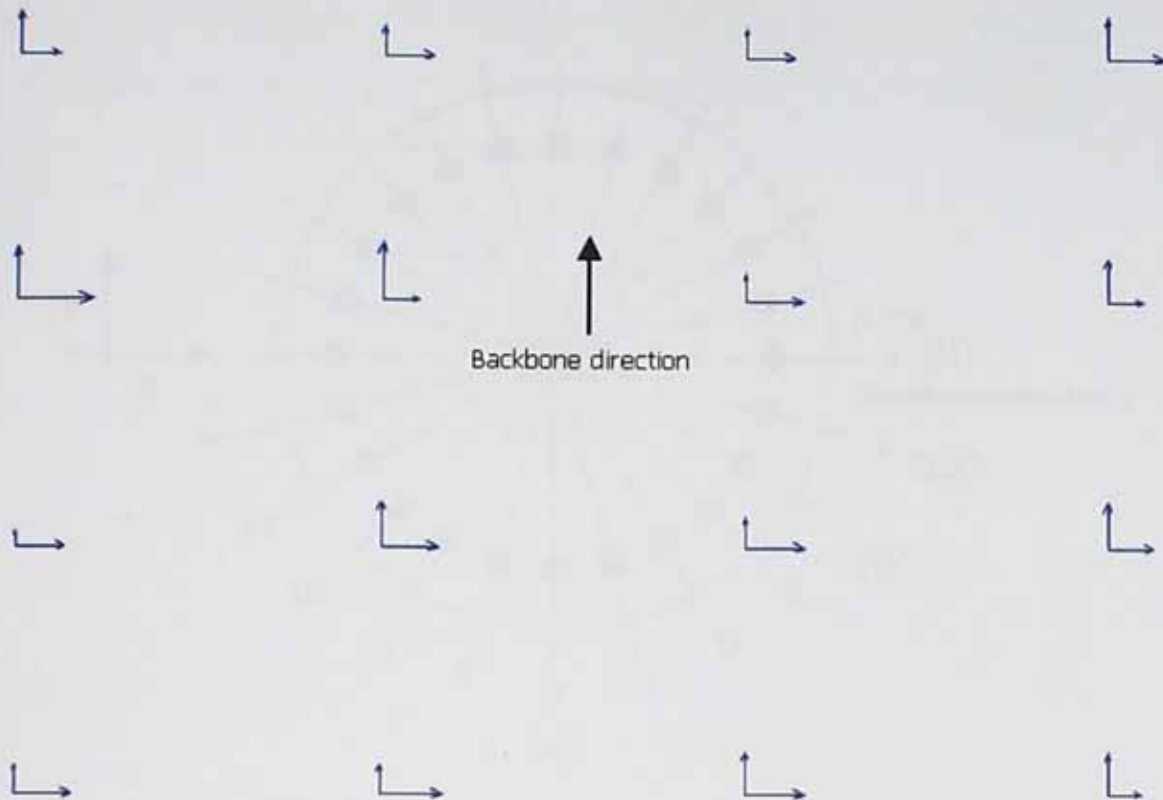


Fig 5.11 Anisotropy behaviour of the large control sample

5.4 Method 3

In previously described experimental work (*Section 3.2.2* and *5.3.1*) it was observed that the strain in the predominant direction of fibres is not affected if the side ends of the sample are gripped or left as free. This has led to the possibility of applying another technique in which the load is applied at various angles to determine strain along a particular direction. The methodology involved the marking of spots along the periphery of a circular sample at an angular interval of 15° and then stretching it along the known value of direction measured in clockwise direction from an axis coinciding with the backbone direction while holding along other directions (*Section 5.3.1*). This provides the possibility of measuring the strain along 12 possible directions as shown in Figure 5.12.

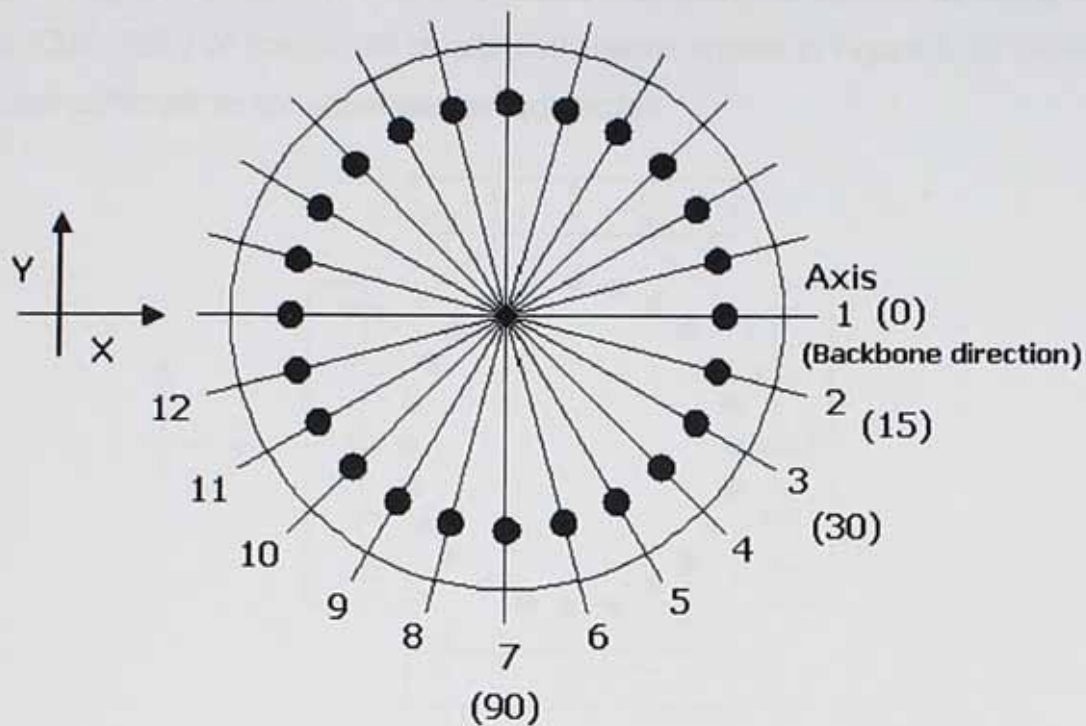


Fig 5.12 Directions of applied load on the circular sample

A circular shaped cutter having diameter of 220 mm was used to cut the samples from different locations along the whole surface of the hide. The sample was then marked with a spot pattern the spots having diameter 4 mm giving the diameter of the grid lines as 130 mm. The validity of the methodology was ascertained by first applying it on a sample dried under 10% uni-axial strain (*Section 4.4.1*). The methodology was then applied on finished samples obtained from different location of a whole hide.

The initial direction of applied load on the sample was parallel to the backbone (0°) referring to a coordinate system with X-axis coinciding with the backbone line as shown in Figure 5.12. The sample was then rotated manually in a clockwise direction for each 15° interval by making sure that each pair of spots was at the same line of action of the central grips along the X-axis. This continued until the starting point was reached. In order to measure ϵ_x for each pair of opposite spots while maintaining $\epsilon_{xy} = 0$, the load was only applied by using the central grip of each set of grips (AB) along X-axis direction. But in the Y-axis direction due to the

circular shape of sample it was only possible to hold the sample by using three grips (CDE, FGH) of the biaxial tensile machine as shown in Figure 5.13. However this was sufficient to constrain lateral contraction.

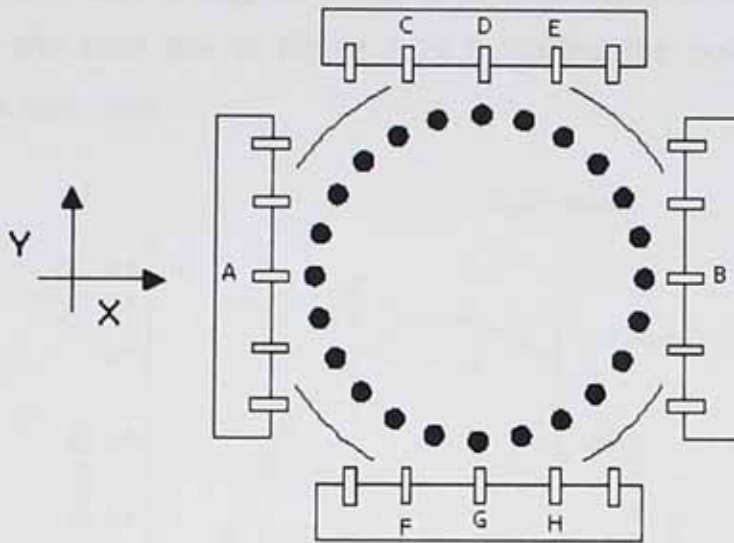


Fig 5.13 Circular shaped sample hold on biaxial tensile machine marked with grids at an interval of 15°

The strain was then measured for each pair of spots (*Section 3.2.2*) at an applied load of 100N.

5.4.1 Results and Discussion

It was observed from the previously described series of experimental work on uniaxial stretching of pre-stretched sample (*Section 4.4.1*) that as the angle measured between lines of tightness and the loading axis increases, the strain value also increases (Figure 4.16) and it attains its maximum value when both loading axis and the direction of lines of tightness are orthogonal to each other. Almost the same behaviour was observed for the present series of dried under strain samples. A significant increase in strain values was observed, as the angle between loading axis and lines of tightness increased, with the lowest value of strain close to the direction of pre-stretching as was expected. This increase in

strain values peaks as the loading axis and the preferred fibres orientation becomes orthogonal, beyond that its starts again decreasing following almost the same pattern as it was before. In order to provide a mean of characterising a polynomial function of degree 2 was applied to model the data. The results are shown by the solid line in Figure 5.14 indicating the polynomial function with 0.5% error distortion.

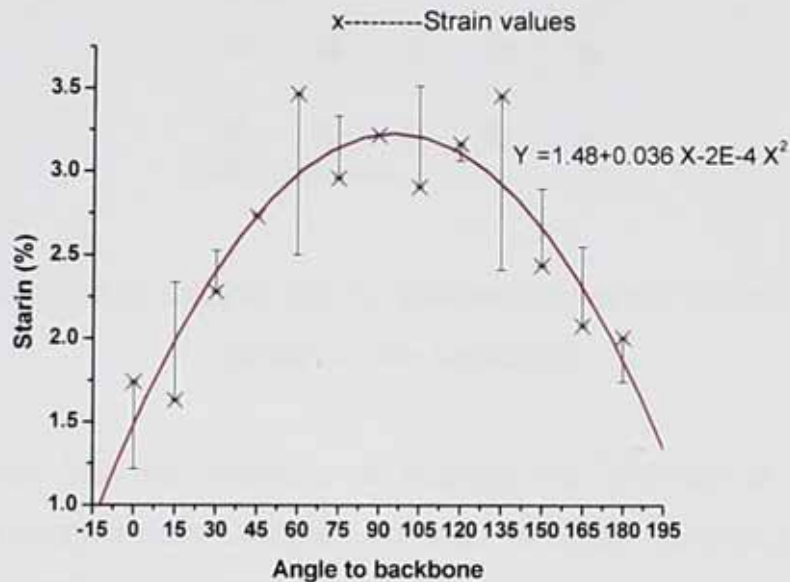


Fig 5.14 Strain along different degrees in a circular sample cut from dried under strain leather

It was observed (Figure 5.14) that the curved pattern is almost symmetric about the high orientation of fibre and the loading axis. The possible reason may be predominate orientation of the fibres about 90° . In Figure 5.15 the direction for few loading axis e.g. 0, 60, 90 and 120° are shown. It can be estimated that the majority of fibres orientation along 60 and 120° will be alike.

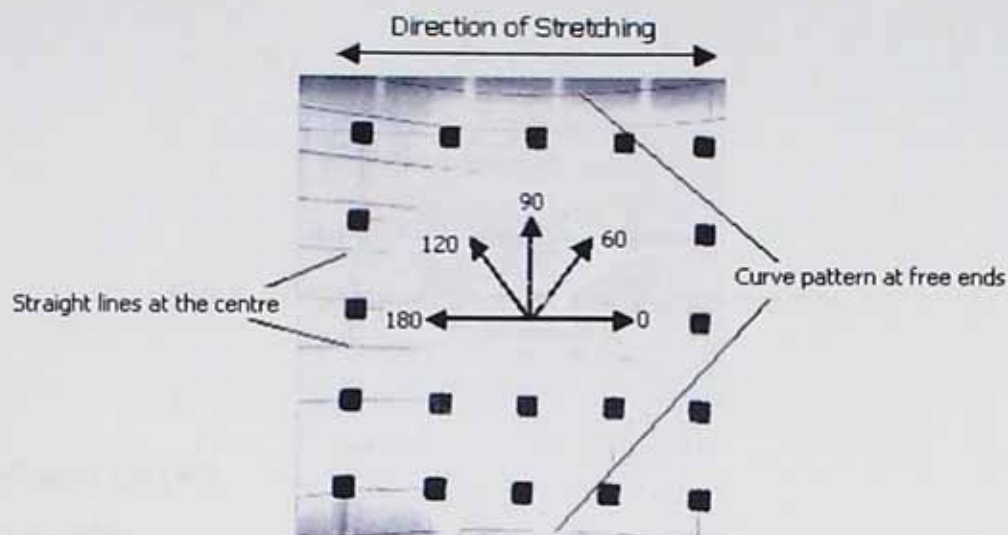


Fig 5.15 Direction of loading axis for sample dried under strained stretched parallel to the backbone

Due to complex internal structure of leather, the analysis of their material properties can become quite complex. In order to better describe the mechanical behaviour of leather as observed from our experimental results further mathematical modelling was applied.

5.4.2 Mathematical Modelling

The main objective of this research was to determine as accurately as possible the direction of lines of tightness over the whole surface of a hide. It would therefore be advantageous if a mathematically defined curve could be fitted to the data which would allow a precise estimate of the angle of minimum strain. A piece of software known as OriginPro 7 was used for mathematical modelling. A *Gaussamp* function was investigated. The equation of the function is defined as follows.

$$y = y_0 + Ae^{-\frac{(x-x_c)^2}{2w^2}} \longrightarrow (5.1)$$

A curve of equation (5.1) is shown in Figure 5.16

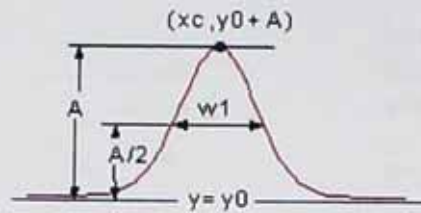


Fig 5.16 Sample curve for Gaussamp function

Where

$$2w = w1/\text{sqrt}(\ln(4))$$

y = Strain value

A = Area for xy curve,

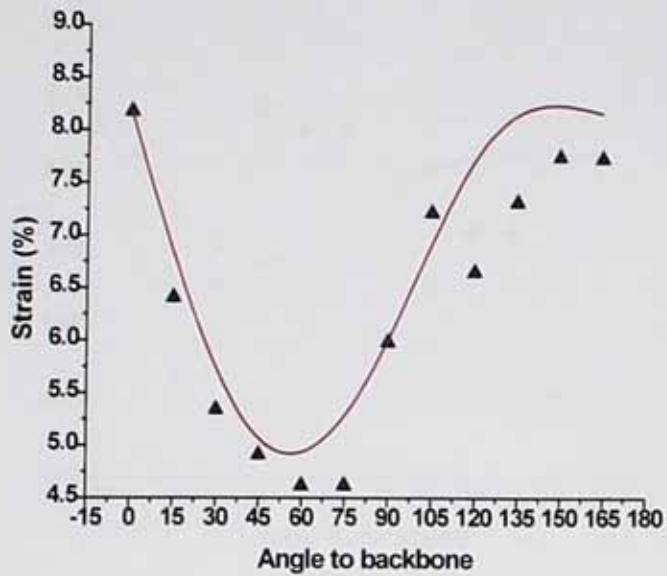
x = Orientation of fibres

w = width of the curve

The following assumptions were made

The predominant direction of fibre orientation and therefore line of tightness is approximately parallel to the backbone and so lower strain values are expected along this direction. Therefore the initial strain measurement axis is set parallel to the backbone (Axis 1 in Figure 5.12). A decision then needs to be made as to whether the parameter 'A' is positive or negative. This will depend on the quality of data. If peak is best defined then 'A' is selected as positive. If a trough is best defined then 'A' is selected as negative. If we selected 'A' as negative then x_c will represent the direction of minimum stretching (i.e lines of tightness). If we selected 'A' as positive x_c will give direction of maximum stretching (assuming symmetry the direction of minimum stretching or lines of tightness could be estimated as at 90° to this direction, Fig 5.17.b).

The application of the *Gaussamp* model to the butt, neck and belly regions is shown in Figure 5.17(a) to (c) respectively while the results for these regions are attached in *Appendix E*.

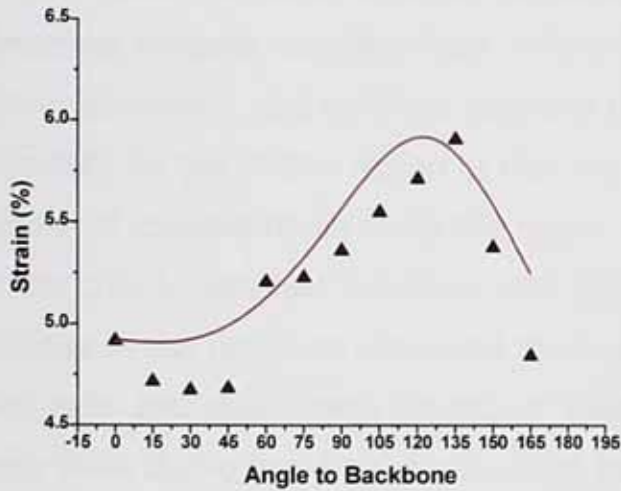


Butt Region
 Model: GaussAmp
 Equation:
 $y=y_0+A*\exp(-0.5*((x-xc)/w)^2)$

R² = 0.88907

y0	8.176	
xc	59.85796	±3.18255
w	35.93991	±2.85058
A	-3.559	

(a)

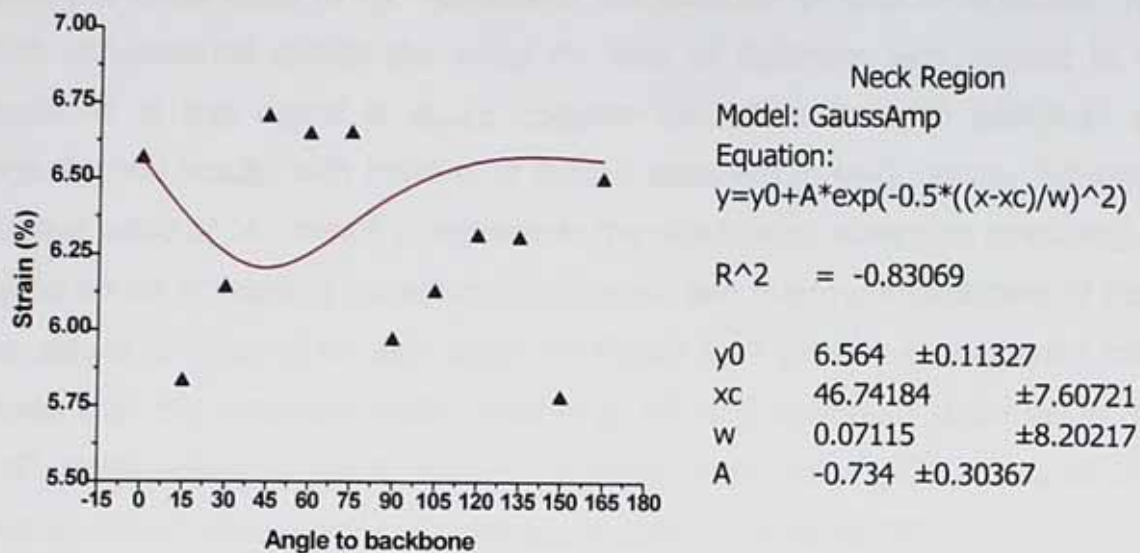


Belly Region
 Model: GaussAmp
 Equation:
 $y=y_0+A*\exp(-0.5*((x-xc)/w)^2)$
 Weighting:
 y No weighting

Chi²/DoF = 0.04199
 R² = 0.80231

y0	4.917	±0
xc	120.51986	±4.83525
w	25.43466	±4.99481
A	0.88744	±0.14594

(b)



(c)

Fig 5.17 Results of applied model on butt (a), belly (b) and neck (c) regions.

It was observed while applying equation (5.1) on the data collected after stretching samples obtained from different location of the finished leather, a strong correlation was obtained between the experimental and analytical values especially for the middle region of hide i.e. butt. The possible reason is the high density of collagen fibres along this region and also while stretching under strain on the drier to obtained maximum area yield the force exerted by the clips is less effective in this region as compared to the edges of the hide. Along other regions (like belly and neck where density of collagen is less) the influence of applied force while drying is more likely to affect these regions due to their location near the edges, so there was a large variation in strain values along the different loading axis. The curve pattern of the analytical model was correlated by using y_0 as input value in equation (5.1) and determined x_c representing the direction of lines of tightness or direction of maximum stretching

It can be observed from Figure 5.17 (a) that the applied model gives its best fit value with residual value of 0.89 for negative value of "A", with x_c having

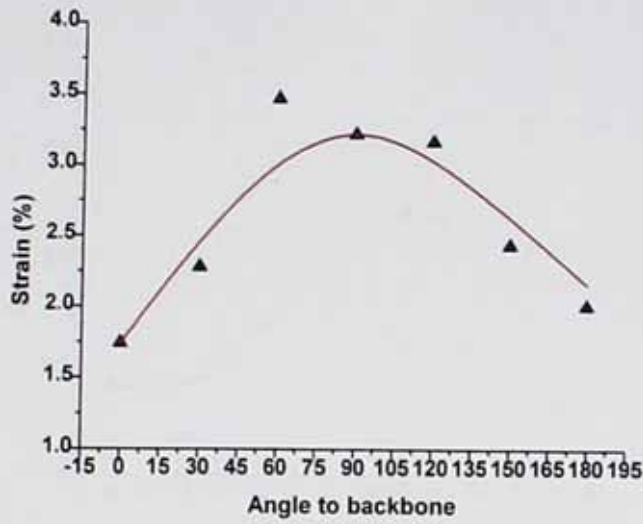
analytical value close to 60° represents the direction of lines of tightness. Also from experimental results the value for lines of tightness with respect to the backbone in this region is at 75° . Similar correlation between analytical and experimental results with residual of 0.81 is observed in belly region, but with a positive value of "A", hence x_c represents the direction of maximum stretching. As stated earlier (Chapter 1) direction of minimum and maximum stretching of fibres are almost orthogonal to each other. In Figure 5.17 (b) the experimental result shows that the minimum strain value is at 45° and maximum strain value is at 135° , while analytical results shows maximum strain value i.e. x_c close to 125° , thus analytical value of lines of tightness is expected close to 35° .

However due to low density of fibres in neck region as shown in Figure 5.17 (c), a large variation in strain values was observed along different directions with low residual value of -0.83 and x_c close to 46° , while experimental results shows the direction of lines of tightness at 15° .

The model therefore is suitable for the region where the fibres are oriented in preferred directions.

When applying the model on pre-stretched sample at an interval of 30° instead of 15° , a strong correlation was obtained between experimental and analytical results. Also the model fitted well for the butt and belly region, but in neck region, due more than one peak, the model does not fit so well. As an alternative approach (Figure 5.17c) a polynomial function of degree five was applied for neck region. The results for an interval of 30° are shown in Figure 5.18 (e). The degree of fit is only marginally improved and is still very poor.

It is concluded that the butt and belly regions can be modelled reasonably well using the *Gaussamp* equation.

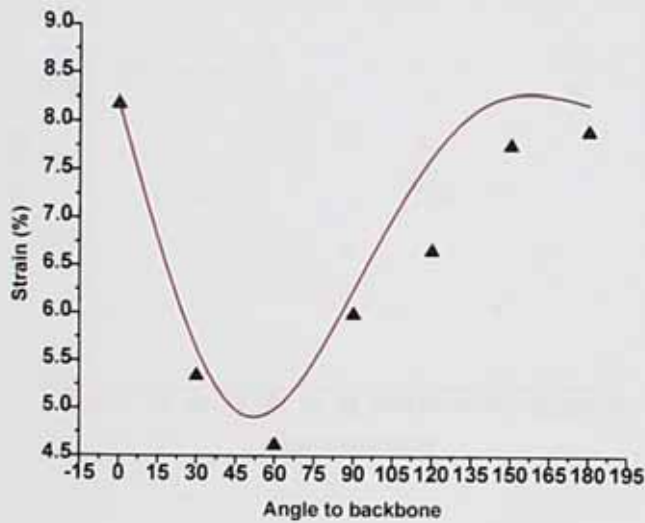


Pre-Stretched sample
 Model: GaussAmp
 Equation:
 $y = y_0 + A \cdot \exp(-0.5 \cdot ((x - x_c) / w)^2)$

$R^2 = 0.87497$

y0	1.74	±0
xc	91.97936	±7.01394
w	46.64835	±5.47695
A	1.48	±0

(a)

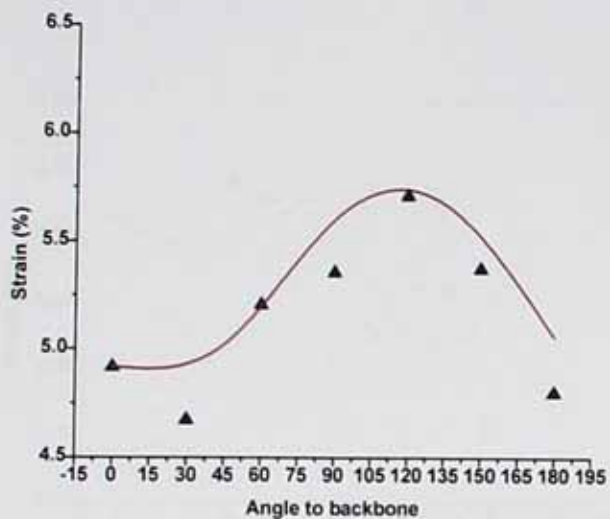


Butt Region
 Model: GaussAmp
 Equation:
 $y = y_0 + A \cdot \exp(-0.5 \cdot ((x - x_c) / w)^2)$

$R^2 = 0.79917$

y0	8.176	±0
xc	61.54697	±6.32882
w	36.74153	±5.52862
A	-3.56	±0

(b)

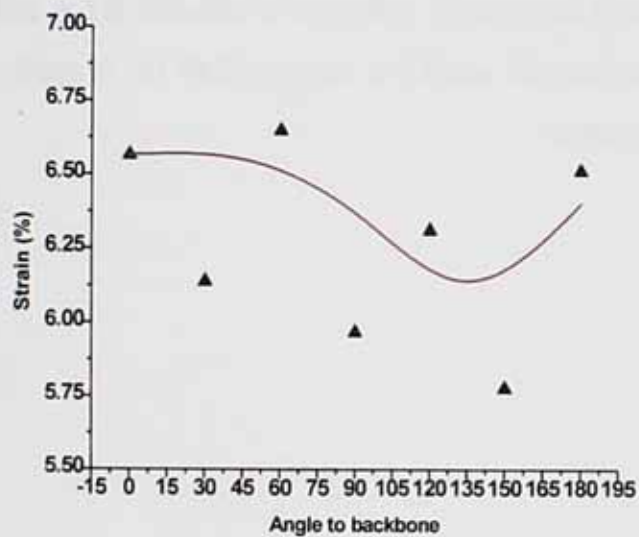


Data: Belly Region
 Model: GaussAmp
 Equation:
 $y = y_0 + A \cdot \exp(-0.5 \cdot ((x - x_c) / w)^2)$
 Weighting:
 y No weighting

Chi²/DoF = 0.03415
 R² = 0.83185

y₀ 4.917 ± 0
 x_c 116.82372 ± 7.30447
 w 28.58248 ± 7.21273
 A 0.7885 ± 0.17311

(c)

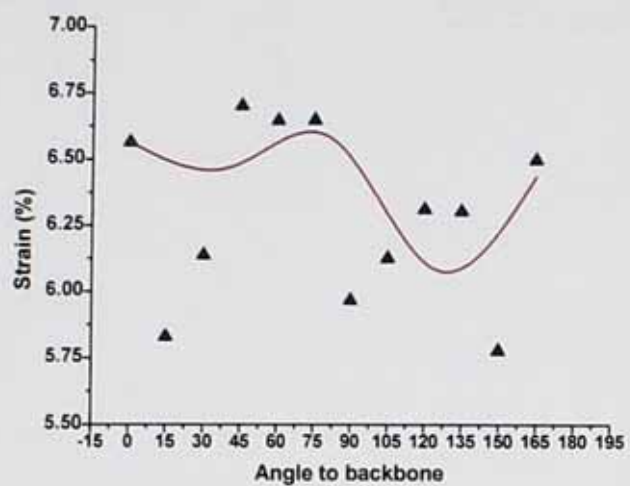


Neck Region
 Model: GaussAmp
 Equation:
 $y = y_0 + A \cdot \exp(-0.5 \cdot ((x - x_c) / w)^2)$

R² = 0.22994

y₀ 6.564 ± 0
 x_c 122.49378 ± 41.42456
 w 61.27481 ± 39.03965
 A -0.426 ± 0

(d)



Neck Region
 Model: Poly5
 Equation: $y = A_0 + A_1x + A_2x^2 + A_3x^3 + A_4x^4 + A_5x^5$
 Weighting:
 y No weighting
 Chi²/DoF = 0.09436
 R² = 0.43747

A0	6.564	±0
A1	-0.07282	±0.03336
A2	0.00317	±0.00163
A3	-0.00005	±0.00003
A4	2.9131E-7	±1.9006E-7
A5	-6.2433E-10	±4.6362E-10

(e)

Fig 5.18 Results of applying *Gaussamp* model to (a) Pre-stretch leather (b) Butt Region (c) Belly Region (d) Neck Region and (e) Polynomial function to Neck Region

CHAPTER 6

6 Proposed System

It was observed from all three methods (*Lateral contraction, Uni-axial constrained and Angular stretching*) that they can be successfully applied to gain information about the lines of tightness in a hide. However if some technique is to be successfully implemented into a real industrial environment, it has to be accurate, fast and easy to use by a non-technical person. Finally, financial aspects must be considered, because they can often be the dominant reason a technique is chosen. The main objective of the research was to develop enough understanding to be able to indicate how to apply a technique on the whole hide. Therefore the selected imaging and stretching system for measuring lines of tightness should be capable of fulfilling the industrial requirement.

6.1 Lateral Contraction Method

Considering first the lateral contraction method, which required the uni-axial application of load along the whole sample. The commercial application of this method would either require one camera capable of capturing an image of the whole hide when it is stretched along corners or a number of cameras each focussing on a specific marked region. The Poisson's ratio values for each region would then be determined separately. If one camera is used then firstly it should have enough sensor size to capture the image of a whole hide having an average surface area (*Field of view of the camera*) of about 1.5 x 2.5 meters [1]. Secondly the resolution of that camera needs to be enough to resolve the marked circular array of dots, which are much smaller in size (4~5 mm in diameter) as compare to the size of the hide. It has been mentioned (*Section 2.5.3*) that as the field of view increases the sensor size of the camera also increases which consequently increases the cost of camera. The application of this method also requires holding the hide uniformly and the uni-axially applied force should be evenly distributed along the irregular edges of the hide. The applied load should be large enough to facilitate an accurate measurement of the lateral contraction. Due to variation in fibre density from one region to another, a relatively large amount of applied load

is required along the edges (Belly) to produce a small amount of strain in the middle portion (Butt). This may result in inducing set along the edges [2]. This is demonstrated in Figure 6.1 where a whole hide marked with a uniform array of spots is shown held along its edges by using grips.

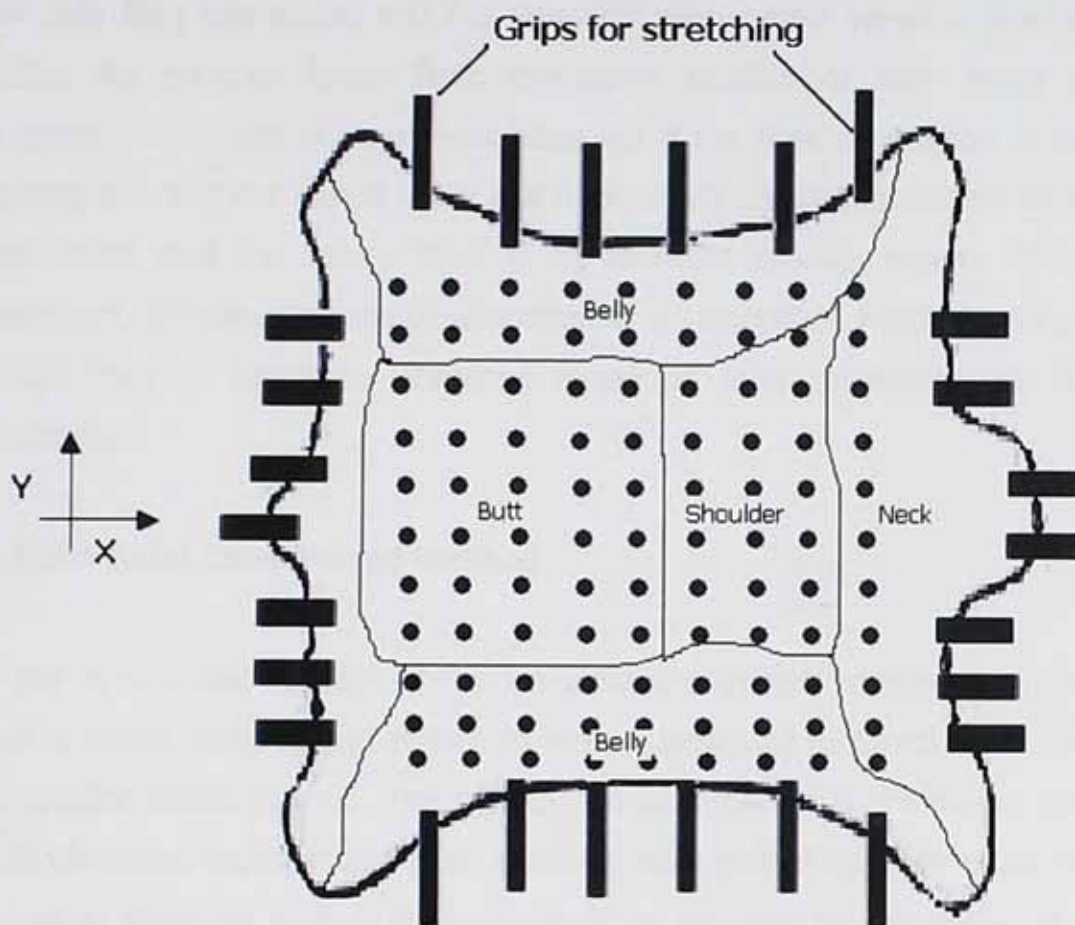


Fig 6.1 Schematic view of a whole hide marked with a uniform array of spots. Grips in X or Y direction use to stretch the whole hide to produce direct strain along that direction and contraction in the lateral direction.

In this method the load has to be applied in either the X or Y direction by actuating all grips along that specific direction. The strain measurement involves the consideration of the whole surface area before and after application of load. This will result in imposing a high demand on the processing speed owing to the analysis of huge amounts of data. The amount of processing data depends upon the number of spots marked on the surface of hide. If normal adult shoe parts are considered e.g. vamp, toe cap, quarter (*Section 1.4*) with size of 10 x 10 cm (100

cm²) and an average area of hide 1.5 x 2.5 m (37,500 cm²), it will give 375 possible locations along the whole surface of the hide to measure the lines of tightness, thus it has to process 375 triangles (*Section 5.2.4*). Considering the previous results (*Section 4.5.2*) no relation has been found between the angle of principle fibre orientation and the Poisson's ratio except when comparing these values for samples taken from the same location of hide along different orientation. The higher value was observed if the fibre orientation is along the loading axis and the lowest value if it is perpendicular to the loading axis. It was also found that the values tend to be different in each region. This creates significant difficulties for the development of an algorithm, which would unequally assign lines of tightness directions based on local measurements of lateral contraction.

6.2 Uni-Axial Constrained Method

If the commercial aspects of the uni-axial constrained method are considered then a similar imaging and stretching system would be required as for the lateral contraction based method. This method would require that the hide is held along both directions together and then actuating each pair of opposite grips instead of actuating them all at one time. It therefore requires the designing of a more complicated stretching system having the capability of actuating each opposite pair of grips at one time whilst other pairs remain fixed and hold the hide. The local strain is measured by considering each row and column of dots falling across the line of action of each pair of opposite grip. The strain values for each direction will then be accumulated to represent the results in vector form. It has been observed from previous results (*Figure 5.9 (a) to (d)*) that the lines of tightness are oriented along that loading axis representing a relatively shorter length of vector. Additionally, along some regions where length of vector was very short it was possible to measure the exact orientation of lines of tightness. Therefore the results of this method will give more information about assuming the angle of fibres orientation, as compared to the Poisson's ratio based method, as the

shorter length of vector will represent the orientation. However, the complexity of the stretching system, the use of an imaging system to produce a large field of view (area of hide), and the processing and accumulation of the information to analyse the data of each pair of grips for each row and column is still there.

6.3 Angular Stretching Method

Finally the industrial application of the third approach based on local stretching of the sample in a known direction requires a considerably simpler imaging and stretching system. This method requires marking a circular array of spots over the whole surface of hide as shown in Figure 6.2.

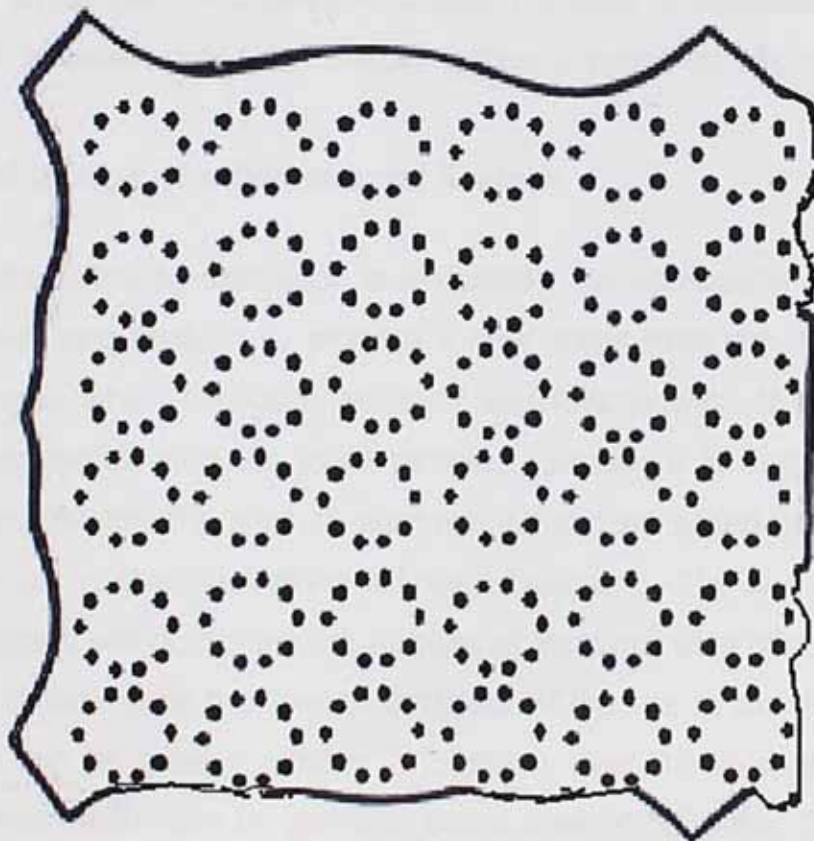


Fig 6.2 Schematic view of whole hide marked with circular array of spots

The greater the number of marked circular arrays of spots over the surface area of the hide, the higher will be the extracted information about lines of tightness.

In this method each circular pattern is analysed individually resulting in a smaller field of view, thus lowering the camera's requirements and its associated cost. The measurement of strain involves the stretching along a diameter of two opposite spots on the circumference of circular pattern. The separation between the spots (diameter of circular pattern) will determine the field of view of camera, and may be much smaller in comparison with the field of view (length or width of hide) required in previous methods. The stretching system is required to stretch only a portion of hide thus reducing the complexity of design and fabrication. This method also reduces the induction of "set" in any region of hide as load can be applied only over the selected circular pattern located at any region of hide e.g. Butt, Belly. The stretching of any region will not have any influence on other regions. The direction of stretching for each pair of grips is also known and thus the minimum strain value will give the direction of lines of tightness within $\pm X^\circ$. Therefore it is proposed that a commercial system is based on this method.

6.4 Proposed Design of a Commercial System

The focus of the following discussion is to consider the application of engineering design principles and analysis to propose a new linear stretcher for determining lines of tightness, which has good accuracy and functionality. It was concluded from the experimental work on large samples (*Section 6.3*) that the proposed system for determining the lines of tightness should be based on a method in which the sample is stretched along a known direction. The size (diameter) of the circular pattern will determine the number of locations over the surface of the hide required to determine the lines of tightness. If the size of the circular pattern is small there can be greater number of patterns over the surface of the hide. Hence more information can be gathered about lines of tightness. The necessary size of circular patterns can also be determined by considering the maximum dimension of the shoe part. There are different numbers and sizes of the parts required for a pair of shoes depending upon the type of shoe, which is to be manufactured (*Section 1.4*). Considering common parts of a normal shoe, the

quarter has the longest length in comparison with other parts (vamp, tongue etc). Therefore the size (e.g. diameter) of the circular pattern is determined by the length of the quarter.

There are several uni-axial (Dartec, Instron) and bi-axial (Deben) stretchers available today and some are commercially available. New systems for leather processing, for example, spray dryers, sammying machines and drying processors are being introduced on a regular basis, but to the author's knowledge no system has been introduced which could be used to stretch the leather non-destructively. However there is a move to the introduction of in-line processes for the leather industry in which operations are linked together, that is, sammying, drying and area measurement may all be performed by one machine together with stretching and toggling as one operation. The presently proposed system could be combined with any existing system of in-line machinery in order to reduce manufacturing time and labour cost. The best possible location for proposed system would be before the application of the finish. Because the hide must be marked with circular pattern of arrays on the surface the marks should not effect on the final products since they will be covered by the finish.

It has been observed during experimental work on large pieces taken from belly and neck regions that leather curls in a lateral direction due to low compactness of fibres in these regions. The design of a mechanical system needs to comply with required design constraints e.g. the applied load should remain fixed for all possible stretching directions with out inducing any set in the leather. The camera should be located in such a way that a high resolution of the marked grid pattern can be achieved. The assembly holding the camera should be fixed to avoid any change in the working distance while capturing images and should be capable of translating from one region to the next along the leather surface.

6.5 System Description

The proposed system would operate as follows:

The hide is marked with circular pattern of arrays before it is fed for stretching. If considering a quarter size of 10 cm, then the diameter of the circular pattern will be equal to 10 cm. Thus, the total number of circular patterns will be 477 over the surface area of 375,00 cm². This is achieved by an engraved printing cylinder placed horizontally with another cylinder above it. The bottom of the lower cylinder takes up the printing colour from a trough, the excess being scraped off by a closely fitting steel blade. As the leather is passed between the cylinders it acquires a pattern of spot circles over its surface as shown in Figure 6.3. It is then subjected to stretching and image analysis.

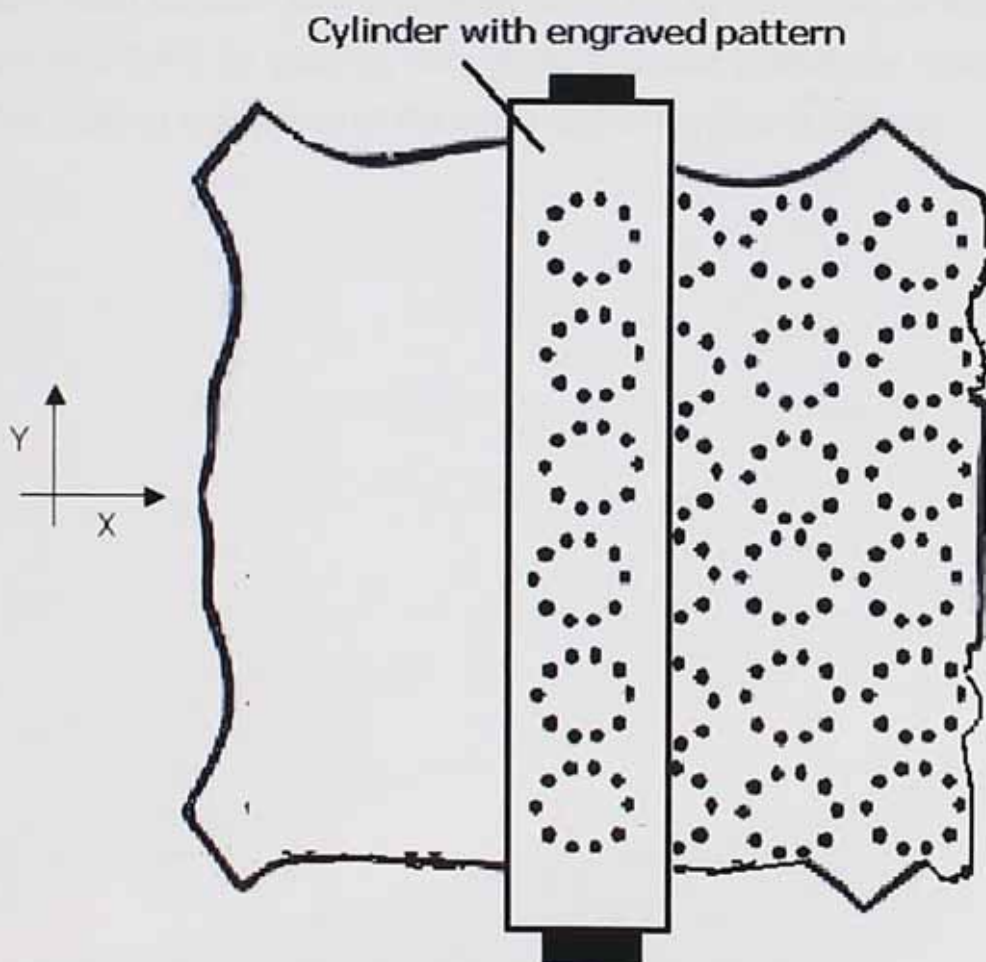


Fig 6.3 Circular pattern of arrays on the surface of leather obtained by using cylinders

There are two possibilities of marking the pattern over the surface of hide. Either it would be marked over the grain side or over the flesh side. The advantage of using the flesh side is that due to the water absorbing property of leather, the trough can be filled with water which is later taken up by the absorbing material held by the engraved pattern. After absorbing water the surface can give a better contrast in comparison with its background.

A design of the mechanical system for leather stretching, which complies with the stated boundary conditions or constraints has been developed. It has the mechanism of stretching the hide in five directions over its surface using upper and lower grips mechanisms. This is achieved by holding the hide using pairs of ten pneumatically controlled grips located along the periphery of a circular plate with a 30° difference between each axis of each pair of opposite grips (see Figure 6.4). Each opposite pair of grips produces the stretch along its axis while holding the hide firmly by pressing through its thickness against the lower pair of grips. The working mechanism of the upper and lower grips is different.

6.5.1 Upper Grip Mechanism

The conceptual model of the upper grid mechanism has shown in Figure 6.4.

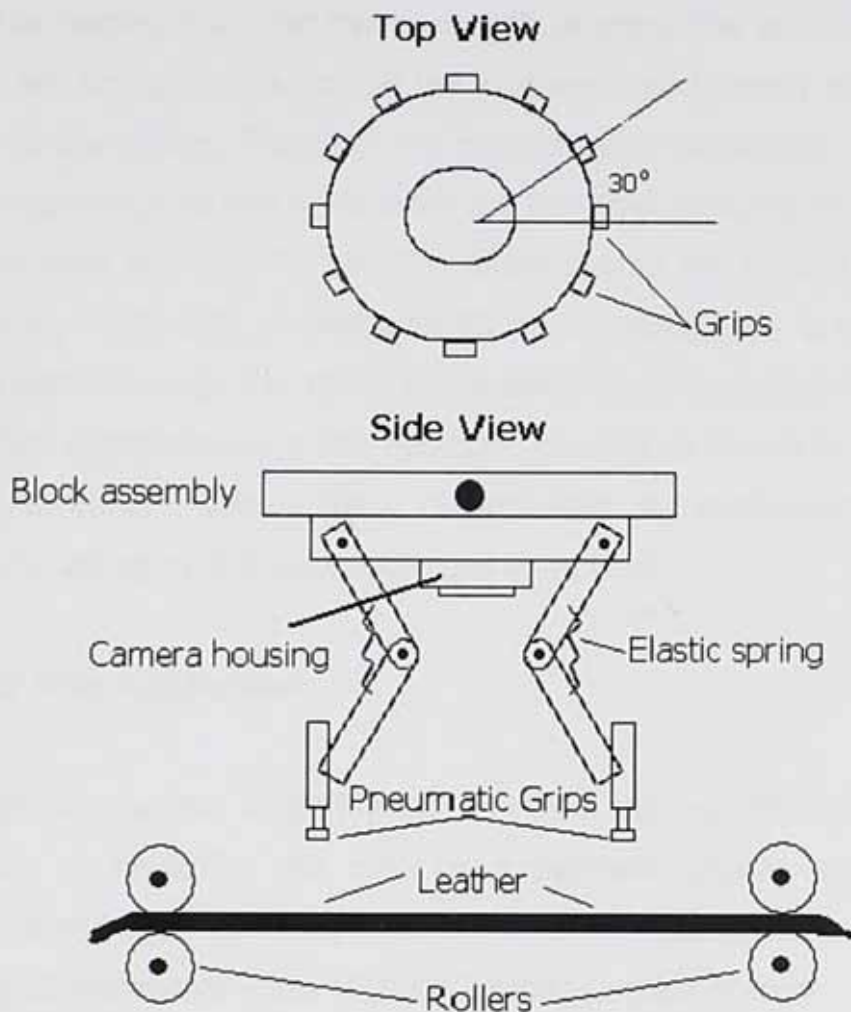


Fig 6.4 Rollers to move leather along its length while the block assembly will translate along its width thus focussing each circular pattern over the surface.

All the pictures for proposed system were developed as 2-D models using the *Auto CAD 2004* software by Autodesk Inc USA. The circular plate has 12 extended slots along its outer surface to hold the pneumatically controlled grips. These pneumatic grips are connected to the circular plate through planar linkages, or

mechanisms in which the principal motion takes place within a single plane. To hold the links at the desired position without obstructing the camera and light housing, an elastic spring is attached to the links. The leather is fed along its width through the rollers. It is then stretched by displacing the upper grips outward while holding it against the lower pair of grips. The outward movement of the grips will straighten the links at the joint and consequently an elastic force will develop in the springs. This force will diminish after the desired load has been applied through the grips and it has been set free thus bringing the pair of grips back to their initial position. This whole mechanism for the grips is carried by a block assembly, which rests on sliding tracks located along both its ends. A driven lead screw passes through the middle of the assembly and controls its movement in the direction perpendicular to the backbone (Y-axis) as shown in Figure 6.4 to locate the desired grid pattern along Y-axis, while the movement of the hide along X-axis is carried by the rollers attached to its end.

6.5.2 Lower Grip Mechanism

The lower grip mechanism is slightly different from the top mechanism, and has the capability of stretching the hide by a hydraulic double acting actuator mounted on a moveable assembly. This assembly is attached to a thick circular plate having 12 rectangular slots with spring-loaded grips in them. The slots are located at angles 30° around plate. Shown in Figure 6.5, is a top view of the lower grip mechanism.

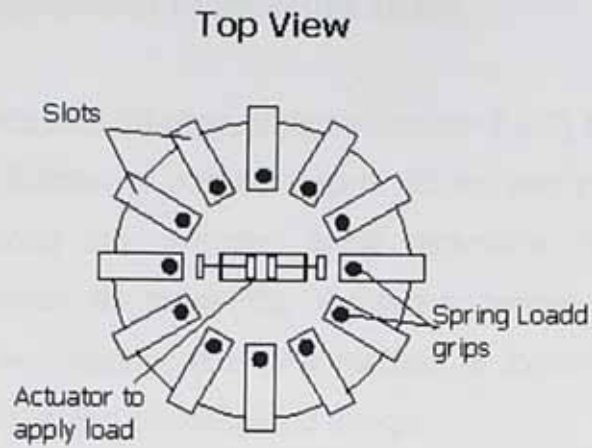


Fig 6.5 Lower grip mechanism

The assembly holding the actuator rests on a bearing that allows rotation. The rotation of the actuator to apply load on the desired pair of grips is controlled by the stepping motor, which is attached to the actuator assembly by spur gears. The whole mechanism has shown in Figure 6.6.

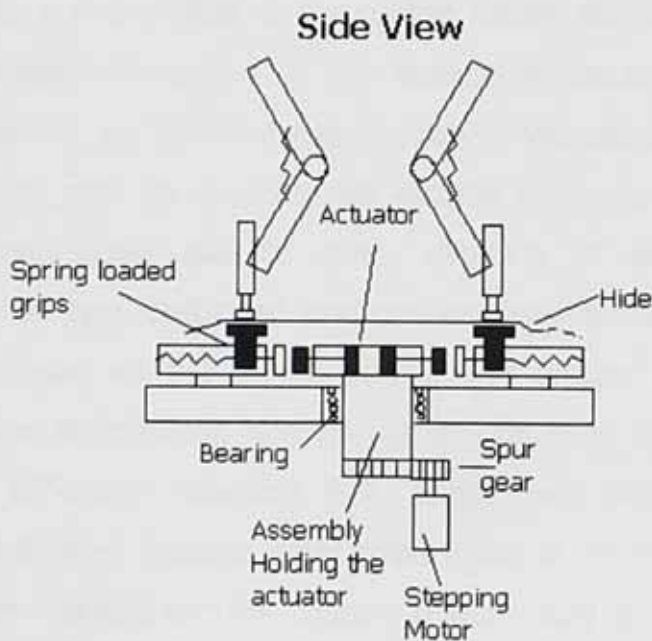


Fig 6.6 Mechanism to locally stretch the hide in a given direction

6.5.3 Software Development to measure strain

It has now been conclusively demonstrated (*Section 3.2.1*) that the images can be captured after application of desired load or stroke and the *lines of tightness* can be measured along any direction using technique demonstrated earlier (*Section 3.1.3*). However to make the technique further user free with its industrial application we introduced a new method to locate the position of the circular spot on deformed and un-deformed image.

6.5.4 Digital Spot- Displacement measurement

The Digital Image Correlation is a well-developed whole-field method for measuring both in-plane strains and rotation. This technique is hard to be used by non-technical person, specially working for the leather industry. However we have been able to apply this technique using *LabVIEW*[®] by providing some tools on the front panel, which are controlled by the coding written on the block diagram. The core of digital image correlation in this application depends on the ability to recognize two similar, yet different image pattern. We adopted this technique as the marked circular spot on un-deformed sample will no longer be circular after application of load/stroke due to flimsy property of leather however best correlation between two (deformed and un-deformed spot) could still be found. The application based on the comparison of two images acquired at different states, one before deformation and the other one after for each pair of grips located at 30° difference (*Section 6.5*). These two images are referred as reference and deformed images. After acquisition of 10 images for 5 different direction of each marked circular pattern (Figure 6.3) by a CCD camera, the images are digitised and stored in computer hard disk for analysis. The marked circular spot with relatively high contrast as compared with the background, in the reference image is characterised by drawing a rectangular subset, an (n x m) pixel area with circular spot in it. The corresponding subset also an (n x m) pixel area, in the deformed image is estimated at a certain location with specified

range. The deformed image is correlated with the reference image to determine the displacement of image subsets between the two images by a fine search routine, pixel by pixel, within the specified range in the deformed image.

The measurement of lines of tightness starts by measuring the distance between the two marked spots on reference and deformed image to determine the strain values for each pair of grips with known direction using following steps

Step 1.

Load all images of a circular pattern (before stretching).

Step 2.

Start with the images captured for axis parallel to the backbone direction and consider it as 0° e.g. parallel to the backbone direction.

Step 3.

Load the reference image of known direction (e.g. 0°) and apply BCG function if the contrast between spot and the background is not enough to be distinguished.

Step 4.

Draw a rectangular around the spot to be searched, click OK after selection.



Fig 6.7 Storing information for the spot to be searched.

Step 5.

Select the whole rectangular region between the grips with all the spots specially end spots in its.

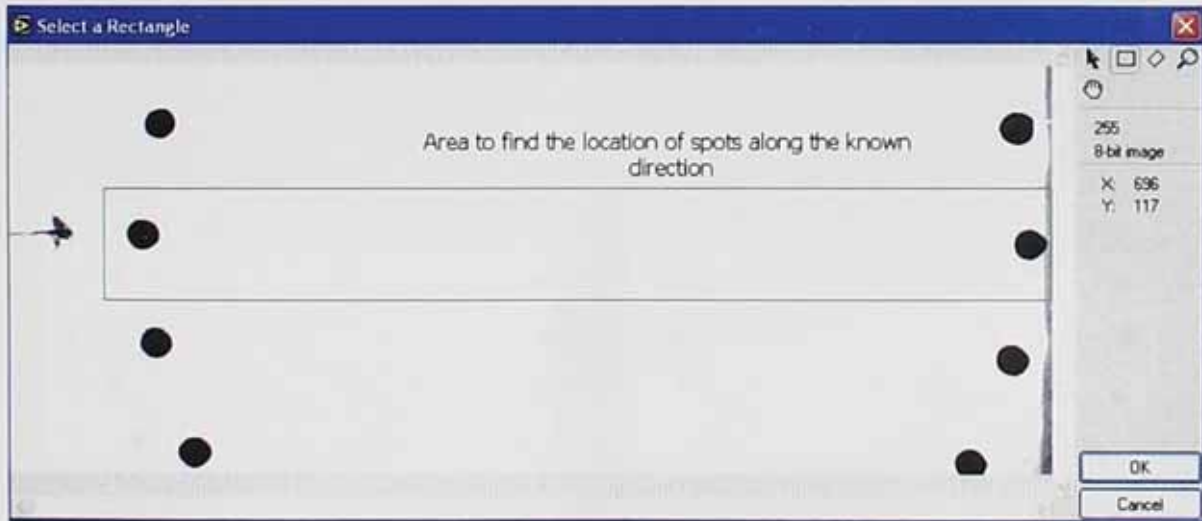


Fig 6.8 Reference Image

Step 6.

Apply Step 5 on deformed image.

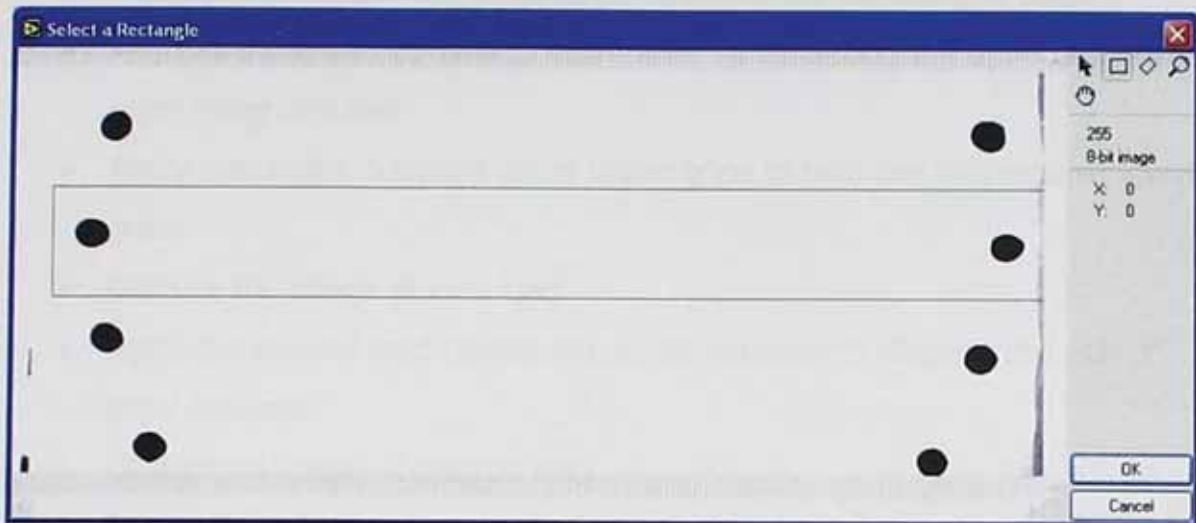


Fig 6.9 Deformed Image

In the result we will get the distance between the end spots of reference and deformed image, which can be used later to find strain and consequently the lines of tightness.

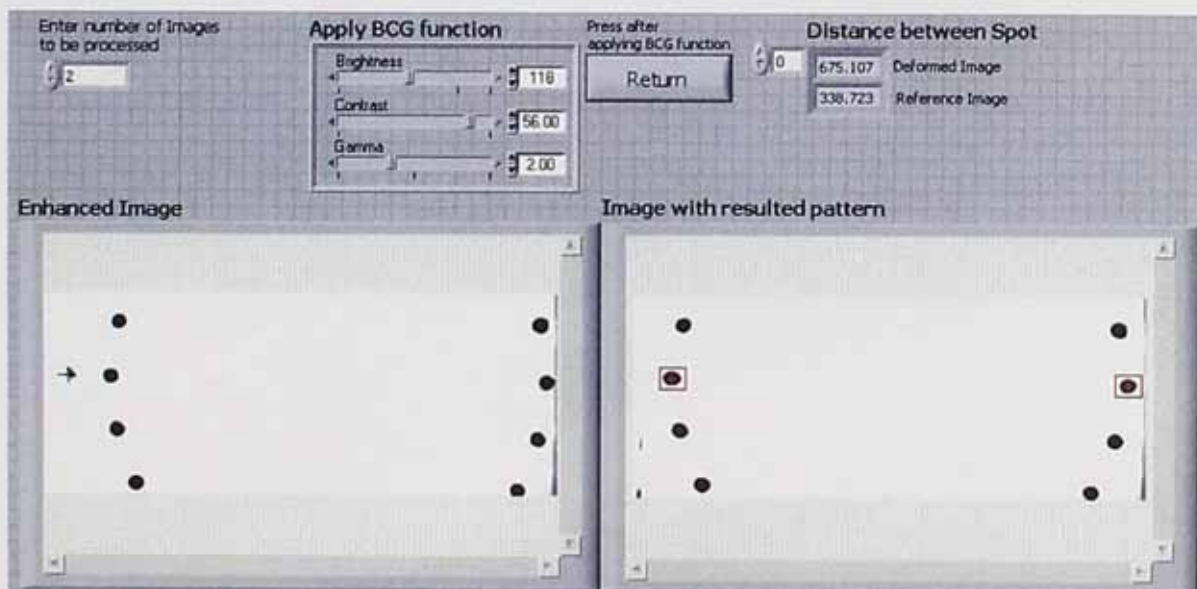


Fig 6.10 Reference and deformed image with distance between spots in pixels

The full process will involve

- Feed the hide through rollers between the lower and upper grips
- Translate the upper and lower grips to locate the circular grid pattern
- Align all the grips opposite to each other by displacing the upper and lower grips along one axis
- Apply pneumatic pressure on all upper grips to hold the hide against lower grips
- Capture the image at zero load
- Apply the desired load (pressure) on the actuator to displace the pair of grips outward
- Capture an image at desired load
- Rotate the actuator against all other pair of grips by stepping motor
- Perform image analysis for each pair of marked circular pattern

The whole process is indicated in the following diagram and actual programming for the industrial application of the whole process is shown in *Appendix F*.

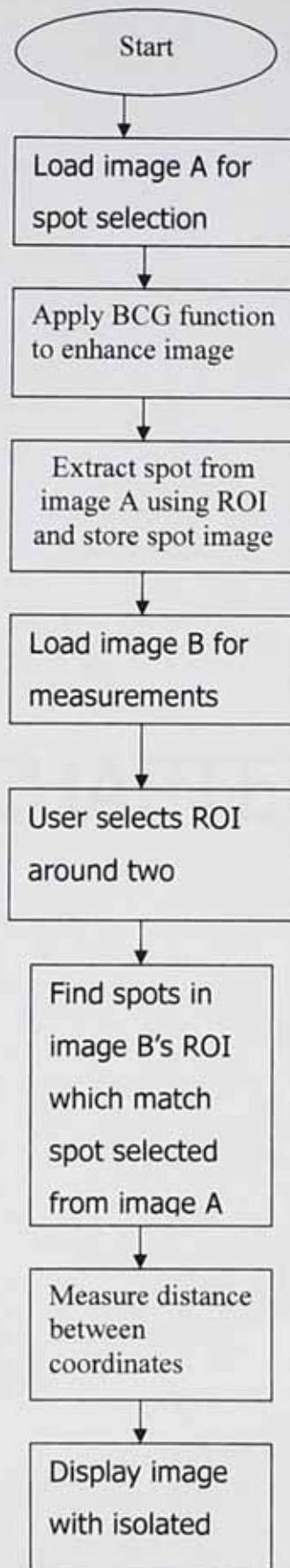


Fig 6.11 Diagram showing steps to locate position of spot in images

7 Characterization of Polymers

7.1 Introduction

The study of the physical and chemical properties of polymers is a branch of polymer science. It is concerned with the structure, properties, and behavior of polymers. The study of polymers is important because they are used in a wide variety of applications, from plastics to fibers to rubbers.

CHAPTER 7

7 Conclusion and Future work

7.1 Conclusion

This research involved the determination of the feasibility of using an image analysis technique to characterise strain distributions in leather and consequently characterise the lines of tightness. It is concluded that:

- The image analysis system developed can measure strain in leather accuracy of 0.5% when it is stretched in tension. The stress-strain behaviour of leather when determined using image analysis shows a "J" shaped curve (as found when conventional methods are used). A key advantage of the new strain measurement technique is that it is possible to gather extra information about the stress-strain behaviour of a sample of leather by determining strain in different sections along its gauge length. The methodology can also differentiate the behaviour of leather in terms of its position and orientation within different sections of the hide.
- The technique allows accurate measurement of lateral strain in leather samples when they are subject to tensile straining. The methodology is thus very good for directly measuring Poisson's ratio in soft highly deformation materials such as leather and rubber. It is particularly good for viscoelastic materials such as leather because it makes an immediate determination of strain before any relaxation can occur (this is almost impossible to achieve with conventional strain measurement techniques). The Poisson's ratio of leather found using this technology varies from 0.30 to 1.5 depending upon the location of sample on the hide. This variability is due to differences in the way fibres in the leather are aligned and interwoven. Higher values of Poisson's ratio are observed in the belly region due to a low packing density of fibres there as compared with butt region where fibres are more

compacted together and the density is somewhat higher. Often high (i.e. > 0.5) values of Poisson's ratio are found with leather samples and this means that their gross volume reduces as they are stretched. This is due to fibres coming closer together as stretching occurs. Leather can also, under some circumstances, show auxetic behaviour ($PR < 0$) where volume increases on stretching. This occurs in leather where fibres have been aligned preferentially in one direction.

High Poisson's Ratio values are observed in samples in which the applied strain and predominant fibre orientation axis are in the same direction. Relatively lower values occur when the applied strain and predominant fibre orientation axis are perpendicular to each other. It is also observed that Poisson's ratio does depend on whether or not leather is stretched prior to drying; values as high as 2.5 may be observed in material dried under strain in comparison with a value of 0.32 for leather dried without applying strain. This behaviour may be explained using a microstructural model which assumes that, during leather deformation, fibres don't themselves stretch but rotate into the stretching axis. This model predicts experimental trends very well; for example predicting higher values of Poisson's ratio when both fibre orientation and loading axis are parallel to each other.

- When large square pieces of leather are stretched along one axis the local measurement of the ratio of lateral strain to axial strain can be used to indicate lines of tightness. However the method is not very reliable, as relatively large amounts of strain in the axial direction are required in order to produce significant strain in the lateral direction. On small rectangular pieces with known direction of lines of tightness it is the case that along these lines the ratio of lateral to direct strain values is high. However with large pieces, due to fibre bundle entanglement, the lateral strain produced in one location may affect the strain values within other nearby locations. Also, measuring the ratio of lateral and axial strain for different regions over the surface of hide is not sufficient to give complete information about lines of

tightness. The industrial application of this method to investigate lines of tightness would require the designing of a system to hold and stretch whole hides (which have an average dimension of 1.5 x 2.5 m).

- A method based on stretching square pieces of leather, marked with a rectangular array of spots, along a set of parallel axes in the x and y direction can be used to indicate local anisotropy and effectively indicates the location of lines of tightness by determining the position of the spots before and after stretching. However the problem of stretching the whole hide along its length and width still persists.
- A system based on stretching relatively small circular regions of the hide by applying load along different axis (e.g. 0 to 180° at 15° intervals) is the most reliable approach to achieving an industrial system for determining the direction of lines of tightness. It requires a printing cylinder to mark circular arrays of spots by a removable printing material along the surface of hide, while the load is applied successively through a pair of grips within a circular gripping system. Mathematical modelling of data obtained from this method using a Gauss amplification function is moderately successful and can be used to indicate the location of lines of tightness using strain/loading axis with an interval of 30°. However in regions of the hides where the density of fibres is less (belly, neck) the straining/loading grip axes require a 15° interval to correctly assign the direction of lines of tightness. Since these regions are used to click quarter and back strips of the shoe pair (shoe portions which are subjected to less mechanical action in shoemaking) the methodology of stretching the hide at angular intervals of 30° may be sufficient to investigate the direction of lines of tightness where it is most important to do so (i.e. in the butt and shoulder regions).

7.2 Future Work

- The industrial application of the method of stretching leather in a known direction requires the manual selection of the marked spot along that known direction. This step needs to be made part of an algorithm, which is capable of rotating the imaging window for each pair of grips locating with a 30° difference.
- Further software development is required so that image capturing and application of load along each pair of grips can be controlled by one front panel which should also be capable to placing of the upper assembly holding the camera at a specified location of a circular pattern.
- If a high resolution camera is used then it should be possible to determine strain values without marking a piece of leather if the camera is focussed on flesh side of the hide as, on this side, there should be a better contrast between naturally occurring surface features thus eliminating the need to mark spots. This should be the subject of further investigation.

References

- 1) Thorstensen, T. C., "Practical Leather Technology", 1993, Krieger Publishing Company.
- 2) "The Fibre Structure of Leather", Leather Conservation Centre, 1981
- 3) O'Flaherty, F. and Roddy W. T., "The Chemistry and Technology of Leather", Volume IV- Evaluation of Leather, 1977, Krieger Publishing Company.
- 4) Otunga, M. G., "Effect of Drying Under Strain on the Mechanical Properties of Leather", 2002, PhD Thesis
- 5) Hiedemann, E., "Fundamentals of Leather Manufacture", 1993, Eduard Roether KG, Darmstadt.
- 6) Attenburrow, G. E. and Wright, D. M., "Studies of the mechanical behaviour of partially processed leather", J. Amer. Leath. Chem. Ass., 89, 1994, pp. 387-398.
- 7) Maeser, M., "The Effect of hide location and cutting direction on the tensile properties of upper leathers", J. Amer. Leath. Chem. Ass., 55, 1960, pp. 501-531.
- 8) Bienkiewicz, K., "Physical Chemistry of Leather", 1983, Malibord, Florida.
- 9) Benham, P. P. and Crawford R. J., "Mechanics of Engineering Materials", Longman Singapore Publishers, 1988
- 10) Attenburrow, G. E., "The rheology of leather - a review", J. Soc. Leath. Technol. Chem., 77, 1993, pp. 107-113
- 11) Mitton R.G., "Some physical properties and their variability in hide belly leather and goat skin", J. Soc. Leath. Technol. Chem., 29, 1945, pp. 269-277
- 12) Mann, C. W., Randall, E. B. et al, "The sampling of side upper leather" J. Amer. Leath. Chem. Ass., 46, 1951, pp. 248-253
- 13) Vos, A. and van Vlimmeren, P. J., "Topographic differences in physical properties", J. Soc. Leath. Technol. Chem., 57, 1993, pp. 93-98

- 14) Ward, A. G., and Brookes, F. W., "Relationship of mechanical properties to structural variation through the thickness of skin and leather" J. Soc. Leath. Technol. Chem , 49, 1965, pp. 312
- 15) Wright, D .M. and Attenburrow, G. E. in XXIII IULTCS Congress Proceedings, London, UK, 1977, p, .686.
- 16) Wright, D. M. and Attenburrow, G. E., "The set and mechanical behavior of partially processed leather dried under strain", J. of Mat. Sci., 35, 2000, pp.1353-1357.
- 17) Liu, C.-K., Latona, N.P., Lee,J., "Effects of drying methods on chrome-tanned leather" J. Amer. Leath. Chem. Ass., 99, 2004, pp. 205-210.
- 18) Mitton, R. G., "Mechanical properties of leather fibres", J. Soc. Leath. Technol. Chem., 29, 1945, pp. 169-194.
- 19) Dieckman, "Leather Manufacturers", Sept 1968.
- 20) Spiers, C.H. and Pearson, M.S., "The shrinkage and plastic flow of chrome leather during drying", J. Soc. Leath. Technol. Chem, 47, 285, 1963,
- 21) Whittaker, R.E., "The viscoelastic properties of leather and poromerics", J. Soc. Leath. Technol. Chem, 59, 1975, pp. 172-180.
- 22) Sturrock, E. J., Attenburrow, G. E., Boote, C., Meek, K. M., "Psuedo-affine behaviour of collagen fibres during the uni-axial deformation of leather", J. Mater. Sci., 37, 2002, pp. 3651-3656.
- 23) Humpherys,G. H. W., "The Manufacture of Sole and Heavy Leathers", 1966, Pergamon Press.
- 24) Landmann, W., "The Machines in the Tannery", 2003, Joseph Ward Colour Printers, Dewsbury, West Yorkshire.
- 25) <http://www.tanware.com/en/measuring/area.html>
- 26) Long, J. V. A., "An Introduction to Shoemaking", 1948, The Shoe and Leather News, London.

- 27) Yu, W. and Attenburrow, G. E., "Studies of the bending behaviour of chrome tanned leather", *J. Soc. Leath. Technol. Chem.*, 81, pp. 152-155.
- 28) Miller, R.G., "Manual of Shoemaking", 1989, Clarks Ltd, Street.
- 29) Maeser, M., "An engineer look at Leather" *J. Amer. Leath. Chem. Ass.*, LVIII, 1963, pp. 456-493.
- 30) SATRA Bulletin, January 2003, Northamptonshire, UK
- 31) Buke, E. and Kendall, G., "Evaluation of two dimensional bin packing using the no fit polygon", *Computers and Industrial Engineering Conference*, Melbourne, Australia, 1999.
- 32) Clay, P. and Crispin, A. J., "Automation lay planning in leather manufacturing" , 17th National Conference on Manufacturing Research, *Advances in Manufacturing Technology*, Vol,15, 2001, pp. 257-262.
- 33) Crispin, A. J., Clay, P., Taylor, G. E., Bayes, T., Reedman, D., "Genetic algorithms applied to leather lay plan material utilization", *Journal of Engineering Manufacture*, 2003, 217, pp. 1753-1759.
- 34) E. J. Sturrock, G.E. Attenburrow, C. Boote and K. M. Meek, "The effects of biaxial stretching of leather on fibre orientation and tensile modulus", *J. Mater. Sci.*, 39, 2004, pp. 2481-2486.
- 35) Osaki, S., "Distribution Map of Collagen Fiber Orientation in a Whole Calf Skin", *The Anatomical Record*, 254, 1999, pp. 147-152.
- 36) Graham Rowley, "Modern shoe making no. 57", SATRA technology centre, 1999, Northamptonshire, United Kingdom.

- 37) Komanowsky, M., "Thermal stability of Hide and Leather at different moisture contents", J. Amer. Leath. Chem. Ass., 86, 1991, pp. 269-280.
- 38) D. C. Reedman, I. C. Howard, D. R. Hayhurst, J. Lin, "Modelling of the performance of leather in a uni-axial shoe last simulator", Journal of Strain Analysis, 27 (4), 1992, pp. 187-196.
- 39) D. N. O'Leary and Attenburrow, G.E., "Differences in strength between the grain and corium layers of leather", J. of Mat. Sci., 31, 1996, pp.5677-5682.
- 40)<http://www.wmin.ac.uk/ITRG/IS/DPI/HIW/2Image%20acquisition%20Notes.pdf>
- 41)http://www.analog.com/processors/resources/technicalLibrary/manuals/training/materials/pdf/dsp_book_Ch23.pdf
- 42)<http://www.csc.liv.ac.uk/~aa/Courses/COMP316/lecture4bw.pdf>
- 43)<http://scholieren.ewi.tudelft.nl/mkt/onderwijs/beeldbewerkingcollegesheets.pdf>
- 44)<http://www.doom9.org/index.html?capture/introduction.html>
- 45)<http://www.machinevisiononline.org/public/articles/articlesdetails.cfm?id=7>
- 46) Klinger, T., "Image Processing with LabVIEW and IMAQ Vision", Prentice Hall, 2003.
- 47) National Instruments, "IMAQ Vision for Lab VIEW", 2000, pp. 6-2
- 48) Kovas, J., "Understanding video calliper accuracy", www.mivos.com

- 49) Billmoyer, F. W., "Textbook of Polymer Science" 1971, J. Wiley New York
- 50) <http://publib.upol.cz/~obd/fulltext/physic38/physic38-11.pdf>
- 51) Asseban, A. *et al*, "Speckle photography on heat transfer studies" The Homepage of optical methods in heat and mass transfer 2000.
- 52) Johnson, P., "Strain field measurements in industrial applications using dual beam digital specklephotograpy", Volvo Aero corporation, Division of Experimental Mechanics, Lulea University of Technology, 1998.
- 53) Mo, N. and Shelton, J.C., "Medical Engineering and Physics, 20, 1998, 594-601.
- 54) Shigeyoshim, Osaki *et al*, "A new approach to collagen fibre orientation in cow skin by the microwave method", Cellular and Molecular Biology, 39(6), 1993, pp. 673-680.
- 55) Liu, C.-K. and Latona, N.P., "Non destructive evaluation of leather based on acoustic emission", J. Amer. Leath. Chem. Ass., 99, 2004, pp. 251-257.
- 56) Kronick, P.L. and Buechler, P.R., "Fibre orientation in calfskin by laser light scattering or X-ray diffraction and quantitative relation to mechanical properties" J. Amer. Leath. Chem. Ass., 81, 1986, pp. 221-229.
- 57) Kronick, P.L. and Buechler, P.R., "Fibre orientation and small deformation modulus of stretched, partially dried hide" J. Amer. Leath. Chem. Ass., 83, 1988, pp. 115-124.

- 58) Long, A.J., Jardine, P., Deadman, T., "The use of acoustic emission to detect grain crack during the lastometer test" J. Soc. Leath. Technol. Chem., 85, 2004, pp. 80-84
- 59) Hoang, K., Wen, W., Nachimuthu, A., Jiang, X.L., "Achieving automation in leather surface inspection", Computers in Industry, 34, 1997, pp. 43-54.
- 60) Breuckmann, E.K., "Measurement of grain structures using 3D scanning", World Leather, August/Sept 2001, pp. 44
- 61) Haynes, A.R. and Coates, P.D., "Semi-automated image analysis of the true tensile drawing behaviour of polymers to large strains", Journal of Material Science, 31, 1996, pp. 1843-1855.
- 62) Marcellier, H. *et al*, "Optical analysis of displacement and strain fields on human skin", Skin Research and Technology, 7, 2001, pp. 246-253.
- 63) Jarrett, R.M. and Sykes, R.L., "Analysis of video recordings to investigate mechanical operations", J. Soc. Leather Tech. Chem., 72, 1987, pp. 94-96.
- 64) Fung, Y.C., "Foundations of Solid Mechanics", Prentice Hall, 1968, p.353.
- 65) Lakes, R.S., "The time dependent Poisson's ratio of viscoelastic materials can increase or decrease", Cellular Polymers, 11, 1992, 466-469.
- 66) "Marks' Standard Handbook for Mechanical Engineers", McGraw-Hill Book Company, Eighth Edition, 1978, p. 5-18.
- 67) Staab, G. H, "Laminar Composites", Elsevier, 1999, p.19

- 68) Khashaba, U.A., "In-plane shear properties of cross-ply composite laminates with different off-axis angles", *Composite Structures*, 65 (2), 2004, pp 167-177
- 69) Goertzen, D.J., Budney, D.R., Cinats, J.G., "Methodology and apparatus to determine material properties of the knee joint meniscus", *Medical Engineering & Physics*, Vol19 (5), 1997, pp. 412-419.
- 70) Attenburrow, G.E. and Wright, D.M., "Studies of the mechanical behaviour of partially processed leather", *J. Amer. Leath. Chem. Ass.*, 89, 1994, pp. 387-398.
- 71) <http://www.measurementsgroup.com/guide/ta/pc/pcb1.htm>
- 72) Liu, J.Y., "Analysis of off-axis tension test of wood specimens", *Wood and Fibre Science*, 34(2), 2002, pp. 205-211.
- 73) Papanicolaou, G.C., Zaoutsos, S.P., Kontou, E.A., "Fibre orientation dependence of continuous carbon/epoxy composites nonlinear viscoelastic behaviour", *Composites Science and Technology*, 64, 2004, pp. 2535-2545.
- 74) Hearn, E. J, "An Introduction to the Mechanics of Elastic and Plastic Deformation of Solids and Structural Materials (3rd edition)", Elsevier, 1997
- 75) Lakes, R.S., "Foam structures with negative Poisson's ratio", *Science*, 235, 1987a, pp. 1038-1040.
- 76) Sevenhuijsen, P. J., "The photonical, pure grid method", *Optics and Lasers in Engineering*, 18, 1993, pp. 173-194.

- 77) Septanika E. G. *et al*, "An automated and interactively large-deformation measurement system based on image processing", *Experimental Mechanics*, 38 (3), 1998, pp. 181-188.
- 78) Frolich, L. M., LaBarebra, M., Stevens, W. P., "Poisson's ratio of a crossed fibre sheath: the skin of aquatic salamanders", *Journal of Zoology*, 232, 2994 pp. 231 252.

Appendix A

No-Fit Polygon Method

In the nesting problem larger shapes must be divided into smaller pieces. This is achieved by arranging the smaller pieces onto the larger shapes so that they do not overlap, they lie within the confines of the larger shapes and the waste is minimized. Only two dimensions are relevant; height and width. It is also characterized by the fact that it works with irregular shapes (polygons).

The No Fit Polygon (NFP) determines all arrangements that two arbitrary polygons may assume such that the shapes do not overlap but so that they cannot be moved closer together without intersecting. To show how the NFP is constructed consider two polygons; P_1 and P_2 . The aim is to find an arrangement such that the two polygons touch but do not overlap. If this can be achieved then we know that we cannot move the polygons closer together in order to obtain a tighter packing. In order to find the various placements the procedure is as follows (see figure 1).

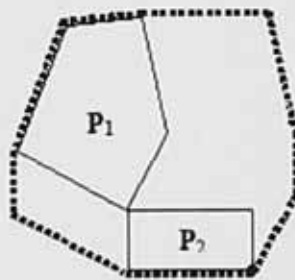


Figure 1 – No Fit Polygon

One of the polygons (P_1) remains stationary. P_2 moves around P_1 and stays in contact with it but never intersects it. P_1 and P_2 retain their original orientation. That is, they never rotate. As P_2 moves around P_1 one of its vertices (the filled circle) traces a line. The NFP is shown as a dashed line. It is slightly enlarged so that it is visible. In fact, some of the edges would be identical to P_1 and P_2 . Once the NFP has been calculated for a given pair of polygons the reference point (the

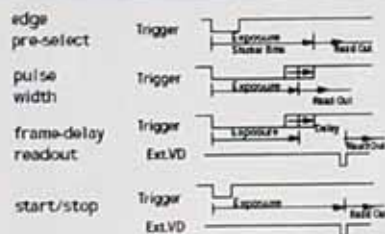
filled circle) of P_2 can be placed anywhere on an edge of the NFP in the knowledge that it will touch, but not intersect, P_1 . In order to implement a NFP algorithm it is not necessary to emulate one polygon orbiting another.

Appendix B

Specifications for CV-A50/A60

Specifications	CCIR	EIA
Scanning system	625 lines 25 frames/sec.	525 lines 30 frames/sec.
CCD sensor CV-A50	Monochrome 1/2" IT CCD	
CCD sensor CV-A60	Monochrome 1/3" IT CCD	
Sensing area	CV-A50 6.4 (h) x 4.8 (v) mm	CV-A60 4.9 (h) x 3.7 (v) mm
Effective pixels	752 (h) x 582 (v)	768 (h) x 494 (v)
Pixels in video output	737 (h) x 575 (v)	758 (h) x 486 (v)
Cell size	CV-A50 8.6 (h) x 8.3 (v) μ m	CV-A60 6.5 (h) x 6.25 (v) μ m
Resolution horizontal	570 TV lines	
Sensitivity on sensor	CV-A50 0.03 Lux, Max gain, 50% video	CV-A60 0.05 Lux, Max gain, 50% video
S/N ratio	CV-A50 59 dB	CV-A60 60 dB
Video output	Composite VS signal, 1.0 Vpp, 75 Ω	
Gamma	0.45 or 1.0	
Gain	Manual - Automatic	
Gain range	0 to +15 dB	
Accumulation	Field - Frame	
Synchronization	Int. X-tal. Ext. HD/VD or random trigger	
Scanning	2:1 interlaced, non-interlaced	
HD sync. input/output	4 V, 75 Ω	
Trigger input	4 V, 75 Ω	
WEN output (write enable)	4 V, 75 Ω	
EEN out. (exposure enable)	4 V, 75 Ω	
Pixel clock output	4 V, 75 Ω	
Shutter	(off), 1/100, 1/250, 1/500, 1/1000, 1/2000, 1/4000, 1/10,000 sec.	
Pulse width control	1.5 H to 1000 H	
Start/stop	1/50 to 1/10,000 sec.	1/60 to 1/10,000 sec.
Long time exposure	1 field to ∞	
Programmable exposure	2.5 H to 252.5 H	
Frame delay readout	Time from PWC trigger input to ext. VD input	
Functions controlled by RS 232C	Scanning format, Trigger mode, Shutter speed, Trigger/WEN polarity, Accumulation, Shutter mode, Programmable exposure, AGC level, White clip, Setup, Manual gain, AGC/manual gain, Internal/potentiometer gain set, Gamma, Pixel clock, Commands and internal adjustments.	
Functions controlled by DIP switches	VD input/output, HD input/output, internal HD and VD 75 Ω termination on/off	
Operating temperature	-5°C to +45°C	
Humidity	20 - 80% non-condensing	
Storage temp./humidity	-25°C to 60°C / 20% - 90 %	
Power	12V DC \pm 10%, 1.5 W	
Lens mount	C-mount	
Dimensions	29 x 44 x 66 mm (HxWxD)	
Weight	150 g	

Trigger/Readout Modes



Connection Description

DC-IN/SYNC

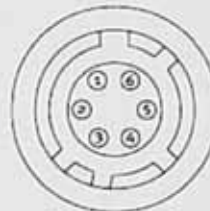


HIROSE HR10A-10R-12P

- Pin
- 1 Ground
 - 2 +12V DC
 - 3 Ground
 - 4 Video output
 - 5 Ground
 - 6 HD input/HD output
 - 7 VD input/VD output
 - 8 Ground
 - 9 Pixel clock output
 - 10 WEN output
 - 11 Trigger input
 - 12 Ground

(Pin configuration compatible with EIAJ standard)

TRIGGER



HIROSE HR10A-7R-6P

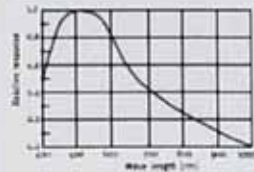
- Pin
- 1 TXD
 - 2 RXD
 - 3 Ground
 - 4 Ground
 - 5 Trigger input
 - 6 EEN output

Plugs for cable:
12 pin: HIROSE HR10A-10P-12S
6 pin: HIROSE HR10A-7P-6S

Ordering Information

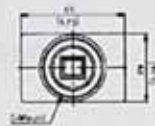
CV-A50C 1/2" Monochrome Camera. CCIR
CV-A60C 1/3" Monochrome Camera. CCIR
CV-A50E 1/2" Monochrome Camera. EIA
CV-A60E 1/3" Monochrome Camera. EIA
MP40 Tripod Adapter (must be ordered separately)

Spectral Sensitivity

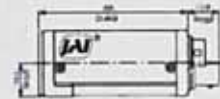


Dimensions

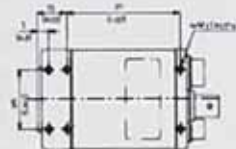
Front view



Side view



Bottom view



Top view



Rear view



Appendix C

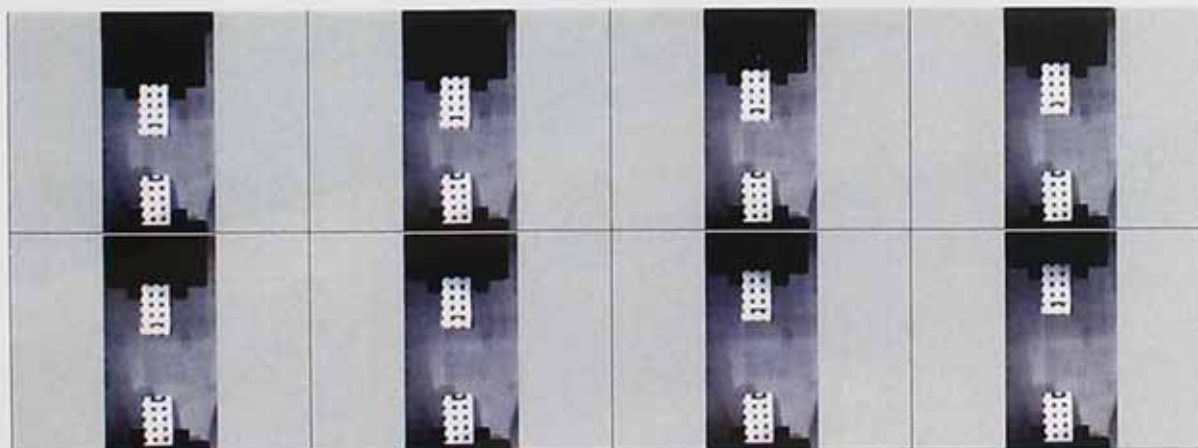
Data for Figure (3.5)

Grid Calibration

Grid Dia	10	Pixels
Applied Stroke	5	mm
Working Distance	300	mm
FOV	288	Pixels (Horizontal)
	570	Pixels (Vertical)

Applied Stroke (mm)	Image Measurement (mm)	Image Measurement (mm)
0	15.92	0
5	20.88	4.96
10	25.83	9.91
15	30.79	14.87
20	35.75	19.83
25	40.71	24.79
30	45.66	29.74
35	50.63	34.71
40	55.59	39.67
45	60.55	44.63
50	65.5	49.58
55	70.46	54.54
60	75.42	59.5
65	80.38	64.46
70	85.34	69.42

Some Images for Figure (3.5)



Data for Figure (3.12)

Load (N)	0	4.1	7.3	9.7	10.6	11.2	12
Stroke (mm)	0	5	10	15	20	25	30
Nominal Strain (%)	0	2.778	5.556	8.333	11.111	13.889	16.667
Section A	0	2.844	5.470	7.877	10.502	12.909	15.534
Section B	0	3.039	5.473	7.905	10.640	13.071	15.807
Section C	0	3.066	6.122	8.163	11.229	13.780	15.821
Section D	0	3.029	6.028	7.572	10.601	13.630	15.145

Appendix D

Data for Figure 4.3

Perpendicular			Parallel		
Load	Strain	Stress	Load	Strain	Stress
0.000	0.000	0.000	0.000	0.000	0.000
0.0092	3.052	0.123	0.0336	3.512	0.448
0.0229	5.301	0.305	0.0954	7.067	1.272
0.0458	8.514	0.611	0.1801	9.564	2.401
0.0755	11.526	1.007	0.2655	13.161	3.540
0.1085	14.217	1.447	0.3555	16.039	4.740

Data for Figure 4.5

Load (N)	0.000	12.2	30.5	76.3	130.5	180.1	252.5
Stress (M Pa)	0.000	0.163	0.407	1.017	1.740	2.401	3.367
Nominal Strain (%)	0.000	3.571	7.143	10.714	14.286	17.857	21.429
Strain A	0.000	3.299	6.341	9.512	12.596	16.195	18.809
Strain B	0.000	3.277	6.643	10.053	13.109	15.899	19.176
Strain C	0.000	3.366	6.776	9.477	12.533	15.456	18.955
Strain D	0.000	2.391	5.277	8.525	11.953	15.201	17.817
Strain E	0.000	3.121	5.461	8.857	10.877	14.135	17.072

Data for Figure 4.6(a)

Load (N)	Strain for Leather Parallel to Backbone							
	0	14.023	30.105	47.342	64.067	83.151	103.317	126.631
Stroke (mm)	0	5	10	15	20	25	30	35
Nominal Strain (%)	0	2.778	5.556	8.333	11.111	13.889	16.667	19.444
A	0	2.556	4.887	7.450	9.775	12.103	14.431	16.992
B	0	2.940	5.554	7.831	10.445	12.405	15.019	17.626
C	0	3.260	5.987	8.160	10.333	13.049	15.206	18.466
D	0	3.277	6.554	9.831	13.108	14.747	16.353	19.630

Data for Figure 4.9

Butt Perpendicular

Stroke 5 mm
 WD 300 mm
 FOV 448pix Horizontal
 580pix Vertical

	Pixels	Direct Strain
Distance (1, 2)	250.87	
Distance (1, 2)	257.25	2.543
Distance (1, 2)	266.18	6.103
Distance (1, 2)	273.30	8.941
Distance (1, 2)	281.03	12.022
Distance (1, 2)	287.92	14.769

Load (KN)	Stroke	
0.0092	5	mm
0.0229	10	mm
0.0458	15	mm
0.0755	20	mm
0.1085	25	mm

Stress (MPa)
0
0.123
0.305
0.611
1.007
1.447

Butt Parallel

Stroke 5 mm
 WD 300 mm
 FOV 448pix Horizontal
 580pix Vertical

	Pixels	Direct Strain
Distance (1, 2)	262.03	
Distance (1, 2)	269.80	2.965
Distance (1, 2)	278.79	6.396
Distance (1, 2)	287.76	9.819
Distance (1, 2)	296.30	13.079
Distance (1, 2)	305.01	16.403

Load (KN)	Stroke	
0.0336	5	mm
0.0954	10	mm
0.1801	15	mm
0.2655	20	mm
0.3555	25	mm

Stress(MPa)
0
0.448
1.272
2.401
3.540
4.740

Data for Figure 4.10

Butt Parallel		Butt Perpendicular	
Direct Strain	Lateral Strain	Direct Strain	Lateral Strain
0	0	0	0
3.512	1.631	3.052	0.694
7.067	4.079	5.301	1.736
9.564	7.082	8.514	4.201
13.161	10.493	11.526	6.979
16.039	14.238	14.217	10.174

Data for Figure 4.11

Poisson's Ratio for different region

Butt Parallel	Butt		Belly		Neck	
	Parallel	Perpendicular	Parallel	Perpendicular	Parallel	Perpendicular
0.464	0.288	0.914	0.790	0.564	0.455	
0.577	0.327	1.056	0.823	0.771	0.516	
0.740	0.493	1.358	0.914	0.952	0.626	
0.797	0.606	1.441	0.943	1.149	0.708	
0.888	0.716	1.510	0.999	1.118		

Poisson's Ratio for Rubber

	0mm		Strain(%)	Lateral Strain(%)	Poisson's Ratio
Distance (4, 5)	66.03	pixels			
Distance (a, b)	74	pixels			
	5mm				
Distance (1, 8)	470.05	pixels	2.844		
Distance (2, 7)	339.04	pixels	3.039		
Distance (3, 6)	202.02	pixels	3.066		
Distance (4, 5)	68.03	pixels	3.029		
Distance (a, b)	73	pixels		-1.351	0.446
	10mm				
Distance (1, 8)	482.05	pixels	5.470		
Distance (2, 7)	347.05	pixels	5.473		
Distance (3, 6)	208.01	pixels	6.122		
Distance (4, 5)	70.01	pixels	6.028		
Distance (a, b)	72.4	pixels		-2.162	0.359
	15mm				
Distance (1, 8)	493.05	pixels	7.877		
Distance (2, 7)	355.05	pixels	7.905		
Distance (3, 6)	212.01	pixels	8.163		
Distance (4, 5)	71.03	pixels	7.572		
Distance (a, b)	71.9	pixels		-2.838	0.375
	20mm				
Distance (1, 8)	505.05	pixels	10.502		
Distance (2, 7)	364.05	pixels	10.640		
Distance (3, 6)	218.02	pixels	11.229		
Distance (4, 5)	73.03	pixels	10.601		
Distance (a, b)	70.8	pixels		-4.324	0.408
	25mm				
Distance (1, 8)	516.05	pixels	12.909		
Distance (2, 7)	372.05	pixels	13.071		
Distance (3, 6)	223.02	pixels	13.780		
Distance (4, 5)	75.03	pixels	13.630		
Distance (a, b)	69.88	pixels		-5.568	0.408
	30mm				
Distance (1, 8)	528.05	pixels	15.534		
Distance (2, 7)	381.05	pixels	15.807		
Distance (3, 6)	227.02	pixels	15.821		
Distance (4, 5)	76.03	pixels	15.145		
Distance (a, b)	69	pixels		-6.757	0.446

Appendix E

Data for Figure 5.17

Butt		Neck		Belly	
Degree	Strain	Degree	Strain	Degree	Strain
0	8.176	0	6.564	0	4.917
15	6.406	15	5.830	15	4.717
30	5.340	30	6.138	30	4.674
45	4.910	45	6.703	45	4.683
60	4.616	60	6.647	60	5.205
75	4.618	75	6.649	75	5.227
90	5.985	90	5.967	90	5.357
105	7.217	105	6.126	105	5.546
120	6.654	120	6.311	120	5.710
135	7.319	135	6.304	135	5.905
150	7.752	150	5.778	150	5.374
165	7.740	165	6.499	165	4.844

Appendix F

Front Panel and Block diagram to apply image analysis technique to determine location of spots along the surface of hide.

First a marked pattern is selected, then along the whole region where the pattern is expected to lie after stretching is selected. The VI will give the location of all the similar marked pattern appeared along the region of interest.

Enter number of Images to be processed

2

Apply BCG function

Brightness 125
 Contrast 56.00
 Gamma 2.00

Press after applying BCG function

Return

Distance between Spot

675.086
 0

Deformed Image
 Reference Image

Number of Matches found

2

Enhanced Image

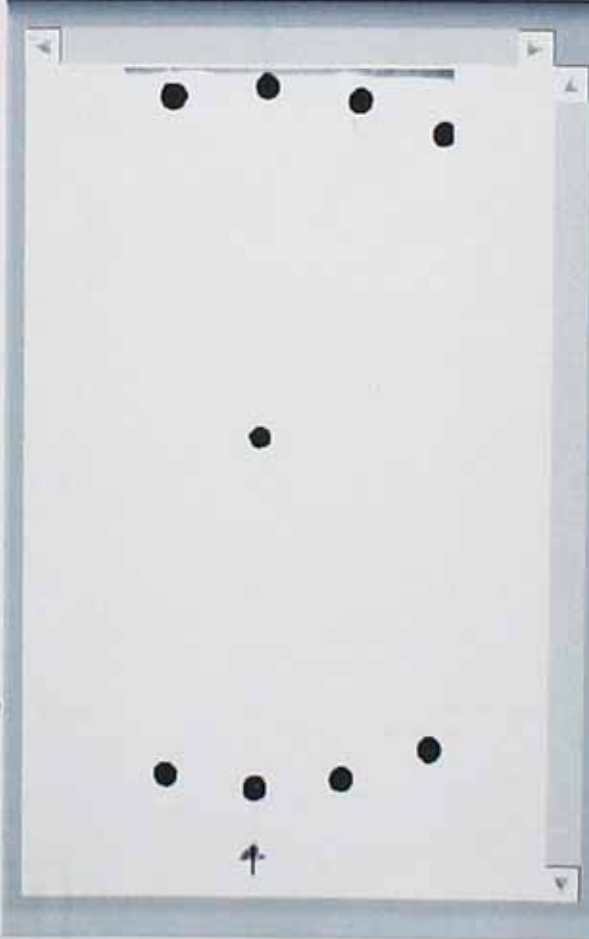
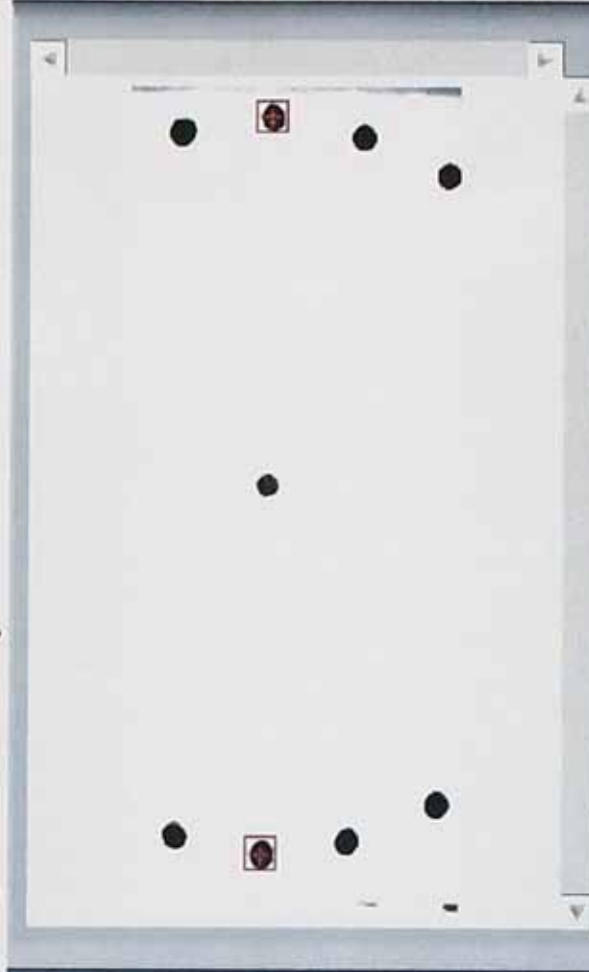


Image with resulted pattern



Settings

Match Mode
 Shift Invariant

Number of Matches Requested

4

Minimum Match Score

900.00

SubPixel Accuracy

Rotation Angle Ranges

0

Start 0.0

End 0.0

Show Search Area

Show Result

Spots Location

0

X 56.19

Y 119.57

X 731.23

Y 127.60

X 0.00

Y 0.00

Publication / Conference / Seminar

- Signal and Image Processing, Honolulu, Hawaii, USA, August 2005
(Paper attached)
- The University of Northampton, internal conference July 2004
- Presentation to Northern group in Leeds Sept 2003
- Seminar in NED university of engineering and technology on Non Destructive Testing August 2005
- Presentation in Leather Research Centre

The Application of Image Analysis to Determine Strain Distribution in Leather
Saqib Kabeer, Geoff Attenburrow, Phil Picton,
Malcolm Wilson
School of Applied Sciences, University
College Northampton, United Kingdom

ABSTRACT

An image analysis system has been developed to investigate the deformation behaviour of leather in a uni-axial direction. This technique provides more information about the stress-strain behaviour of a leather sample along the gauge length as compared to conventional testing, as strain distribution in leather varies from point to point along its surface. This technique could be very helpful in determining strain distribution along the whole hide in a non-destructive way.

1 Introduction

Non-destructive testing (NDT) may be defined as the application of an inspection method to a component or structure in which the test piece is not adversely affected by the testing method. Great achievements have been obtained in this field by the introduction of Holography, Speckle Photography, and Laser Speckle Photography.

These methods have been successfully applied to quantitative measurement of temperature [1], strain field [2] and surface displacement [3]. These methods have some drawbacks like sensitivity to the environment, they require surface preparation, they are non-automated and time consuming. Therefore these methods cannot be successfully applied to measuring strain in leather.

The most important factor for strain measurements especially for leather in a non-destructive way is the delay between the application of stroke and making measurements. Leather, being a viscoelastic material [4], would try to retract its original shape after the application of stroke. Therefore any delay in making measurements would lead to the collection of inaccurate data. Also, the application of a large amount of stroke during measurements would result in the induction of permanent set [4]. Keeping these two factors in mind, there is a need to develop a system which could be very fast so that there is almost no chance for the leather to retrace its shape, and could read the minute displacement along its surface after the application of a small stroke in order to avoid set.

An Image Analysis Technique is therefore applied for the present work. The use of this

technique using digital images to measure strain fields is an emerging area of research in polymer sciences [5] and biomedical science [6]. An early study of the response of leather to mechanical stretching in an setting machine [7] also suggest that the approach is feasible.

1.1 System Set up

A system has been set-up, which allows (i) controlled stretching of the leather (ii) the acquisition of digital images of the stretched leather (iii) quantitative analysis of the images by computer.

The stretching of the leather sample is carried out by a Dartec Tensile Testing machine, while images are captured by a CCD camera with a 12mm lens. The captured images are digitised by the frame grabber provided by National Instrumentation Inc. The whole system is shown in the Figure 1.

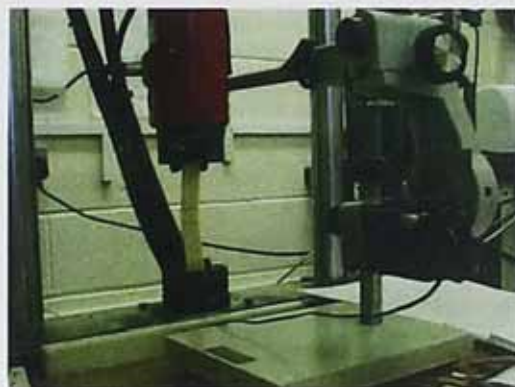


Fig 1 The system

1.2 Software selection and development

Virtual instrumentation (VI) is defined as a combination of hardware and software with computer technologies to create a user defined system. It is possible with virtual instruments, to build measurement and automation systems that suit requirements exactly (user-defined) instead of being limited by traditional fixed-function instruments (vendor-defined). It was decided to use this VI approach which will support research on software development in order to achieve the ultimate aim of providing a strain map.

A software package called "Lab VIEW" was obtained from National Instrumentation Inc. Lab VIEW is an integral part of virtual instrumentation because one of its best features is its front panel facility, which provides an easy-to-use application development environment. It offers features that are easy to connect to a wide variety of hardware and other software.

- *Graphical Programming*

Lab VIEW offers a graphical programming environment making it possible to design custom virtual instruments by creating a graphical user interface on the computer screen through which it is possible to operate the instrumentation program, control selected hardware, analyse acquired data and display results.

It is possible to customise front panels with knobs, buttons, dials, and graphs to emulate control panels of traditional instruments, create custom test panels, or visually represent the control and operation of processes. The similarity between standard flow charts and graphical programs shortens the learning curve associated with traditional, text-based languages.

The behaviour of the virtual instruments is determined by connecting icons together to create block diagrams, which are natural design notations. With graphical programming, systems can be developed more rapidly than with conventional programming languages, while retaining the power and flexibility needed to create a variety of applications.

- *Image Acquisition:*

National Instruments "IMAQ Vision builder" software is a tool for prototyping and testing image processing applications. It provides three types of image acquisitions: snap, grab and sequence. A *snap* acquires and displays a single image. A *grab* acquires and displays a continuous sequence, which is useful, for example when focussing the camera until the whole sample is in imaging window. A *sequence* acquires images according to settings (image acquisition rate) that are specified and send the images to the image browser. The images as acquired by vision builder will be digitised by a frame grabber.

- *Software development*

To prototype the image processing application, an algorithm was build using the IMAQ Vision Builder scripting feature. This scripting feature records every step of the processing algorithm, e.g. open image, select edges, calibrate (convert pixel to real world co-ordinate), and calliper (measure distance between edges). After completing the algorithm for one image it can be used for other images. This feature allows batch processing.

A graphical programme has been developed which automatically process the images to

measure the strain distribution from displacement of marking (lines or dots) on the sample.

2.1 Accuracy of image processing software

There is a need to determine the accuracy of measurements using the image analysis technique before its application for the measurement of strain measurement in leather. The system uses a CVA50 CCD camera having sensor size of 6.4 x 4.8 mm with 12 mm lens for the first series of experimental work (uni-axial stretching).

The minimum recommended working distance for this lens is 300mm. If a sample size of 25 x 220mm is used, this would give a gauge length of around 160mm after using 60mm in grips. The aim is to stretch the sample to a maximum length of around 200mm. Therefore the maximum field of view (FOV) after stretching will be 25 x 200mm.

The working distance required for this FOV (25 x 200mm), Focal Length (25mm) and Sensor Size (6.4 x 4.2mm) can be determined using a basic lens equation. When these values are used the required working distance is approximately 375mm.

2.1.1 Acquiring images

After calculating the working distance and placing the camera at that position the images are acquired. A PCI-1409 image acquisition board was used which features a 10-bit analogue-to-digital converter (ADC) that converts video signals from the camera to digital formats. NI-IMAQ 2.5 driver software is used to acquire the images and IMAQ Vision Builder software to process images.

With this integrated system a live view of the sample can be displayed on the computer screen. If the whole sample still cannot be reproduced on the screen then the dimensions of the imaging window need to be changed. The dimensions of the imaging window should occupy the whole sample. These dimensions are integer value which depicts the number of pixels assign to length and width of the whole image (field of view). The size of the imaging window is obtained by assigning different width and height values. A proper ratio of width and height of the window needs to be obtained until a sharp image without any blurring and image flickering is obtained.

Once the whole sample is in the imaging window an image can be snapped at any time and saved in multiple format e.g. TIFF, PNG, BMP etc for processing at any time.

2.1.2 Calibration by using grid

The process of calibrating a camera involves determining the intrinsic parameters, such as focal length, and extrinsic parameters, such as the position and orientation of the camera with respect to a co-ordinate frames. This process often relies on the use of calibration patterns with known geometry.

The most commonly used calibration pattern is the grid pattern consists of black circular pattern with white background to give strong features. This involves the extraction of pattern features (in pixels), and equating them with real world measurements (mm, cm). Once it has been achieved the intrinsic or extrinsic parameters of the camera cannot be changed but the pattern can be replaced by the sample.

After the imaging system has been set up and images acquired, the images can be analysed to extract valuable information about the object under inspection i.e. strips. These strips are pasted with the grid of known diameters and centre to centre distance. It is called the calibration grid and is supplied by *national instruments*, having diameter of 4mm and centre to centre distance of 1cm. This is shown in Figure 2.



Fig 2 Grid used for calibration

It is been suggested that the diameter of the grid when measured by image analysis software should be 6 to 10 pixels. Although the calculated working distance for the field of view of the system is 375mm, the camera can be placed in a position that can get the two strips within the field of view even after the application of stroke. But the diameter of the grid should not be less than 6 pixels. If the camera is moved nearer to the object the magnification can be increased by assigning more pixel values to the grid. As soon as the camera moves away from sample the assigned pixel values will be reduced.

The test procedure was to hold these strips with jaws and to drive the displacement rod (upper jaw) and capture images at every applied step. The typical image used for calibration and for accuracy of measurement by using software is shown in Figure 3.

On the calibration device a set of targets (dots) is placed and the difference between them measured using image processing after the application of stroke. To measure the displacement between upper and lower strips

the tools from IMAQ Vision builder were used to create the analysis algorithm which is called *script*. This script can then be used for other images to perform same analysis.

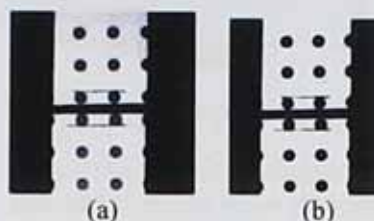


Fig 3(a, b) Effects of brightness, contrast and gamma function

The script writing starts after the saved image is loaded and displayed on the screen. IMAQ BCGLookup was applied by varying the amounts of Brightness, Contrast and Gamma across the whole image to highlight details of significant area e.g. grids at the expense of the background. The results are shown in Figure 3 (b). The grids can be isolated from the background by thresholding the whole image. Thresholding consists of segmenting the image into two regions - a particle region and background region. It converts the image from greyscale with pixel values ranging from 0 to 255, to a binary image, with pixel values 0 or 1. Pixels outside the thresholds interval are set to zero and are considered as part of the background area. Pixels inside the threshold interval are set to 1 and considered as part of particle area.

As the image has been converted from greyscale to a binary image the process is known as *blob analysis (binary large objects)*. Blob analysis is used to find statistical information such as size of blob or number, location and presence of blob within the region. A morphological filter was applied to search for only circles on the grid. This is achieved by eliminating the border objects which would result in few circular grids of interest. The processed binary image is then passed by applying the BasisParticle function by which the position of each blob can be located by considering top left corner as an origin. The actual results of processed image after application of these steps are shown in Figure 4.

Once the coordinates of each blob has been determined the distance between them can be calculated using the calliper command of the software. This will give the distance between two dots in pixels which can be transformed into millimetres using the calibration command.

The transformation is carried out by equating the known distance value between two dots

which is 10mm with the pixel values as calculated by the software.

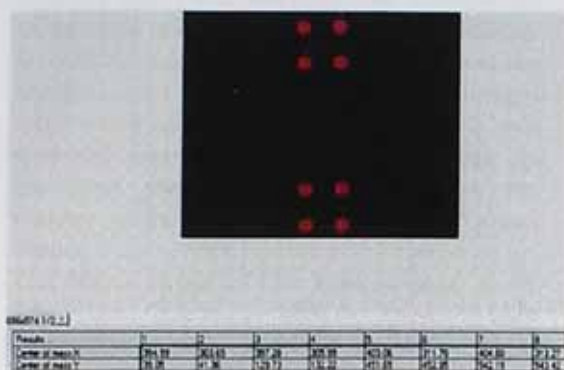


Fig 4 Location of blob on image

Finally, by using this correlation, the actual displacement (in mm) of the bottom lowest and top most dots on upper and lower strips respectively can be determined e.g. dot 4 and 6 or 3 and 5 in Figure 4.

2.1.3 Measurement by image analysis software

The setup consists of following parameters:

- Camera CVA50
- Lens 12mm
- Working distance 300mm
- FOV 696 x 574 pixels

Using this setup 15 images were captured after the application of 5mm strokes. Then by applying the above technique the separation between strips is measured using image analysis software. An approximately linear relation is obtained with a correlation factor of 0.99 and a residual of ± 0.01 mm.

It can be concluded from the above graph that a stroke of 5mm can be measured with in an accuracy of ± 0.01 mm with the existing setup.

3 Measurement of Strain distribution in rubber

Once the accuracy of displacement measured by image analysis technique has been determined there is a need to find the accuracy of strain measurement using the same technique.

The technique was applied on a rubber sample, to measure the strain distribution along its gauge length. Rubber was used because it is a homogeneous material with well-known characteristics. The stress-strain behaviour of rubber is sensitive to variations in chemical composition and process parameters such as cure time. However the general behaviour of rubber when it is stretched is shown in Fig 5.

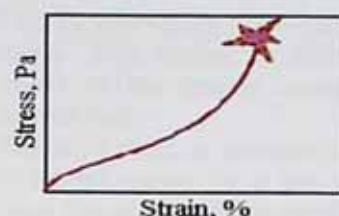


Fig 5 Stress-Strain behaviour of rubber

At first (bottom left of diagram) the rubber is reluctant to stretch under the applied force, so the curve rises steeply (large increase in stress to cause a little strain). Then there is a range of stress where the rubber extends more or less proportionately to the effort applied. Finally the rubber gets very resistant to stretching, as shown by the steeply rising curve, until it finally breaks.

3.1 Experimental setup

In this experimental work, a rubber sample (220 x 25 mm) marked with equidistant dots of 4mm diameter along its gauge length is used to detect the degree of strain distribution in a uni-axially stretched direction. The sample is shown in Figure 6.

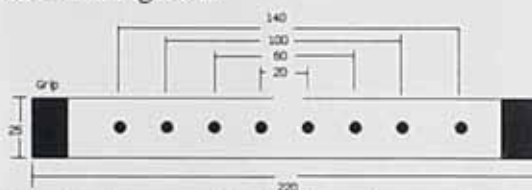


Fig 6 Rubber sample, all dimensions are in mm

The sample is gripped at its ends on tensile testing machine and the CCD camera is placed in a way that the whole sample can be viewed on the imaging window. In order to avoid perspective error the camera is placed in a way that the sample should be projected perpendicular to it.

As the camera does not move during the test in the current equipment configuration, strains can be measured by the relative movement of the dots with reference to an image of undeformed shape. To obtain the series of images at different stroke rate the sample is then uni-axially stretched with a load cell speed of 60 mm/min until a stroke length of 30 mm is achieved, as field of view is constrained. During this extension of the sample, images were automatically captured after the application of every 5 mm stroke. Although images can also be captured by using the snap and grasp feature of the software, this would result in a delay between capturing the image and the application of the required stroke, thus allowing a discrepancy of results.

Therefore in order to avoid error in acquiring images after the application of every 5 mm stroke, a front panel has been built with the use of controls and indicators. Controls simulate instrument-input devices and supply data to the block diagram of the VI. Consecutive images were obtained at a fixed interval of 5 mm stroke by providing a skip table to the user on the front panel. This table describes the number of frames to skip after each acquired frame.

The frame speed of the camera used is 25 frames/sec, thus in the table the frames to skip are multiples of 5, which is controlled using graphical codes on the block diagram. The front panel and acquired images are shown in Figure 7 and 8 respectively.

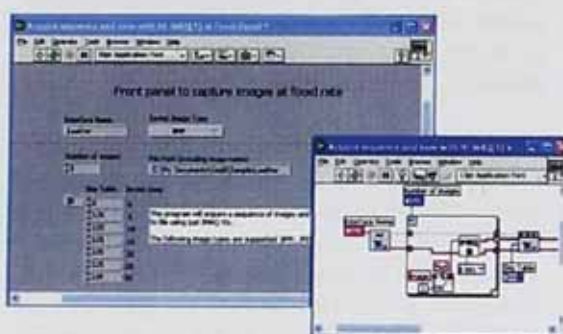


Fig 7 Front panel and Block diagram for continuous image capturing at different stroke rate

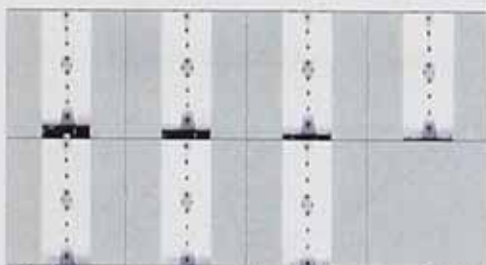


Fig 8 Images captured at different strokes

Subsequent images and load data are captured at regular intervals under the control of accurate timing facility. Images are saved to analyse later. The magnitude of load after the application of each stroke is recorded automatically by the software used to operate the tensile testing machine.

3.2 Image processing

Detection of the relative movement of dots on the sample for each acquired image is the main region of interest, so after every application of stroke all marked dots should be in the imaging window.

To detect these dots all the images were assigned a greyscale value ranging from 0 to

255 by converting the image into an 8-bit image. This results in different grey level values to the sample background and the marked dots.

The same script as mentioned in section 2.1.2 is applied except for a few changes e.g. not using the calibration command as the system is measuring strain which is a dimensionless quantity so the measurements can be in either units i.e. no of pixels or mm are acceptable. The resulted image and the script are shown in Figure 9 (a) and (b) respectively.

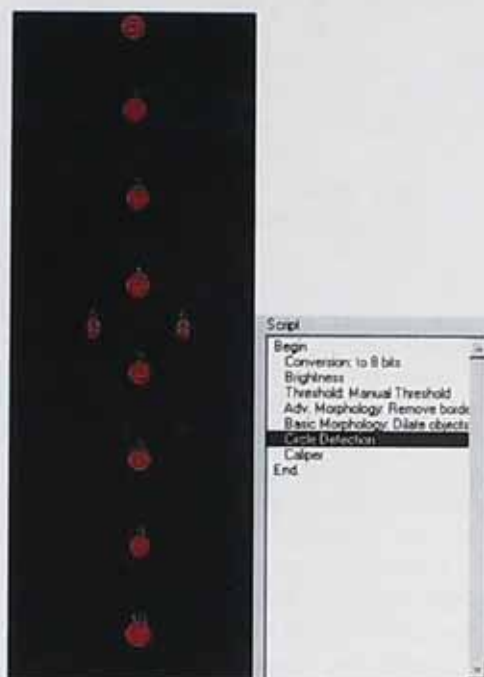


Fig 9 (a, b) Resulted image and script

After applying the script the location of the each dot is determined. Using the calliper command the displacement between the dots before and after stretching the sample uniaxially is calculated. The whole sample is divided into four different sections A, B, C, and D with lengths of 140, 100, 60 and 20mm respectively. The relative movement of marked dots on a sample was used to determine the mean strain in each section (A, B, C, and D). When the strain values for each section are plotted against the applied load as measured using image analysis technique the graph followed the same pattern as shown in Figure 7. Due to the limited field of view the full stroke length where the sample breaks cannot be shown. The results are shown in Figure 10. A uniform strain response was expected for rubber. When the best fit polynomial function with 4th degree of polynomial was applied (as shown in above figure) a residual of ± 0.5 resulted. This means that strain can be measured with in an accuracy of $\pm 0.5\%$.

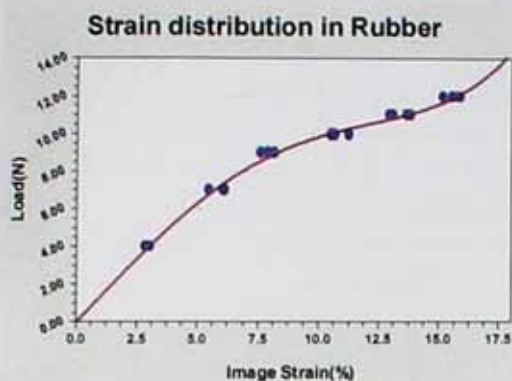


Fig 10 Strain measurement in rubber by image analysis at various loads

It can be observed from the graphs, that in the case of rubber strain for any given load in each section is almost same, as the data points overlap each other. The load-strain curve in Figure 10 is highly non-linear as expected from rubber [9].

When the same procedure was applied to determine the strain distribution in leather this strain is different for each section. The curves are again highly non-linear but concave to load axis giving a "J" shaped curve as expected [4]. By applying the best fit curve of 4th degree of polynomial the curve almost show a "J" shape with a very high residual of around ± 12 . This shows that the strain distribution in leather is not same for its each section. The results for strain are shown in Figure 11.

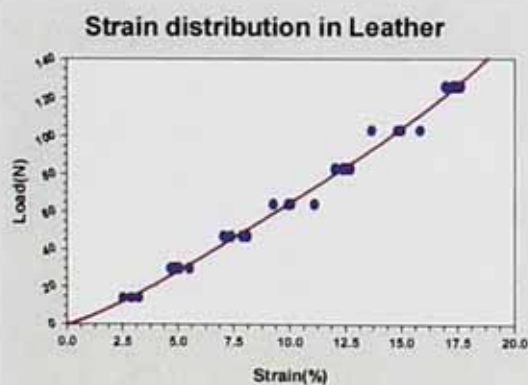


Fig 11 Strain measurement in leather by image analysis at various loads

4 Conclusions

A system has been set up to capture digital images of materials being stretched in order to measure the stress-strain characteristics. The system has been calibrated using a range of materials including rubber, to show that it can accurately take measurements without damaging the material. The aim of the system is to measure the characteristics of leather, which is a non-homogeneous material. This

paper has shown that the stress-strain characteristics of a strip of leather can be accurately determined.

Reference:

- 1) Asseban, A et al, "Digital speckle photography and speckle tomography in heat transfer studies", *Optics and Laser Technology*, 32, 7-8, p. 583-592, 2000
- 2) Sjoedahl, M et al, "Applications of digital speckle photography in experimental Mechanics", in "Optical Inspection and Micromasurements II", SPIE Proc. Vol 3098, pp.195-203, 1997
- 3) Strain field measurements in industrial applications using dual beam digital speckle photography, Peter Johnson Volvo Aero corporation, Division of Experimental Mechanics, Lulea University of Technology, 1998.
- 4) Ning Mo, Julia C. Shelton, "Medical engineering and Physics, 20 (1998), 594-601.
- 5) Attenburrow, G.E., "The Rheology of Leather -A Review", *J. Soc. Leath. Technol. Chem.*, 77, 1993, pp. 107-113.
- 6) Haynes, A.R. and Coates, P.D., "Semi-Automated Image Analysis of the True Tensile Drawing Behavior of Polymers to Large Strains", *Journal of Material Science*, 31, 1996, pp. 1843-1855.
- 7) Marcellier, H. *et al*, "Optical Analysis of Displacement and Strain Fields on Human Skin", *Skin Research and Technology*, 7, 2001, pp. 246-253.
- 8) Jarrett, R.M. and Sykes, R.L., "Analysis of Video Recordings to Investigate Mechanical Operations", *J. Soc. Leather Tech. And Chem.*, 72, 1987, pp. 94-96.
- 9) J.Kovas, "Understanding video calliper accuracy", www.mivos.com
- 10) F.W. Billmoyer, "Text book of Polymer Science" 1971, J. Wiley New York